Free-Space Quantum Electrodynamics with a single Rydberg superatom

Masterarbeit von
Christoph Braun
30.09.2017

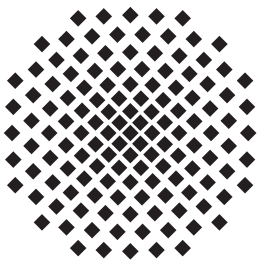

Universität Stuttgart
5. Physikalisches Institut

Hautpbericht:	Prof. Dr. Tilman Pfau
Mitbericht:	Prof. Dr. Peter Michler
Betreuer:	Prof. Dr. Sebastian Hofferberth

Quantenelektrondynamik eines einzelnen Rydbergatoms ohne Einschluss der gekoppelten Lichtmode

Zusammenfassung
Im Rahmen dieser Arbeit wurde untersucht, wie sich ein zwei-plus-ein Levelsystem verhält, wenn es von wenigen Photonen einer einzigen propagierenden Mode getrieben wird.

Um die extremen Anforderungen an sowohl Moden-Anpassung als auch Moden-Überlapp, die im Falle der Kopplung eines einzelnen Photon an ein einzelnes Atom gestellt werden, nicht erfüllen zu müssen und dennoch ein stark gekoppeltes System untersuchen zu können wurde das Konzept des Superatoms herangezogen. Ein Ensemble von Atomen, beispielsweise ein Molekül, oder wie hier eine Atomwolke, weist dabei die charakteristischen Merkmale eines einzigen Atoms, beziehungsweise eines Modell-Systems auf. Um der hier behandelten Atomwolke die Eigenschaften eines zwei-plus-ein Niveau Systems aufzuzwingen wird die Eigenschaft der Rydbergblockade ausgenutzt. Existiert eine Rydberganregung, kann innerhalb eines durch den Blockaderadius definierten Volumens kein weiteres Rydbergatom angeregt werden. Die Atomwolke wird hierzu dahingehend maßgeschneidert, so dass sie zwar kleiner als der Blockade Radius ist, gleichzeitig jedoch eine möglichst hohe atomare Dichte aufweist. Sind diese Anforderungen erfüllt, so kann in der gesamten Wolke nur eine einzige Anregung Platz finden, welche gleichzeitig von der Gesamtheit der einzelnen Atome getragen wird, was zu verstärkter Kopplung an das Lichtfeld führt.

Diese kollektive Verstärkung stellt die Quintessenz der präsentierten Arbeit dar. Sie resultiert nicht nur in einer deutlich verstärkten Wechselwirkung zwischen Licht und Materie, sondern führt auch dazu, dass eine fixe Phasenrelation zwischen den Atomen eine gerichtete Emission des gestreuten Lichts zur Folge hat. Die hier vorgestellten Messungen sind die ersten Messungen eines einzelnen stark an propagierende Photonen ohne künstlichen Modeneinschluss gekoppelten Zwei-Niveau Systems, in denen die kohärenten Effekte einzelner Photonen sowohl in der aus dem System emittierten Intensität sowie in den Korrelationen zwischen einzelnen Photonen beobachtet werden konnten. Der das System verlassende Lichtpuls weist hoch nicht-klassische Eigenschaften auf, mit periodisch super- und subpossinischer Modulation. Um das System physikalisch in Kontext setzten zu können werden zunächst Konzepte der Resonator Quantenelektrodynamik eingeführt und später mit der Freiraum Quantenelektrodynamik kontrastiert.

Free-Space Quantum Electrodynamics with a single Rydberg superatom

Abstract
In the course of this thesis the behavior of a two-plus-one levelsystem driven by a propagating few-photon light-mode was investigated.

To overcome the stringent requirements regarding mode matching as well as mode overlap, which need to be optimized to achieve significant coupling to an individual atom, and still investigate a strongly coupled system we utilize the concept of a superatom. An ensemble of atoms, e.g. a molecule or like here an atom cloud, that resemble the essential properties of an individual atom or model-system is called superatom. To provide the atomic cloud discussed in this thesis with the properties of a two-plus-one level system the Rydberg blockade, which prevents further Rydberg excitations inside a certain distance, is utilized. The atomic cloud for that purpose is tailored such that it is smaller than a single blockade radius, but still allows for a high atomic density. If these requirements are met, the cloud can only host a single excitation, which simultaneously is shared among all constituents of the atomic ensemble leading to an increased coupling strength.
eines einzelnen stark an propagierende Photonen ohne künstlichen Modeneinschluss gekoppelten Zwei-Niveau Systems This collective enhancement represents the quintessence of the presented work. It does not only result in a significantly increased coupling between light and matter but also implicates a fixed phase relation among the individual constituents, which leads to directed emission of the scattered light. The measurements presented in this thesis are the first investigations of a single two-level system strongly coupled an individual propagating few-photon light-mode in free space, in which the coherent effects of individual photons could be observed on the one hand in the outgoing intensity, on the other hand in the correlations among individual photons. The outgoing light field recovers highly non-classical properties with periodic sub- and super-possonian statistics. To put the system into a physics context, the concepts of cavity quantumelectrodynamics are introduced and contrasted with free space quantum electrodynamics.

Declaration

I hereby declare that this submission is my own work and that, to the best of my knowledge and belief, it contains no material previously published or written by another person, except where due acknowledgment has been made in the text. This is a revised version, in which minor corrections have been made.

Christoph Braun

Publications

The work discussed in this thesis was published in:

- Asaf Paris-Mandoki*, **Christoph Braun***, Jan Kumlin, Christoph Tresp, Ivan Mirgorodskiy, Florian Christaller, Hans Peter Büchler, and Sebastian Hofferberth
  Free-Space Quantum Electrodynamics with a single Rydberg superatom;
  Physical Review X 7, 41010 (2017)

Furthermore, in the framework of this thesis following articles have been published:

- Ivan Mirgorodskiy, Florian Christaller, **Christoph Braun**, Asaf Paris-Mandoki, Christoph Tresp, and Sebastian Hofferberth
  Electromagnetically induced transparency of ultra-long-range Rydberg molecules;
  Physical Review A 96, 11402 (2017)

- Christoph Tresp, **Christoph Braun**, and Sebastian Hofferberth
  Superatom schluckt einzelnes Photon;
  Physik in Unserer Zeit 48, 59 (2017).

* These authors contributed equally to this work.

Contents

1 Introduction

In 1801 Thomas Young's double-slit experiment provided evidence for the wave nature of light [1]. Its fast oscillating nature was then investigated about 80 years later by Heinrich Hertz [2], who also shortly thereafter found that electrodes illuminated with UV-light created *longer*, as Hertz described it, discharge sparks compared to non illuminated ones [3]. Following the 1896 formulated description of the spectra of black-body radiation by Willy Wien, in 1901 Max Planck could, deviating from his previous work, explain the obtained experimental spectra with by the introduction of *energy elements* [4–8]. These *energy elements'* energy E had to be related to their frequency ν by $E = h\nu$ with a proportionality factor h, today known as *Planck's constant* [8]. However the two main findings, discrete *energy elements* on the one hand and on the other hand the uniform intensity of an emitted electromagnetic field, as established by James Clerk Maxwell, were not easily compatible [9, 10].

In 1905 Albert Einstein heuristically assumed that there might not only be finite numbers of, e.g. atoms and electrons inside a ponderable body, but also a non-continuous energy distribution considering the process of light creation and conversion, and in particular explaining the aforementioned photoelectric effect - the idea of photons was born [10]. Inspired by the ideas of Einstein and Planck, Louis de Broglie combined the two energy relations found from relativity $E = m_0c^2$, where m_0 and c correspond to a body's rest mass and the speed of light, and black-body radiation $E = h\nu$. He postulated that a photon eventually might fulfill both simultaneously and vice versa for a solid body, resembling the particle-wave duality. Furthermore he deduced a *phase-* and *group*-velocity for both a photon as well as a solid particle [11, 12]. Finally de Broglie revolutionized the understanding of both light and matter, also influencing Schrödinger, who *invented* the equations describing the behavior of quantum systems [12–16]. Schrödinger himself was never keen on believing that it would ever be possible to observe quantum systems, where individual atoms and photons interact [17].

The previously described developments laid the foundation of the basis of quantum mechanics as we know it today; the wealth of this field of physics is still being explored today, in basic research and now also applied in many modern technologies. With the unprecedented technological advancements in the 20th and 21st century, among them radio, semiconductor and laser technology, studies of individual photons interacting with individual atoms more and more came to reality. Eventually culminating in the study of individual photons interacting with single atoms in a cavity, implementing the seminal Jaynes-Cummings model; or even excited atoms interacting with the vacuum-field inside a cavity could be observed [18–22]. These investigations show in an impressively clean manner the interaction of a single quantum of energy that is coherently hopping between an individual atom and a mode of a resonator, representing the most basic system in quantum electrodynamics (QED). Considering the advancements in direct implementations of quantum mechanics, the advent of laser cooling, made it possible to prepare a system extremely close to absolute zero temperature. Being able to achieve these incredibly low temperatures, it was possible to create a close to macroscopic quantum mechanical system, a Bose Einstein condensate, where individual particles become indistinguishable, incorporate their wave character and occupy one large quantum state [23–25], prepared by light.

Light-matter interactions form the basis for a vast number of processes and applications, ranging from vision to photosynthesis as well as imaging, spectroscopy or optical information processing and communication.

Though being very important, the interaction of light and matter is usually incredibly weak, yet the interaction strength can be increased by a cavity around the system of interest. The cavity increases the time a photon interacts with a system, or in other terms boosts the interaction strength between

the photon and the system. The strong increase in coupling strength nonetheless comes at the cost of access to the electric-field interacting with the atom, as it is well trapped inside the cavity [26]. The realization of a system being able to still interact strongly with an atom while maintaining access to the light field enables the observation of non-classical states of light prepared by on the fly processing of photons in the system. Many research teams worldwide focus on the realization of such a system in free space [27–29] and try to come close to *reversed spontaneous emission*, i.e. the perfect excitation of an atom with a single photon. While such systems were elusive for a long time, the emerging field of waveguide QED got close to this goal, by strongly confining the photon's transverse directions, e.g. in a tapered optical fiber, while not significantly modifying its longitudinal properties. In these systems first applications are being implemented such as photon routing, photon absorption, switches and chiral channels [30–35]. One prominent modification of the waveguide approach consists of the idea of coupling a system to a *chiral* channel offering a propagation-direction-dependent light-matter interaction [36].

A direct utilization of quantum mechanical principles for quantum coherent applications requires an interface enabling the communication between distant quantum systems [37] in a coherent manner, thus requiring efficient, rather deterministic, interaction of single quanta and single emitters. Where emitters do not necessarily need to be individual atoms.

In this thesis, first the basic steps required to perform the later discussed experiments will be presented. A theoretical framework first considering cavity systems and later systems coupled to a propagating channel will be presented. The cavity systems will be discussed in order to provide a broader context considering strongly coupled emitter-photon systems. The main experimental achievement presented in this thesis, the deterministic preparation of the first Dicke state in a superatom, based on the Rydberg blockade will be presented [38, 39]. The preparation of this state does not only result in super-radiance of the spontaneous emission, but, due to the Rydberg blockade, also the collectively amplified coherent coupling [40], thus enabling the observation of coherent Rabi oscillations in a single pass. Using the superatom approach the otherwise stringent requirements regarding mode-matching to the dipole emission pattern and mode overlap with the atom are significantly reduced, hereby overcoming the otherwise fundamentally limited coupling strength of a single atom to free-space [41].

2 The Setup

This section shall give a brief overview of the different experimental stages required to achieve an Rydberg superatom consisting of $\approx 10^4$ ^{87}Rb atoms. It will not discuss the full experimental parameters, optics and electronics used to implement the respective stages, it will rather try to convey the idea of each technique and why it is essential for the measurements presented later on.

2.1 The Magneto Optical Trap

Every experiment starts by loading a magneto optical trap (MOT) from a room temperature background gas of ^{87}Rb and ^{85}Rb providing a pressure of 10^{-10} mbar in an ultra-high vacuum chamber. The atoms are decelerated and captured by six pair-wise counter-propagating laser beams, red-detuned to the D_2-transition in ^{87}Rb, intersecting at the center of an magnetic quadrupole field. The MOT captures atoms slower than the capture velocity, which is defined such that an atom entering the MOT region is at rest once it reaches the opposite edge of the MOT region. In order to cool one requires a dissipative force slowing atoms down, but simultaneously a conservative force trapping the slow atoms. Therefore an atom in the MOT experiences both a dissipative and a conservative force restoring the atoms position towards the center. The whole procedure, of simultaneously decelerating and trapping, works due to the interplay of polarization, magnetic field and vectorial velocity. An atom travelling in the opposite direction of a red-detuned laser beam will, due to the Doppler effect, be more likely to scatter photons compared to an atom at rest, since it effectively experiences the light to be closer to resonance. Thus atoms traversing the cloud will always scatter more photons from the beam towards which they are travelling. The scattered light emitted from the atom is randomly directed, the laser beam thereby reduces the velocity component pointing against the propagation direction of the laser field, thus constituting the dissipative force decelerating the atom, while the atom is moving towards the laser beam. This process is commonly referred to as optical molasses [42]. The dissipative force in fact provides a slowing down of atoms, but it does not provide any spatial confinement or restoring force dragging an atom towards the trap center. The spatial confinement arises to due the aforementioned interplay of polarization and magnetic field. The trapping potential arises due to the internal level structure, enabling the possibility to use the magnetic field to spatially modify the scattering rate of each atom. As indicated in Fig. 1, the magnetic field shifts the different excited states for an atom at e.g. $z' > 0$ such that the detuning of the transition, which is being addressed by the beam propagating in negative z-direction is closer to resonance than the one addressed by the counter-propagating beam. The atom will be pushed towards the center. In the end the complex interplay of the dissipative and restoring force provides a cold atomic cloud. Fig. 1 oversimplifies the real physical picture, as there is no closed cycling transition in Rubidium due to the two meta-stable ground states; it is therefore necessary to shine in an additional laser to pump the atoms back into the cycle with a repump laser. The final atom number and temperature depend on a variety of experimental parameters, e.g. beam balance, beam overlap, polarization quality and are very hard to predict.

In the current realization we trap about $15 \cdot 10^6$ atoms after $\approx 1\,\mathrm{s}$ at a temperature of $\approx 45\,\mu\mathrm{K}$. By further increasing the magnetic field the atomic cloud can be spatially compressed and thus the atomic density increased before loading the atoms into a far off-resonant dipole trap, corresponding to the next experimental step. The atoms are detected via absorption imaging, where each atom scatters photons of a resonant laser beam thus casting a shadow onto the detector. The amount of missing photons then directly relates to the number of atoms stacked along the beam direction.

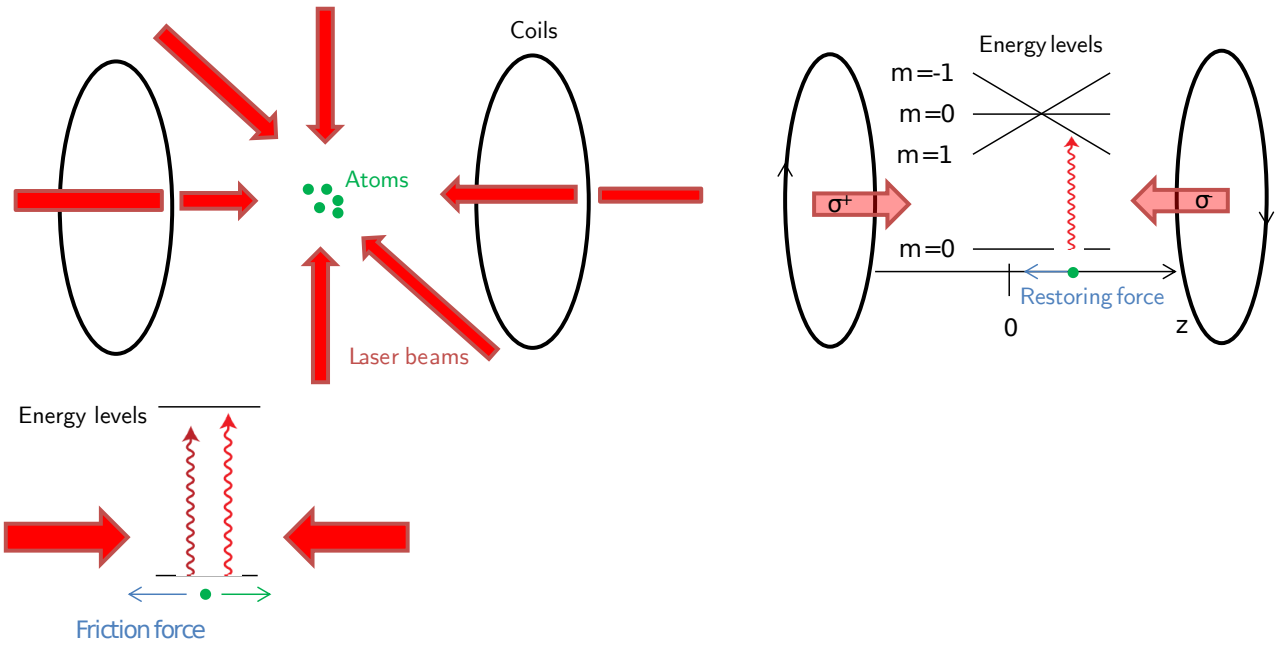

Fig. 1: Schematic of a magneto optical trap **(top left)** Experimental Realization: Six beams (red arrows) are pairwise counter-propagating intersecting at the trap center. Two coils create a magnetic quadrupole field providing a magnetic field gradient to trap atoms using radiation pressure. **(bottom left)** Atoms scatter light from a red-detuned laser beam only while travelling fast enough against its propagation direction, the random scattering events result in a net momentum transfer in direction of the laser beam thus decelerating the atoms. **(right)** Generic trapping schematic for an atom with a single ground an three excited states. In the center of the trap the excited states are all degenerate as there is no magnetic field. In the outside region the magnetic field shifts the $m_F = \pm 1$ state closer to resonance with the respective beam. Thus an atom located right of the center will experience a net restoring force towards the center indicated by the blue arrow.

The temperature of the cloud can be extracted from a time series of absorption images, since the temperature corresponds to a characteristic velocity distribution, thus by measuring the expansion of the cloud the temperature can be determined.

2.2 The Optical Dipole Trap

After having loaded the MOT, the experiment proceeds by loading the atoms into a far off-resonant optical dipole trap (ODT) at 1070 nm in order to create a cold, dense, optically thick atomic medium.

An atom in a far off-resonant laser field is only very weakly interacting with the laser field, thus for trapping purposes fairly high powers are required in order to achieve a significant trapping potential. In a simplified picture an atom can be considered as charge distribution which is polarized by the electrical field $\mathbf{E}$ of the trapping laser resulting in a dynamic polarization $\mathbf{p}$ oscillating at the laser frequency, i.e. $\mathbf{p} = \alpha \mathbf{E}$, where α is the atom's dynamic polarizabilty. The dynamic dipole then again interacts with the electric field leading to a potential proportional to the laser intensity I, $U_{\text{dip}} \propto \mathbf{p} \cdot \mathbf{E} \propto I$. It is thus plausible that the trapping potential is only a second order effect, which does only contribute little heating [43].

The response to a far detuned laser field shall briefly be discussed by considering a two-level system weakly coupled to a classical laser field $\mathbf{E} = \mathbf{E}_0 \cos(\mathbf{k}\cdot\mathbf{r} - \omega t)$, the ground state shall have zero energy and the excited state $\hbar\omega_e$. The Rabi frequency will be given by $\Omega = \langle e|-\mathbf{d}\cdot\mathbf{E}|g\rangle/\hbar$, where $\mathbf{d} = e\mathbf{r}$, the dipole operator with e the elementary charge. Diagonalizing the Hamiltonian describing the system in the rotating wave approximation

$$H = \hbar(\omega - \omega_0)\sigma^\dagger\sigma + \hbar\Omega(\sigma^\dagger + \sigma), \tag{1}$$

where $\sigma^\dagger$ is the operator exciting an atom, and σ leading to an relaxation from the excited to the ground state, one finds the eigenenergies

$$\mathcal{E}_\pm = \frac{\hbar}{2}\left(-(\omega - \omega_e) \pm \sqrt{(\omega - \omega_e)^2 + \Omega^2}\right). \tag{2}$$

In the limit of $|(\omega - \omega_e)| \gg \Omega$, the eigenenergies can be approximated to give

$$\mathcal{E}+ = -(\omega - \omega_e) - \frac{\Omega^2}{4(\omega - \omega_e)} \tag{3}$$

$$\mathcal{E}- = \frac{\Omega^2}{4(\omega - \omega_e)}. \tag{4}$$

In the presented limit the excited state population will be negligible, still the driving field leads to an energy correction. For a red-detuned laser an atom in the ground-state, in the limit $\Omega/(\omega - \omega_0) \to 0$, experiences an energy correction leading to a lower energy with increasing field strength. It follows that the higher the intensity is, the higher is the trapping potential, this term is referred to as a.c. Stark-shift.

As a rubidium atom is not a two-level-system, the trapping potential results from two main contributions, the D_1- and D_2-transition interacting with the laser field. In the current setup the two dipole-trap beams cross under an angle of 32 °, focused to a 40 μm $1/e^2$ beam waist, with at maximum 11 W of power in each arm. The trapping potential can then be calculated, neglecting polarization of the trapping beams, which would lead to to different trap depths for different m_F levels, using [43]

$$U_{\mathrm{dip}}(\mathbf{r}) = \frac{\pi c^2 \Gamma}{2\omega_0^3}\left(\frac{2}{\Delta_2} + \frac{1}{\Delta_1}\right), \tag{5}$$

where Γ is the excited state decay rate, ω_0 the resonant angular frequency and $\Delta_{\{1,2\}}$ the detuning from the respective $D_{\{1,2\}}$-transition. For the presented values the trap is at maximum $U_{\mathrm{trap}} = h \times 23.8\,\mathrm{MHz} = k_B \times 1.14\,\mathrm{mK}$ deep. The harmonic approximation of the trapping potential gives trap frequencies of $\nu_{\{x,y,z\}} = \{2.53, 0.71, 2.63\}\,\mathrm{kHz}$. The given values correspond to the maximum values, the power in the trap can be adjusted using an acousto-optic modulator, which is controlled in a closed loop. An absorption image of the cloud after loading and cooling the atoms is depicted in Fig. 2. The dipole trap contains $\approx 140,000$ atoms at a temperature of $\approx 5\,\mu$K and is depicted shortly after releasing the cloud from the trap. To reduce atom loss that would occur when evocatively cooling the atomic cloud to lower temperatures, we use Raman Sideband cooling as intermediate cooling step.

2.3 The Raman Sideband Cooling

The Raman Sideband Cooling was implemented during my Bachelor Thesis [44] in Stuttgart and finalized and characterized by Christoph Tresp [45]. Raman sideband cooling requires atoms to be

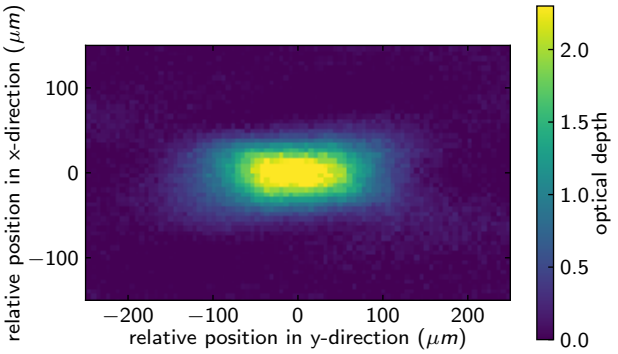

Fig. 2: Absorption image after $t_{tof} = 20\,\mu$s time of flight. The cloud contains 14×10^4 atoms at a temperature along the long direction and short direction of the cloud of $T_x = 2.5\,\mu$K and $T_y = 6.7\,\mu$K.

trapped inside a strongly confining potential, essential for a net cooling effect is the effective reduction of motional energy due to light scattering. The recoil energy $E_r = \hbar^2 k^2/(2m)$ is the kinetic energy, an atom at rest will have, after absorbing or emitting a 780 nm photon. Placing the system in the Lamb-Dicke regime, where atoms trapped in a potential with an energy spacing much larger than the recoil energy effectively inhibits heating [46]. The strong confinement in the present in experiment is provided by a stationary three dimensional optical lattice derived from two propagating and one retro-reflected laser beam, detuned to the red of the $|5S_{1/2}, F = 1\rangle \rightarrow |5P_{3/2}, F = 2\rangle$ transition. In this implementation the lattice does not only provide the trapping potential but is also driving the Raman transitions between adjacent m_F-levels and their degenerate neighboring motional states, as depicted in Fig. 3 by the double arrows; the Raman transitions are second order transitions via a virtual excited state. To achieve a significant rate for the Raman transitions that lead to a lower motional quantum number n, the states $|n, m_F\rangle$ and $|n-1, m_F-1\rangle$ are shifted into degeneracy with a magnetic field. As the reversed process is equally likely an atom in $|5S_{1/2}, F = 1, m_F = -1, n'\rangle$ will be pumped to $|5P_{3/2}, F = 0, m_F = 0, n'\rangle$ with resonant σ^+-polarized laser light thus removing the motional quanta which have been transferred to potential energy. Atoms in the motional ground state in $|5S_{1/2}, F = 1, m_F = 0, n = 0\rangle$ are pumped to the dark-state $|5S_{1/2}, F = 1, m_F = 1, n = 0\rangle$, which is entirely decoupled from any pumping light. If the dark-state, i.e. the motional ground state is largely populated the atoms are adiabatically released, such that no heating occurs. Raman Sideband cooling in the current implementation is utilized to reduce the temperature of atoms simultaneously held in the optical dipole trap, in order to increase the density after cooling. This cooling technique is superior to evaporative cooling, as it is fast, and provides close to no atom loss. The performance of the previous implementation was characterized in [45].

2.4 The Dimple Trap

Achieving a cloud smaller than the Rydberg cloud is not possible in the previously described ODT. To achieve a significant reduction in cloud size we shine in an additional focused trapping laser at 850 nm. The laser beam is elliptically shaped with $1/e^2$ intensity widths $w_{\text{long}} \approx 25\,\mu$m and $w_{\text{short}} \approx 6\,\mu$m along the long and short axis. The potential resulting from the dimple beam with a power of 250 mW is 400 μK.

The strongly confining axis is aligned such that it penetrated by the photons probing the dynamics of the Rydberg system, making the system a effective 0d-geometry, as the entire physics of the

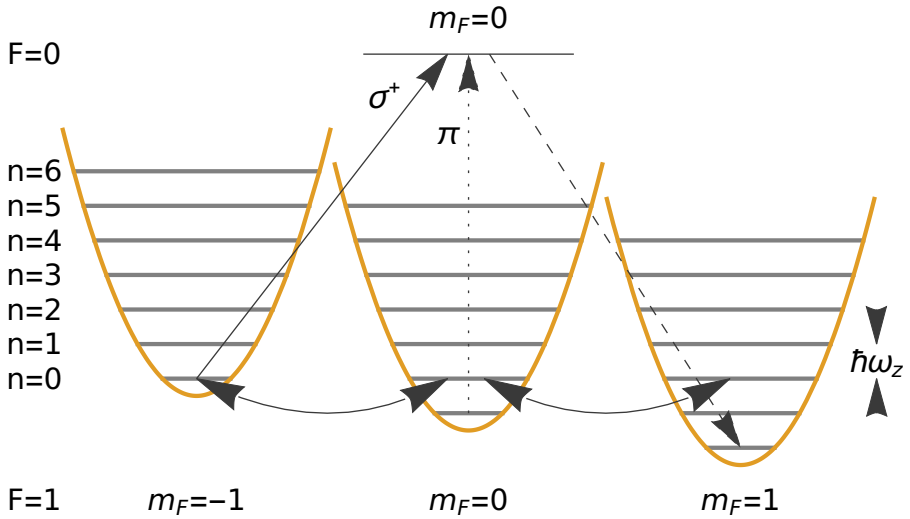

Fig. 3: Schematic working principle of Raman Sideband cooling. An offset magnetic field shifts states $|n, m_F\rangle$ and $|n-1, m_F-1\rangle$ into degeneracy enabling Raman transition among them. Additionally a resonant pump laser will transfer atoms from $|5S_{1/2}, F=1, m_F=-1, n'\rangle$ to $|5P_{3/2}, F=0, m_F=0, n'\rangle$, a weak π-polarized laser will pump atoms in the motional ground state from $|5S_{1/2}, F=1, m_F=0, n=0\rangle$ to the dark-state $|5S_{1/2}, F=1, m_F=1, n=0\rangle$, which is entirely decoupled from any transitions.

atomic cloud do happen in a single blockade radius which does not allow for position dependent effects in the presented experiments, as the exact position of the excitation is irrelevant. In a future implementation the dimple beam will be split in order to provide multiple traps hosting multiple spatially separated atom clouds.

3 Cavity Quantum Electrodynamics - light is trapped

The interaction of a single photon with an individual atom is incredibly small, by making the system interact with the same photon for $\approx 4 \times 10^9$, the interaction becomes significant [26, 47]. And enables the observation of fundamental quantum processes in nature, such as direct observation of the quantized nature of photons [22], or the energy splitting of a single atom coupled to a cavity. The cavity enhances the electric field of each photon and thus the atom-photon interaction. This way very small effects can lead to a significant modification of the physical properties, which will be theoretically studied in the following.

3.1 Jaynes-Cummings Model

The seminal Jaynes-Cummings model describes the interaction of a two-level system coupled to a stationary bosonic photon field, any dynamics occurring in this systems originate from energy exchange between the two coupled systems [20]. This system was and still is of great interest as it represents the textbook example of quantum electrodynamics, where the two simplest systems coherently interact and exchange energy. The system was extensively studied in many variations using individual atoms in Fabry-Perot cavities, superconducting qubits coupled to transmission lines and trapped ions[47–54].

The setting for this model is as follows, a quantized electric field $\mathbf{E}_{\mathbf{k},\zeta}(\mathbf{r},t)$ interacts with an atom or molecule exhibiting only two levels of opposite parity with energy E_g and E_e. The electric field reads

$$\mathbf{E}_{\mathbf{k},\zeta}(\mathbf{r},t) = \boldsymbol{\epsilon}_{\mathbf{k},\zeta}\sqrt{\frac{\hbar\omega}{2\epsilon_0 V}}\left(\mathrm{e}^{i\mathbf{k}\cdot\mathbf{r}}\, a_{\mathbf{k},\zeta}(t) + \mathrm{e}^{-i\ \mathbf{k}\cdot\mathbf{r}}\, a^\dagger_{\mathbf{k},\zeta}(t)\right) \tag{6}$$

$$= \boldsymbol{\epsilon}_{\mathbf{k},\zeta}\sqrt{\frac{\hbar\omega}{2\epsilon_0 V}}\left(\mathrm{e}^{i(\mathbf{k}\cdot\mathbf{r}-\omega t)}\, a_{\mathbf{k},\zeta}(0) + \mathrm{e}^{-i(\mathbf{k}\cdot\mathbf{r}-\omega t)}\, a^\dagger_{\mathbf{k},\zeta}(0)\right), \tag{7}$$

and will be assumed to be constituted by a single mode $\mathbf{k},\zeta$ with polarization $\boldsymbol{\epsilon}_{\mathbf{k},\zeta}$, which is perpendicular to its propagation direction $\mathbf{k}$, the creation and annihilation operators $a_{\mathbf{k},\zeta}(t)$ and $a^\dagger_{\mathbf{k},\zeta}(t)$, which for now, like already assumed in Eq. 7 shall be assumed to be stationary, i.e. $a_{\mathbf{k},\zeta}(t) = a_{\mathbf{k},\zeta}(0)\,\mathrm{e}^{i\omega t}$, create and annihilate a photon carrying $\hbar\omega = \hbar|\mathbf{k}|/c$ of energy, where c is the vacuum speed of light, $\hbar$ the reduced Planck constant and ϵ_0 the permittivity of free space. The electric field is for simplicity uniform inside the quantization volume V, the mode profile would correspond to a normalized multiplicative factor. It immediately follows, that the smaller the quantization volume, the bigger the electric field per photon. The creation and annihilation operators fulfill the bosonic commutation relations, i.e.

$$[a_{\mathbf{k},\zeta}(0), a^\dagger_{\mathbf{k},\zeta}(0)] = 1 \tag{8}$$

$$[a_{\mathbf{k},\zeta}(0), a_{\mathbf{k},\zeta}(0)] = [a^\dagger_{\mathbf{k},\zeta}(0), a^\dagger_{\mathbf{k},\zeta}(0)] = 0. \tag{9}$$

The action of the creation and annihilation operators on a state containing n photons is given by

$$a_{\mathbf{k},\zeta}(0)\,|n_{\mathbf{k},\zeta}\rangle = \sqrt{n_{\mathbf{k},\zeta}}\,|n_{\mathbf{k},\zeta}-1\rangle \tag{10}$$

$$a^\dagger_{\mathbf{k},\zeta}\,|n_{\mathbf{k},\zeta}\rangle = \sqrt{n_{\mathbf{k},\zeta}+1}\,|n_{\mathbf{k},\zeta}+1\rangle \tag{11}$$

$$a^\dagger_{\mathbf{k},\zeta}a_{\mathbf{k},\zeta}(0)\,|n_{\mathbf{k},\zeta}\rangle = n_{\mathbf{k},\zeta}\,|n_{\mathbf{k},\zeta}\rangle\,, \tag{12}$$

where the combination of the operators in Eq. 12 yields the number of quanta in that mode, thus multiplied by $\hbar\omega_{\mathbf{k},\zeta}$ gives the energy in the respective mode neglecting the vacuum- or ground state energy. Considering now first the uncoupled system made up of the atomic Hamilton operator H_A and the field Hamiltonian H_F, where the indices $\mathbf{k}, \zeta$ will be dropped from now on and $E_g = 0$,

$$H_A = \hbar\omega_0 \left|e\right\rangle \left\langle e\right| \tag{13}$$

$$H_F = \hbar\omega \left(a^\dagger a + \frac{1}{2}\right). \tag{14}$$

The eigenstates are product states of the respective Hamiltonians and will be denoted as orthonormal states $|m, n\rangle$, where index m denotes the atomic state and n the photon number, they obey

$$(H_A + H_F)\left|m, n\right\rangle = \hbar\left(\delta_{m,e}\omega_0 + n\omega + \frac{1}{2}\right) \tag{15}$$

$$\langle m, n|m', n'\rangle = \delta_{m,m'}\delta_{n,n'}. \tag{16}$$

In leading order the interaction of a photon with an electric field occurs due to the dipole part of the interaction, assuming that the spatial variation of the electric field is much larger than the size of an atom. The interaction Hamiltonian thus reads

$$H_{\text{int}} = \mathbf{d} \cdot \mathbf{E}_{\mathbf{k},\zeta}(\mathbf{0}, t) = -e\mathbf{r} \cdot \mathbf{E}_{\mathbf{k},\zeta}(\mathbf{0}, t), \tag{17}$$

with e the elementary charge, where the atomic matrix elements are given by the expectation value of the dipole operator $\langle e|\mathbf{d}|g\rangle = \mathbf{d}_{eg} = \mathbf{d}_{ge}$, where the last equality assumes a real matrix element. The dipole operator can thus be written as

$$\mathbf{d} = \mathbf{d}_{eg}(\left|e\right\rangle \left\langle g\right| + \left|g\right\rangle \left\langle e\right|). \tag{18}$$

For simplicity the electric field shall be a single mode field, the interaction then results in

$$H_{\text{int}} = \mathbf{d}_{eg}\Big(\left|e\right\rangle \left\langle g\right| + \left|g\right\rangle \left\langle e\right|\Big) \cdot \boldsymbol{\epsilon}_{\mathbf{k},\zeta}\sqrt{\frac{\hbar\omega}{2\epsilon_0 V}}\Big(\mathrm{e}^{-i\omega t}\, a_{\mathbf{k},\zeta}(0) + \mathrm{e}^{i\omega t}\, a^\dagger_{\mathbf{k},\zeta}(0)\Big), \tag{19}$$

introducing the coupling strength $\hbar g = \mathbf{d}_{eg} \cdot \boldsymbol{\epsilon}_{\mathbf{k},\zeta}\sqrt{\frac{\hbar\omega}{2\epsilon_0 V}}$ and explicitly stating the time evolution of the operator $\left|e\right\rangle \left\langle g\right| \to \left|e\right\rangle \left\langle g\right| \mathrm{e}^{i\omega_0 t}$, with $\hbar\omega_0 = E_e - E_g$ yields

$$H_{\text{int}} = \hbar g\Big(\left|e\right\rangle \left\langle g\right| \mathrm{e}^{i\omega_0 t} + \left|g\right\rangle \left\langle e\right| \mathrm{e}^{-i\omega_0 t}\Big)\Big(\mathrm{e}^{-i\omega t}\, a_{\mathbf{k},\zeta}(0) + \mathrm{e}^{i\omega t}\, a^\dagger_{\mathbf{k},\zeta}(0)\Big) \tag{20}$$

$$\begin{aligned} = \hbar g\Big(&\mathrm{e}^{i(\omega_0-\omega)t}\left|e\right\rangle \left\langle g\right| a_{\mathbf{k},\zeta}(0) + \mathrm{e}^{-i(\omega_0-\omega)t}\left|g\right\rangle \left\langle e\right| a^\dagger_{\mathbf{k},\zeta}(0) \\ &+ \mathrm{e}^{i(\omega_0+\omega)t}\left|e\right\rangle \left\langle g\right| a^\dagger_{\mathbf{k},\zeta}(0) + \mathrm{e}^{-i(\omega_0+\omega)t}\left|g\right\rangle \left\langle e\right| a_{\mathbf{k},\zeta}(0)\Big). \end{aligned} \tag{21}$$

Assuming $|\omega_0 - \omega| \ll \omega_0 + \omega$, the terms in Eq. 21 with exponents $\propto (\omega_0 + \omega)$ will oscillate much faster compared to the slow dynamics $\propto (\omega_0 - \omega)$, and will average out very fast on the time scale of the slow dynamics. For sufficiently small photon numbers, or as long as the energy of an excitation is small compared to the coupling strength, it is well justified to drop these terms, this approximation is called rotating wave approximation. Considering the system from another perspective the terms oscillating at $\pm(\omega_0 + \omega)$ correspond to the process of exciting the atom and simultaneously adding one more photon to the field and de-exciting the atom and annihilating one photon, i.e. these processes do not conserve the number of quanta in the system. Note that even though the number of quanta is not conserved the entire Hamiltonian does not violate energy conservation as it satisfies

$\frac{\mathrm{d}H_H(t)}{\mathrm{d}t} = i/\hbar[H_H(t), H_H(t)] + \partial H_H(t)/\partial t = 0$ in the Heisenberg picture, as the $H_H(t)$ does not show any explicit time-dependence[55]. The assumption to drop the dynamics of the fast oscillating terms, in many cases is as coarse as restricting the level structure to just two levels, since the detuning to the next level usually corresponds to a similar energy- hence timescale compared to the fast oscillating terms, thus the rotating wave approximation is usually as well justified as the restriction to two levels[56]. In principle the Rabi model can be solved analytically but is reaching beyond the scope of this work [57]. The Schrödinger equation for the Jaynes-Cummings model, dropping the vacuum-field term, then reads

$$\begin{aligned} H_{JC} =& H_A + H_F + H_{int} && (22)\\ i\hbar\partial_t |\Psi\rangle =& H_{JC} |\Psi\rangle && (23)\\ =& \Big(\hbar\omega_0 |e\rangle\langle e| + \hbar\omega a^\dagger a + \hbar g(|g\rangle\langle e| a^\dagger + |e\rangle\langle g| a)\Big) |\Psi\rangle . && (24) \end{aligned}$$

Plugging a state that includes all possible states of the atom and photon,

$$|\Psi\rangle = \sum_{n=0}^{\infty} \Big(c_{g,n} |g,n\rangle + c_{e,n} |e,n\rangle \Big), \tag{25}$$

into the Schrödinger Eq. 24 and projecting with $|e,n\rangle$ and $|g,n+1\rangle$ results in two coupled differential equations

$$i\partial_t \begin{pmatrix} c_{g,n+1}(t) \\ c_{e,n}(t) \end{pmatrix} = \begin{pmatrix} (n+1)\omega & g\sqrt{n+1} \\ g\sqrt{n+1} & n\omega + \omega_0 \end{pmatrix} \cdot \begin{pmatrix} c_{g,n+1}(t) \\ c_{e,n}(t) \end{pmatrix}. \tag{26}$$

The dynamics of the Jaynes-Cummings model are fully described within a subspace containing only two coupled adjacent levels, thus the Hamiltonian breaks up into blocks of dimension 2×2. Diagonalizing the Hamiltonian one finds the energies of the coupled system

$$\mathrm{E}_{+,-} = \frac{\hbar}{2}\Big((2n+1)\omega + \omega_0 \pm \sqrt{4g^2(n+1) + (\omega-\omega_0)^2}\Big) \tag{27}$$

and the corresponding eigenstates of the Hamiltonian

$$|+,n\rangle = \begin{pmatrix} \frac{\sqrt{4g^2(n+1)+(\omega-\omega_0)^2}+\omega-\omega_0}{\sqrt{8g^2(n+1)+\sqrt{2(\omega-\omega_0)\left(\sqrt{4g^2(n+1)+(\omega-\omega_0)^2}+\omega-\omega_0\right)}}} \\ \frac{1}{\sqrt{\frac{4\left(\sqrt{4g^2(n+1)+(\omega-\omega_0)^2}+\omega-\omega_0\right)^2}{g^2(n+1)}+1}} \end{pmatrix}, \tag{28}$$

and

$$|-,n\rangle = \begin{pmatrix} \frac{\sqrt{4g^2(n+1)+(\omega-\omega_0)^2}+\omega-\omega_0}{\sqrt{8g^2(n+1)-2(\omega-\omega_0)\left(\sqrt{4g^2(n+1)+(\omega-\omega_0)^2}-\omega+\omega_0\right)}} \\ -\frac{1}{\sqrt{\frac{4\left(\sqrt{4g^2(n+1)+(\omega-\omega_0)^2}-\omega+\omega_0\right)^2}{g^2(n+1)}+1}} \end{pmatrix}. \tag{29}$$

Introducing the *single photon Rabi frequency* $\Omega_n = 2\sqrt{n+1}g$ and detuning $\Delta = \omega - \omega_0$ the eigenvalues

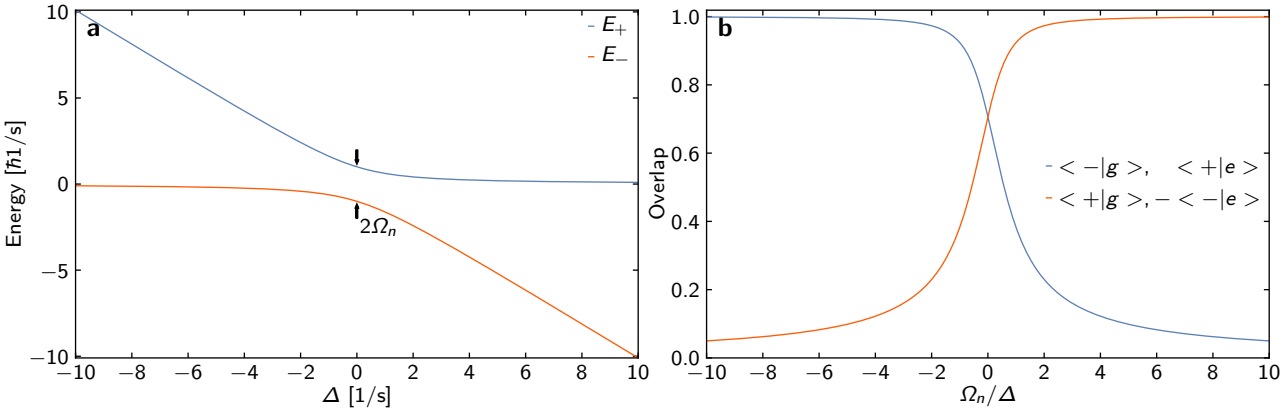

Fig. 4: Energy of the coupled system and relative state contribution to the $|+,n\rangle$ and $|-,n\rangle$ states. **a** The dressed states on resonance show the characteristic energy splitting $2\hbar\Omega_n = 2\hbar 2g\sqrt{n+1}$ (indicated by the black arrows). At any given detuning and Rabi frequency the two states are split by $2\hbar\tilde{\Omega}_n$, if the detuning is large compared to the Rabi frequency, the energy of the dressed states assimilates the bare states' energies with a small correction $\pm\Omega_n/\Delta$. The energy of state $|g,n+1\rangle$ is referenced to zero and $\Omega_n = 1\,\mathrm{s}^{-1}$ in panel **a**. **b** Overlap of the bare and dressed states of given photon number n, which is not stated in the legends. At large detuning the state mixing is relatively small, which is also reflected by the fact that the energy correction can be treated as a perturbation. By adiabatically following one of the dressed states energy with the cavity field radiation resonant to the dressed state, e.g. by following the $|n,-\rangle$, one can transfer the atom from the ground to the excited state.

and corresponding eigenvectors can be cast into a less cumbersome form

$$\mathrm{E}_{+,-} = \frac{\hbar}{2}\Big((2n+1)(\Delta+\omega_0)+\omega_0 \pm \sqrt{\Omega_n^2+\Delta^2}\Big) \tag{30}$$

$$|+,n\rangle = \begin{pmatrix} \sqrt{\frac{\Delta}{2\sqrt{\Delta^2+\Omega_n^2}}+\frac{1}{2}} \\ \frac{1}{\sqrt{\frac{\left(\Delta+\sqrt{\Delta^2+\Omega_n^2}\right)^2}{\Omega_n^2}+1}} \end{pmatrix} \qquad |-,n\rangle = \begin{pmatrix} \frac{1}{\sqrt{\frac{2\Delta\left(\Delta+\sqrt{\Delta^2+\Omega_n^2}\right)}{\Omega_n^2}+2}} \\ -\frac{1}{\sqrt{\frac{\left(\Delta-\sqrt{\Delta^2+\Omega_n^2}\right)^2}{\Omega_n^2}+1}} \end{pmatrix}. \tag{31}$$

Parameterizing the coefficients of the uncoupled states assembling the *dressed states* $|+,n\rangle, |-,n\rangle$ in terms of a rotation of the uncoupled states by a mixing angle θ_n, one finds

$$\tan(2\theta_n) = -\frac{2g\sqrt{n+1}}{\Delta} \qquad \left(0 \le \theta_n < \frac{\pi}{2}\right) \tag{32}$$

$$|+,n\rangle = \sin(\theta_n)\,|g,n+1\rangle + \cos(\theta_n)\,|e,n\rangle \tag{33}$$

$$|-,n\rangle = \cos(\theta_n)\,|g,n+1\rangle - \sin(\theta_n)\,|e,n\rangle\,. \tag{34}$$

The energy eigenvalues of the coupled Hamiltonian are shown in Fig. 4. In order to now investigate the dynamics, the atom shall be in $|\Phi_0\rangle = c_g(0)\,|g,n+1\rangle + c_e(0)\,|e,n\rangle$, with $|c_e(0)|^2 + |c_g(0)|^2 = 1$ at $t = 0$, thus the state

$$|\Psi_n(t)\rangle = \langle +,n|\Phi_0\rangle\,|+,n\rangle\,\mathrm{e}^{-it\mathrm{E}_+/\hbar} + \langle -,n|\Phi_0\rangle\,|-,n\rangle\,\mathrm{e}^{-it\mathrm{E}_-/\hbar} \tag{35}$$

describes the full dynamics of the system for arbitrary initial states. The probability of finding the atom in the excited state can then be calculated by projecting the excited state onto the state vector

$\Psi(t)$ of the system,

$$P_e(t) = |\langle e, n|\Psi_n(t)\rangle|^2 \tag{36}$$

$$= \frac{\Omega_n^2 \sin\left(\frac{t\sqrt{\Delta^2+\Omega_n^2}}{2}\right)}{\sqrt{\Delta^2+\Omega_n^2}} \tag{37}$$

$$= \frac{\Omega_n^2}{2\sqrt{\Delta^2+\Omega_n^2}}\left(1-\cos\left(t\sqrt{\Delta^2+\Omega_n^2}\right)\right), \tag{38}$$

where for simplicity in Eq. 37 and consequently Eq. 38 the initial state was assumed to be $|g, n+1\rangle$. The probability of finding the atom in the excited state shows oscillatory behavior, even though the entire system is in a steady state, since $|+, n\rangle, |-, n\rangle$ are stationary eigenstates of the system. Since the system is "perfect", i.e. not exposed to noise leading to decay or dephasing, the system does not lose any coherence and the oscillations are persistent in amplitude. The phenomenon of coherent oscillatory population transfer is called *Rabi Oscillation*, in this specific case between states $|g, n+1\rangle$ and $|e, n\rangle$. The oscillation angular frequency

$$\tilde{\Omega}_n = \sqrt{\Omega_n^2 + \Delta^2} = \sqrt{4g^2(n+1) + (\omega-\omega_0)^2}, \tag{39}$$

is often referred to as *generalized Rabi frequency*. Not only by increasing the photon number, but also by detuning the field from resonance one can achieve faster oscillations. From Eq. 38 one can identify two limiting cases which are $\Delta \to 0$ and $\Delta \to \infty$. In the first case the time averaged population of both the excited and the ground state is $1/2$, while the oscillation leads to full population inversions, equally spaced in time by $\tau = \Omega_n/(2\pi)$, the Rabi period. In this case, $\Delta \to 0$, the two states $|g, n+1\rangle$ and $|e, n\rangle$ are degenerate, while the dressed states are split by $2\hbar\Omega_n$. If there is only a single quantum of energy, the states directly above the uncoupled ground state $|g, 0\rangle$ exhibit the vacuum Rabi splitting, which has been observed in many systems, ranging from superconducting 3d microwave cavities coupled to Rydberg atoms, over optical cavities coupled to atoms to superconducting qubits coupled to a superconducting $L-C$-resonator [19, 48, 54, 58–61]. The discrete nature of the vacuum Rabi splitting gives direct proof of the quantized nature of light. The dynamics observed in these system are only perfectly sinusoidal, if the initial state was a Fock state of the photon field. In Fig. 5 the vacuum Rabi oscillations of an excited atom entering the empty cavity are depicted for various detunings of the cavity field. In the second case, for large detuning, the atom does hardly transit between the two states and is protected against relaxation to the ground state. This is one striking effect of the cavity, it entirely changes the vacuum density of states for the photons, in this model leaving only one mode behind. For large detuning $\Omega_n/\Delta \ll 1$ the atoms oscillate with very small amplitude and only acquire a different phase over time, thus their energy level is shifted, recovering the *A.C. Stark-shift*. The physical picture changes, if the probability amplitude of photons in the cavity is not perfectly peaked at a single photon number and the photon field is in a coherent state $|\alpha\rangle$ with Possoinian photon number distribution around the mean photon number $\bar{n} = |\alpha|^2$, i.e.

$$|\alpha\rangle = \sum_{n=0}^{\infty} \frac{\alpha^n}{\sqrt{n!}} \mathrm{e}^{\frac{-|\alpha|^2}{2}} |n\rangle, \tag{40}$$

the oscillation amplitude will then collapse but also revive after a certain time [22, 62]. The probability to find the system in the excited state is then given by

$$P_{e,\alpha}(t) = \langle e, n-1| \sum_{n=0}^{\infty} \frac{\alpha^n}{\sqrt{n!}} \mathrm{e}^{\frac{-|\alpha|^2}{2}} |\Psi_{n-1}(t)\rangle, \tag{41}$$

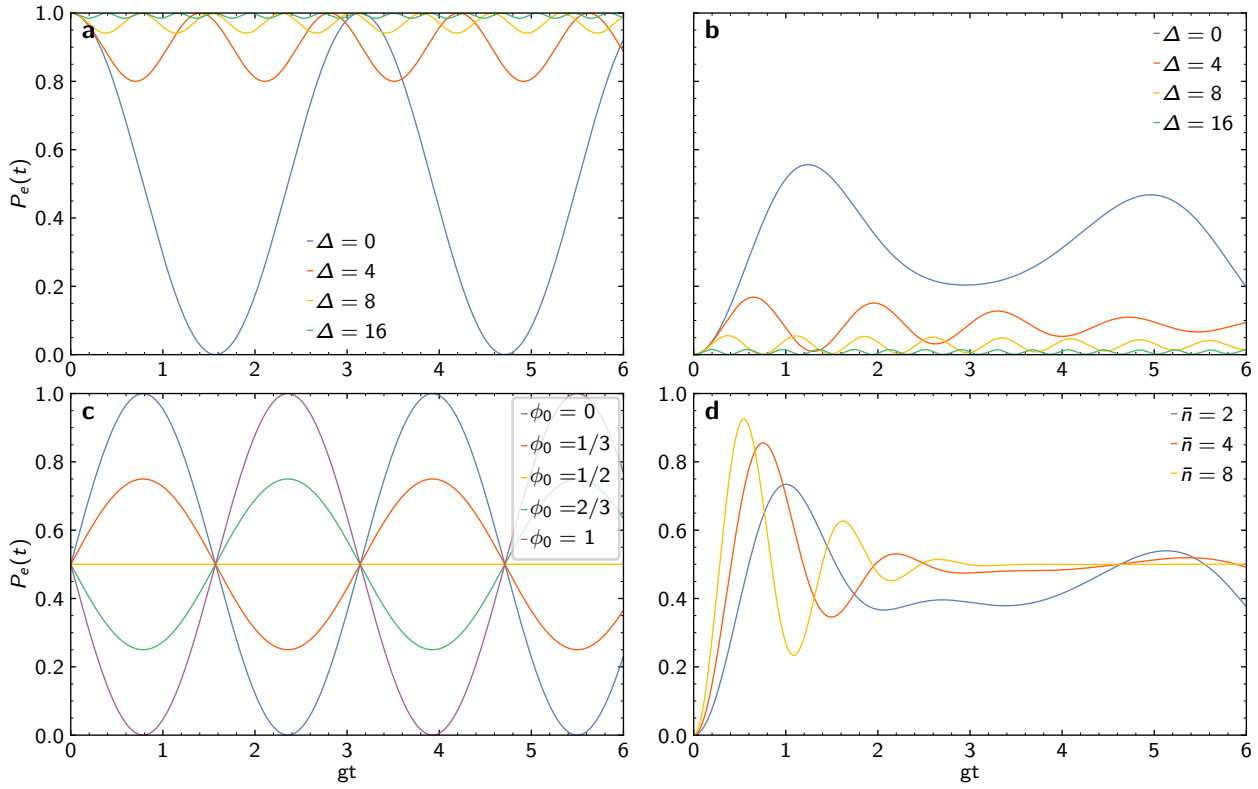

Fig. 5: Rabi oscillations for different detunings, and initial relative phase. **a** for a $n = 0$ photon state and an atom in the excited state and **b** for a coherent state with mean photon number $\bar{n} = 1$ and an atom initially in the ground state. The Rabi oscillations in case of the coherent photon state occur at a faster frequency, due to the admixture of higher photon number states. Since none of the photon numbers of the coherent state clearly dominates, the oscillation occurs at multiple frequencies simultaneously leading to a smaller amplitude compared to the Fock state. With increasing detuning the oscillation frequency is mainly determined by the detuning, thus the oscillations show less of the typical collapse behavior. **c** Rabi oscillations starting from state $1/\sqrt{2}(|g,1\rangle + \mathrm{e}^{i\pi(1/2+\phi_0)}\,|e,0\rangle)$. $\phi_0 = 0$ is the state in which the system would be found after exciting it from the ground state while continuously driving it for $t = \pi/(2\Omega_n)$. By preparing a state with no net phase difference no oscillatory behavior can be observed, all other phases represent intermediate oscillation amplitudes and whether an initial excitation or relaxation occurs. **d** Resonant Rabi oscillations for multi-photon coherent states, compared to **b** the time for a revival of the oscialltaion amplitude increases, whereas with increasing mean photon number the collapse occurs faster.

where $\Psi_{n-1}(t)$ is accounting for the now shifted zero point of energy. The ground state is $|g,n\rangle$, in which the system can be prepared to obtain an entirely coherent energy distribution. Note that the energy of state $\Psi_{n-1}(t)$, is energetically shifted with respect to $\Psi_{n-1}(t)$, which for $n = 0$ already contains one quantum of energy, which corresponds to the contribution of an $n = 1$ Fock state.

The modulation of the Rabi oscillation amplitude occurs due to the fact that all states simultaneously drive the atom, each component at frequency $\bar{\Omega}_n$. If the atom is not initially in a perfectly symmetric superposition $(|g,n+1\rangle + |e,n\rangle)/\sqrt{2}$ its oscillation amplitude will initially collapse. However for relatively low mean photon numbers of the coherent pulse $\bar{n}$ the main contribution, if the atom enters the cavity in the excited state, is the prepared Fock state of the atom, carrying exactly one quantum of energy. Thus the oscillation of the one photon component is strong compared to others,

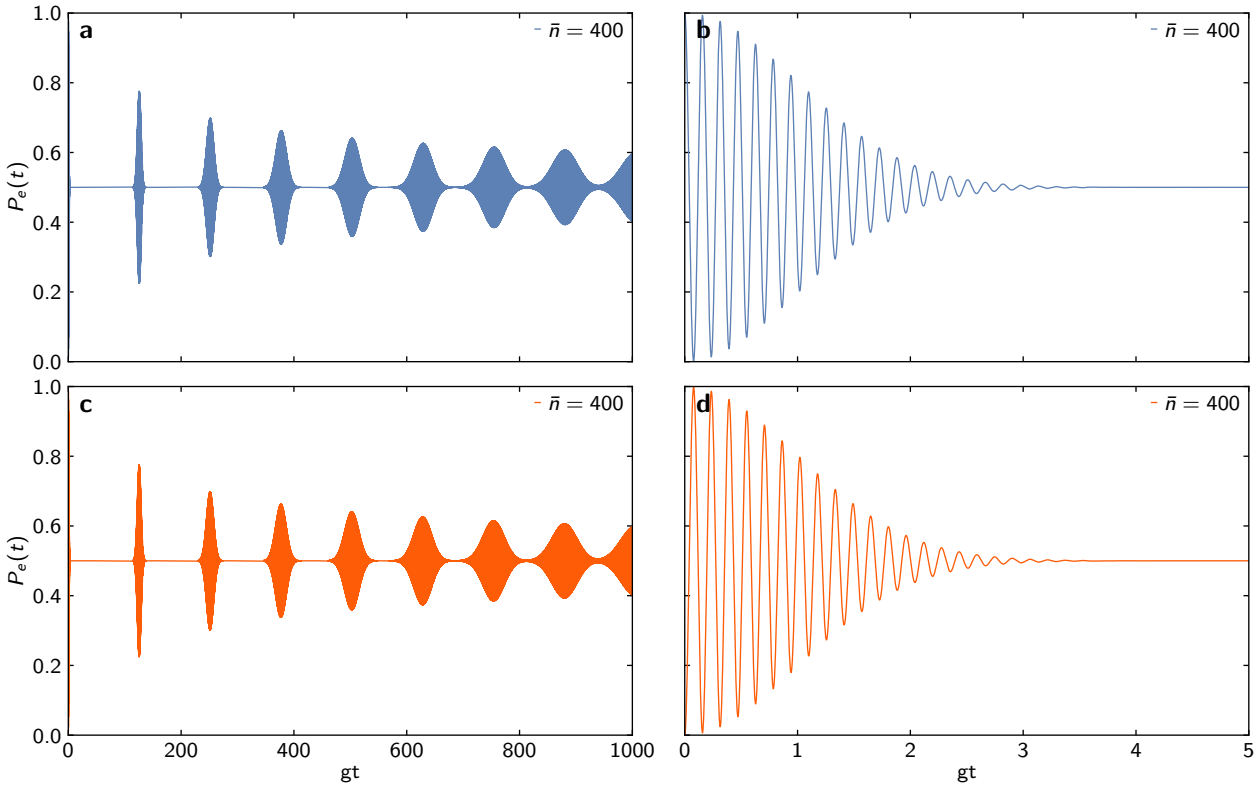

Fig. 6: Rabi oscillations on resonance for a coherent state with mean photon number $\bar{n} = 400$. The amplitude of the Rabi oscillations quickly collapses and stays minimal for a relatively long time, during which the oscillations are out of phase. Consequently the amplitude grows again and collapses multiple times. The behavior is simulated for an atom initially prepared in the excited state (**a** and **b**) and in the ground state (**c** and **d**). (**a** and **c**) show multiple revivals of the oscillation amplitude, while (**b** and **d**) show the initial collapse of the oscillation amplitude after preparing the atom at $t = 0$ in a definite state also showing that the collapse occurs over multiple oscillation periods. The modification of deterministically adding a significant one-photon component into the coherent state is mostly irrelevant for the overall oscillations.

whereas for higher mean photon numbers the effect is not significant anymore, as shown in Fig. 6. For relatively low photon numbers the time it takes for a revival of the oscillation amplitude is relatively short, since the number of oscillations that need to get back in phase is relatively small, cf. Fig. 5 and Fig. 6. Observing this collapse and revival for a coherent state of the photon field also provides direct evidence for the quantized nature of light, and concurrently provides evidence that the description of the coherent state of mean photon number $\bar{n}$ is correct by resolving the individual Fock state components [22]. Even though this model provides great inside into the quantum world, it will never be realized, or if it was realized it could not be measured, since the description of this systems relies on a perfectly isolated quantum system. Nonetheless many current implementations get incredibly close, however the preparation of the cavity field requires a coupling of the cavity to the environment, which will be discussed in the following.

3.2 Photons leaking from and into the cavity

Another effect of the cavity, besides changing the vacuum density of states, is a consequence of the vacuum rabi splitting of $|-,0\rangle$ and $|+,0\rangle$. If one wants to sends photons through the cavity e.g. on the red sideband $\omega_0 - g$, the cavity is resonant for a single photon occupying $|-,0\rangle$, the next photon wanting to enter the cavity will however be off resonant, due to the $\sqrt{n}$ scaling of the energy levels and is thus not be able to enter the cavity [63, 64]. The cavity transmission then shows antibunched photon statistics no matter what the input field is. This effect can only be observed for an imperfect cavity. The cavity mode must decay, otherwise there will be no leakage in either direction - in or out of the cavity. For a superconducting microwave cavity the finesse, i.e. the number of round trips a photon can take inside the cavity before decaying to the outside, can reach values of $4 * 10^9$, corresponding to a photon lifetime of 130 ms [26]. Refining the Jaynes-Cummings model such that light leaking from or into the cavity can be described requires an outside field to couple to the field operators of the cavity mode. The coupling strength shall be called κ, it describes the interaction strength of a external field with the internal cavity mode.

For simplicity the cavity, shall be assumed to be a one-sided cavity. This means one side of the cavity is a perfect conductor, i.e. $r = 1$, while the other side's reflection is $\tilde{r} < 1$. Starting from the Hamiltonian for two coupled one-sided cavities, the field expected inside a cavity while driven with a classical field will be derived, eventually resulting in the master equation of a decaying cavity field coupled to a two-level system. In the rotating frame and applying the slowly varying envelope approximation, such that the coupling can be treated as small perturbation to the isolated cavity modes, the Hamiltonian is given by [56]

$$H = \hbar\omega_1\Big(a_1^\dagger a_1 + \frac{1}{2}\Big) + \hbar\omega_2\Big(a_2^\dagger a_2 + \frac{1}{2}\Big) + \hbar g\Big(a_1 a_2^\dagger + a_2 a_1^\dagger\Big), \tag{42}$$

where the two cavities are denoted by the respective indices. The coupling strength is $g = ct/(2\sqrt{L_1 L_2})$, with c the speed of light in the cavity, $t \in \mathbb{R}$ the transmission between the two cavities and L_i the length of cavity i. By switching to the interaction picture with respect to cavity 2, the uncoupled Hamiltonian reduces to

$$H_0 = \hbar\omega_1\Big(a_1^\dagger a_1 + \frac{1}{2}\Big). \tag{43}$$

Assuming to have a coherent state in cavity 1, which is the equivalent to an incoming coherent laser field, with appropriate phase, incident on cavity 2. This results in the interaction

$$H_{12} = \hbar\mathcal{E}\left(a_1\,\mathrm{e}^{i\omega_2 t} + a_1^\dagger\,\mathrm{e}^{-i\omega_2 t}\right), \tag{44}$$

where $\mathcal{E} = \alpha g$ is the driving amplitude associated with an incident coherent field of amplitude $\alpha \in \mathbb{R}$ by properly choosing the phase of the incident field. Now one can relate the driving rate of the incident field and the cavity decay to find a coupling strength of any coherent input field. The cavity loss $\kappa_{cav,1} = t^2/\tau_1$ corresponds to the probability of losing a photon per round trip time in the cavity $\tau_1 = 2L_1/c$. The coupling strength for a resonant field reads

$$\mathcal{E} = \sqrt{\frac{\kappa P}{\hbar\omega}}, \tag{45}$$

where P is the incident power. Note that the description of a classical field is valid for a coherent state of arbitrary mean photon number [65].

In order to find the coupling strength to not only a mode matched incident field, but all vacuum modes, cavity 2 is assumed to be a multimode cavity. The interaction part of the Hamiltonian thus reads

$$H_{int} = \hbar \sum_q g_q \left(a_1 a_{2,q}^\dagger + a_1^\dagger a_{2,q} \right). \tag{46}$$

If the cavity length is further expanded, at some point the mode spectrum is very dense, thus the sum describing the coupling to different modes can be replaced by an integral, describing the coupling to a continuum of (non-degenerate) modes. Renaming the operators of the cavity to a and $a^\dagger$ and the operators of the continuum or bath to $b(\omega)$ and $b^\dagger(\omega)$ the interaction Hamiltonian yields

$$H_{int} = \frac{\hbar}{\sqrt{2\pi}} \int_0^\infty \mathrm{d}\omega \sqrt{\kappa(\omega)} \left(a b^\dagger(\omega) + a^\dagger b(\omega) \right). \tag{47}$$

The creation and annihilation operators of the bath fulfill the bosonic commutation relations

$$\left[b(\omega), b^\dagger(\omega') \right] = \delta(\omega - \omega'). \tag{48}$$

Now abstracting a little further from the previous example, and redefining the total Hamiltonian of the entire *laboratory* by splitting it into three parts, the system under consideration H_{sys}, the bath H_B and the coupling described by H_{int}. The system now does not necessarily need to be a cavity but can be any system described by some set of operators. For clarity the operator c is one of several possible system operators coupling the system to a bosonic bath, e.g. the modes of the free electromagnetic field. The total Hamiltonian and its contributions read

$$H = H_{sys} + H_B + H_{int} \tag{49}$$

$$H_B = \hbar \int_{-\infty}^\infty \mathrm{d}\omega \omega b^\dagger(\omega) b(\omega) \tag{50}$$

$$H_{int} = \frac{\hbar}{\sqrt{2\pi}} \int_{-\infty}^\infty \mathrm{d}\omega \sqrt{\kappa(\omega)} \left(c b^\dagger(\omega) + c^\dagger b(\omega) \right). \tag{51}$$

Eq. 50 and Eq. 51 are idealized since the integration in principle would only span $[0, \infty)$. However after transforming into a system rotating at the transition frequency ω_t, which is mostly large compared to the systems bandwidth, the integral spans $[-\omega_t, \infty)$ [66]. With the assumption of a finite bandwidth it can be justified to then further expand the lower bound of integration to $-\infty$. The equations of motion for any system operator a and the bath operator b can be found by solving the Heisenberg equation of motion,

$$\partial_t a = \frac{i}{\hbar} [H, a] = \frac{i}{\hbar} [H_{sys}, a] + i \int_{-\infty}^\infty \mathrm{d}\omega \sqrt{\frac{\kappa(\omega)}{2\pi}} b^\dagger(\omega) [c, a] + [c^\dagger, a] b(\omega) \tag{52}$$

$$\partial_t b(\omega) = \underbrace{\frac{i}{\hbar} [H_{sys}, b]}_{=0} - i\omega b(\omega) - i \sqrt{\frac{\kappa(\omega)}{2\pi}} c. \tag{53}$$

Eq. 53 can be formally integrated from an initial time $t_0 \leq t$ to t which results in

$$b(\omega) = b_0(\omega)\, \mathrm{e}^{-i\omega(t-t_0)} - i \sqrt{\frac{\kappa(\omega)}{2\pi}} \int_{t_0}^t \mathrm{d}t'\, \mathrm{e}^{-i\omega(t-t')}\, c(t'), \tag{54}$$

where $b_0(\omega)$ corresponds to the value of $\underline{(}\omega)$ at $t = t_0$. Substituting Eq. 54 in Eq. 52 and explicitly stating the time dependencies gives

$$\begin{aligned}\partial_t a =& \frac{i}{\hbar}[H_{sys}, a(t)] \\ &+ i\int_{-\infty}^{\infty} \mathrm{d}\omega \sqrt{\frac{\kappa(\omega)}{2\pi}} \left(b_0^\dagger(\omega)\, \mathrm{e}^{i\omega(t-t_0)}[c(t), a(t)] + [c^\dagger(t), a(t)] b_0(\omega)\, \mathrm{e}^{-i\omega(t-t_0)} \right) \\ &- \int_{-\infty}^{\infty} \mathrm{d}\omega \frac{\kappa(\omega)}{2\pi} \int_{t_0}^{t} \mathrm{d}t' \left(\mathrm{e}^{i\omega(t-t')}\, c^\dagger(t')[c(t), a(t)] - [c^\dagger(t), a(t)]\, \mathrm{e}^{-i\omega(t-t')}\, c(t') \right).\end{aligned} \tag{55}$$

At this point the evolution of the system depends on the exact history of the bath described by $b(\omega)$, which is linked to the coupling to the system $\kappa(\omega)$. By making the dynamics Markovian, i.e. [56, 66, 67]

$$\kappa(\omega) = \kappa, \tag{56}$$

all bath modes couple equally to the system operator and the integrals can be solved. The system is subject to *white quantum noise*, since the spectrum of the bath system interaction is flat. Defining an input field $b_{in}(t)$ and using the relations

$$b_{in}(t) = \frac{1}{\sqrt{2\pi}} \int_{-\infty}^{\infty} \mathrm{d}\omega b_0(\omega)\, \mathrm{e}^{-i\omega(t-t_0)} \tag{57}$$

$$\int_{-\infty}^{\infty} \mathrm{d}\omega\, \mathrm{e}^{-i\omega(t-t')} = 2\pi\delta(t-t') \tag{58}$$

$$\int_{t_0}^{t} \mathrm{d}t' c(t')\delta(t-t') = \frac{1}{2}c(t), \tag{59}$$

$\partial_t a(t)$ can be calculated since the bath and system are not related at different times. Note that Eq. 59 is not well defined, since the bound of integration is exactly the pole of the δ-function, heuristically it is reasonable, if $\delta(x)$ is symmetric, half of its weight is within the bounds of integration. With the use of Eq. 57, Eq. 59 and Eq. 58 while applying the Markov approximation one finds the *quantum Langevin equation*

$$\partial_t a = \frac{i}{\hbar}[H_{sys}, a(t)] - \left\{ [a(t), c^\dagger(t)] \left(\frac{\kappa}{2} c(t) + i\sqrt{\kappa} b_{in}(t) \right) - \left(\frac{\kappa}{2} c^\dagger(t) - i\sqrt{\kappa} b_{in}^\dagger(t) \right) [a(t), c(t)] \right\}. \tag{60}$$

Eq. 60 relates the state of the system to the input field, however if the field of interest is the field emitted from the system, one can simply redefine the solution found for $b(\omega)$ for $t < t_1$, such that

$$b(\omega) = b_1(\omega)\, \mathrm{e}^{-i\omega(t-t_1)} + i\sqrt{\frac{\kappa(\omega)}{2\pi}} \int_{t}^{t_1} \mathrm{d}t'\, \mathrm{e}^{-i\omega(t-t')}\, c(t'). \tag{61}$$

gives the time evolution of the bath for all future times, the outgoing field can be defined as

$$b_{out}(t) = \frac{1}{\sqrt{2\pi}} \int_{-\infty}^{\infty} \mathrm{d}\omega b_1(\omega)\, \mathrm{e}^{-i\omega(t-t_1)}\,. \tag{62}$$

The same procedure then leads to the *time-reversed* quantum Langevin equation, relating the dynamics of the system to the outgoing field, which reads

$$\partial_t a = \frac{i}{\hbar}[H_{sys}, a(t)] - \left\{ [a(t), c^\dagger(t)] \left(-\frac{\kappa}{2} c(t) + i\sqrt{\kappa} b_{out}(t) \right) - \left(-\frac{\kappa}{2} c^\dagger(t) - i\sqrt{\kappa} b_{out}^\dagger(t) \right) [a(t), c(t)] \right\}. \tag{63}$$

Combining Eq. 54 and Eq. 3.2 and integrating out the frequency behavior using the above definitions it follows

$$b_{out}(t) - b_{in}(t) = -i\sqrt{\kappa}c(t). \tag{64}$$

Eq. 64 allows for the calculation of the output-field, if the dynamics of the system $c(t)$ under the influence of the input field $b_{in}(t)$ are known. Returning to the above example of a cavity, or equivalently a harmonic oscillator, coupled to a continuum of modes, the equation of motion for the annihilation operator reads

$$\partial_t a = -i\omega_0 a - \frac{\kappa}{2}a - i\sqrt{\kappa}b_{in}(t). \tag{65}$$

Already from Eq. 60 follows, that the system is damped, independent of the driving field $b_{in}(\omega)$ and specific system.

To illustrate the solution of Eq. 60 for a simple system the Jaynes-Cummings model coupled to a bath shall be considered. The system then consists of an atom in a single mode cavity, described by Eq. 22, and the field operators a and a_k coupled to a bath. In order to write the equations in a more compact form, the previously defined operators from Eq. 24 are now expressed as spin matrices with the commutation relations

$$\sigma = |g\rangle\langle e| \qquad \sigma_z = |e\rangle\langle e| - |g\rangle\langle g| \tag{66}$$

$$\sigma_z = [\sigma^\dagger, \sigma] \qquad 2\sigma = [\sigma, \sigma_z]. \tag{67}$$

The most interesting quantities are then again, the number of photons in the cavity and the probability of being in the excited state. Furthermore one would be interested in the in- and output of the system, however the system may not be analytically solvable. The equation of motion for the operators of interest read, for simplicity time dependencies are not stated,

$$\partial_t(a^\dagger a) = ig(\sigma^\dagger a - a^\dagger\sigma) - \kappa a^\dagger a - i\sqrt{\kappa}(a^\dagger b_{in} - b_{in}^\dagger a) \tag{68}$$

$$\partial_t(\sigma^\dagger\sigma) = -ig(\sigma^\dagger a - a^\dagger\sigma). \tag{69}$$

To form a closed system, the equations of motion for more operators are needed, namely

$$\partial_t(\sigma^\dagger a) = i\omega_0\sigma^\dagger a - i\omega\sigma^\dagger a - ig(a^\dagger\sigma_z a + \sigma^\dagger\sigma) - \frac{\kappa}{2}\sigma^\dagger a - i\sqrt{\kappa}\sigma^\dagger b_{in} \tag{70}$$

$$\partial_t(a^\dagger\sigma_z a) = -ig(\sigma^\dagger a - a^\dagger\sigma) - 2ig(\sigma^\dagger a^\dagger a^2 - \sigma(a^\dagger)^2 a) - \kappa a^\dagger\sigma_z - i\sqrt{\kappa}\sigma_z(b_{in}a^\dagger - b_{in}^\dagger a), \tag{71}$$

which again require the equation of motion for further operators. Finally solving the full Jaynes-Cummings Hamiltonian while including the bosonic environment requires an infinite set of equations. Eq. 71 e.g. requires the time evolution of $\sigma^\dagger a^\dagger a^2$ and $\sigma(a^\dagger)^2 a$, which would then in turn further expand the amount of operators needed. Nevertheless the system can be solved in a simple case. The environment is assumed to be at zero temperature, i.e. $b_{in}(t) = 0$, therefore the bath creates no photons in the cavity. Furthermore the atom is in the excited state while the cavity is initially empty or alternatively the cavity is in a $n = 1$ Fock state, while the atom is in the ground state at $t = t_0$. In these two specific scenarios any operator quadratic in either the cavity annihilation or creation operator will not contribute and can thus be omitted, such as ($\sigma^\dagger a^\dagger a^2$ and $\sigma(a^\dagger)^2 a$ in Eq. 71. The system can then be analytically solved [68], the solution of the expectation values is depicted in Fig. 7. The excited state still shows oscillatory behavior for small damping $g/\kappa = 10$, is strongly damped for intermediate damping ($g = \kappa$) and enters the overdamped case ($g/\kappa = 0.1$), in which the

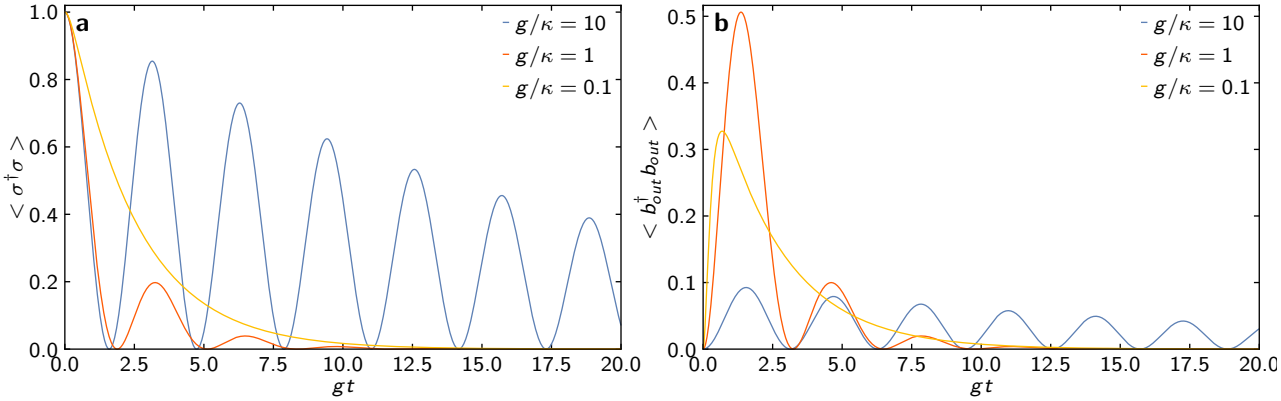

Fig. 7: Single two-level atom in a leaking cavity field for an initially excited atom. **a** Expectation value of the atomic population in the excited state. Depending on the coupling strength of the cavity to the bath, the system exhibits oscillatory behavior over several periods for small photon leakage, eventually leading to an overdamped case, in which the atom and cavity both directly transit to the ground state without oscillating. If the system enters the overdamped regime the excited state exhibits an exponential decay with rate $-4g^2/\kappa$. **b** Outgoing Fock state wave function of the photon leaving the cavity. The atomic behavior essentially dictates the behavior of the outgoing photon.

system settles to its ground state before any oscillation occurs. Utilizing Eq. 64 and the fact that there is no input field, one can find the output of the system to be

$$b_{out}^\dagger b_{out} = \kappa a^\dagger a. \tag{72}$$

To further analyze the system including multiple photons, while later also being able to include a coherent input field, in the following the dynamics will be investigated using a density matrix approach, which in turn is equivalent to the previous description for certain fields [66, 69]. For simplicity the bath or environment of the system will again be assumed to be at zero temperature, thus effects resulting from photons occupying the bath modes, such as stimulated emission and absorption can be safely neglected. The restriction to zero temperature becomes less stringent, if the level spacing of the system is in the optical regime, since even for ambient temperatures the mean photon number due to black body radiation is negligible. The refinement to a coherent input field enables the simple description of the driving field by a constant $\mathbb{C}$-number [65]. The equation of motion for the density matrix is given by

$$\partial_t \rho = \frac{i}{\hbar}[\rho, H_{sys}] + \gamma \mathcal{L}(a)\rho \tag{73}$$

where $\mathcal{L}(a)\rho$ is the Lindblad super-operator for any collapse operator a describing the irreversible coupling of the system to a bath

$$\mathcal{L}(a)\rho = a\rho a^\dagger - \frac{1}{2}\left(a^\dagger a\rho + \rho a^\dagger a\right). \tag{74}$$

To efficiently use the Lindblad master equation and its solution, only a finite set of photon number states of the cavity is taken into account. Relatively low photon numbers in the coherent state require only a small number of Fock states that effectively contribute to the dynamics. The system now is

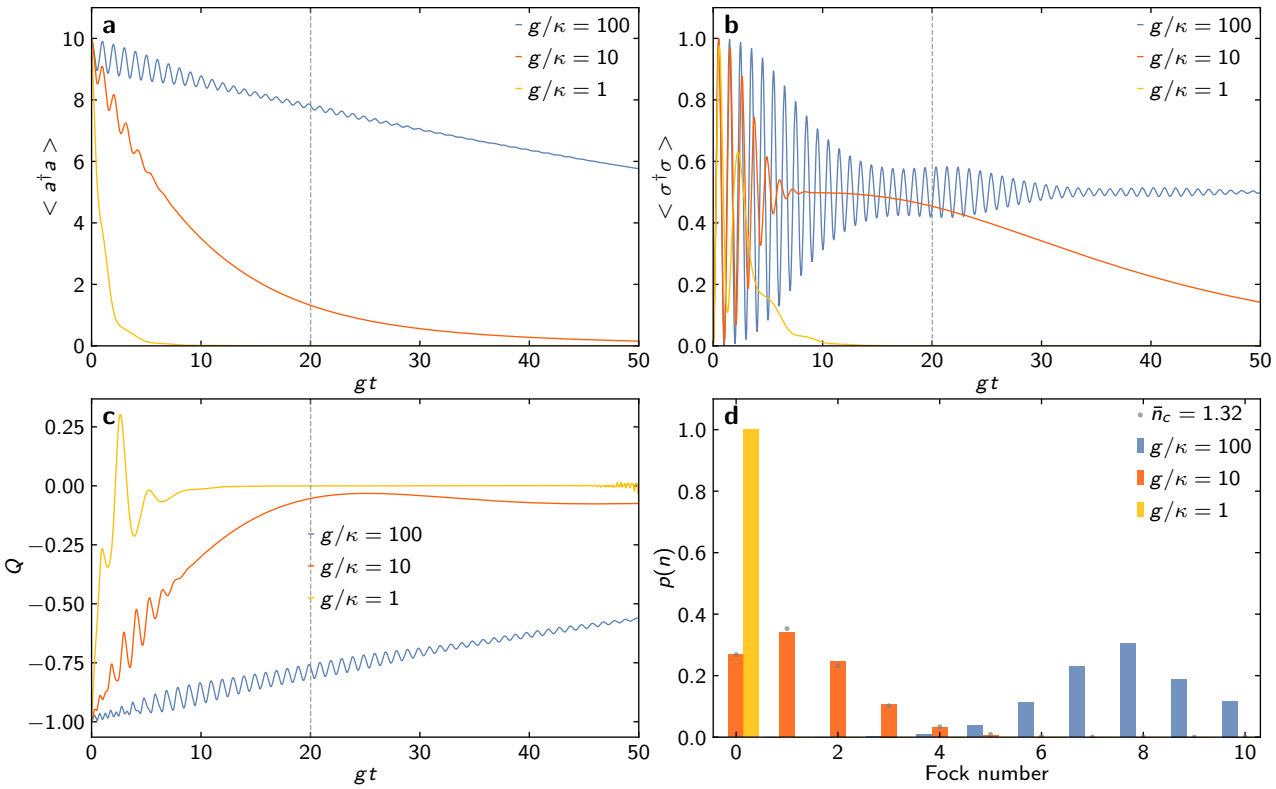

Fig. 8: Leaking cavity initially prepared in a $n = 10$ photon Fock state and an atom in its ground state without driving field. **a** Expectation value of the photon number for different cavity damping rates. The atom interacts with the cavity field such that it rearranges the photons in time by absorbing and stimulated emitting it into the cavity again. Thus the modulation of the mean value is maximally altered by ± 1. **b** Probability of finding the atom in its excited state. Depending on the damping of the cavity field the atom exhibits different behavior. Essentially the characteristic of the oscillation changes, exhibiting revivals for small enough damping, which suggests a broadened photon distribution. **c** Mandel Q parameter of the cavity field. The cavity field initially in a Fock state acquires larger variance for, similar to a coherent state as it decays. **d** Number state distribution of the cavity field. The gray dashed line in **a-c** indicates the position at which the distribution is depicted. The gray points correspond to a coherent state with mean photon number $\bar{n} = 1.32$, the mean photon number of $g/\kappa = 10$ at $gt = 20$.

assumed to be prepared as follows, the atom is initially in its ground state, the cavity is also in a well defined state and the cavity field is resonant to the atom. The system Hamiltonian in this case is again given by the Jaynes-Cummings Hamiltonian in Eq. 22. The damping term already significantly modifies the dynamics, first it provides damping to the overall oscillation amplitude and if the cavity decay is big enough prevents revivals for a coherent state, because the cavity field decays before the oscillations get back in phase. Secondly an initial Fock state of the decays towards a coherent state with reduced mean photon number (cf. Fig. 8). The character of the photonic state can be determined with the aid of the Mandel Q parameter

$$Q = \frac{< (a^\dagger a)^2 > - < a^\dagger a >^2}{< a^\dagger a >} - 1, \tag{75}$$

measuring the deviation from a Poisson distribution. If the photonic state is a coherent state, i.e. Possoin distributed, the Mandel Q parameter $Q = 0$, whereas $Q = 1$ for Fock states. The Mandel Q parameter could also be replaced by measuring the variance of the distribution yet it is a convenient

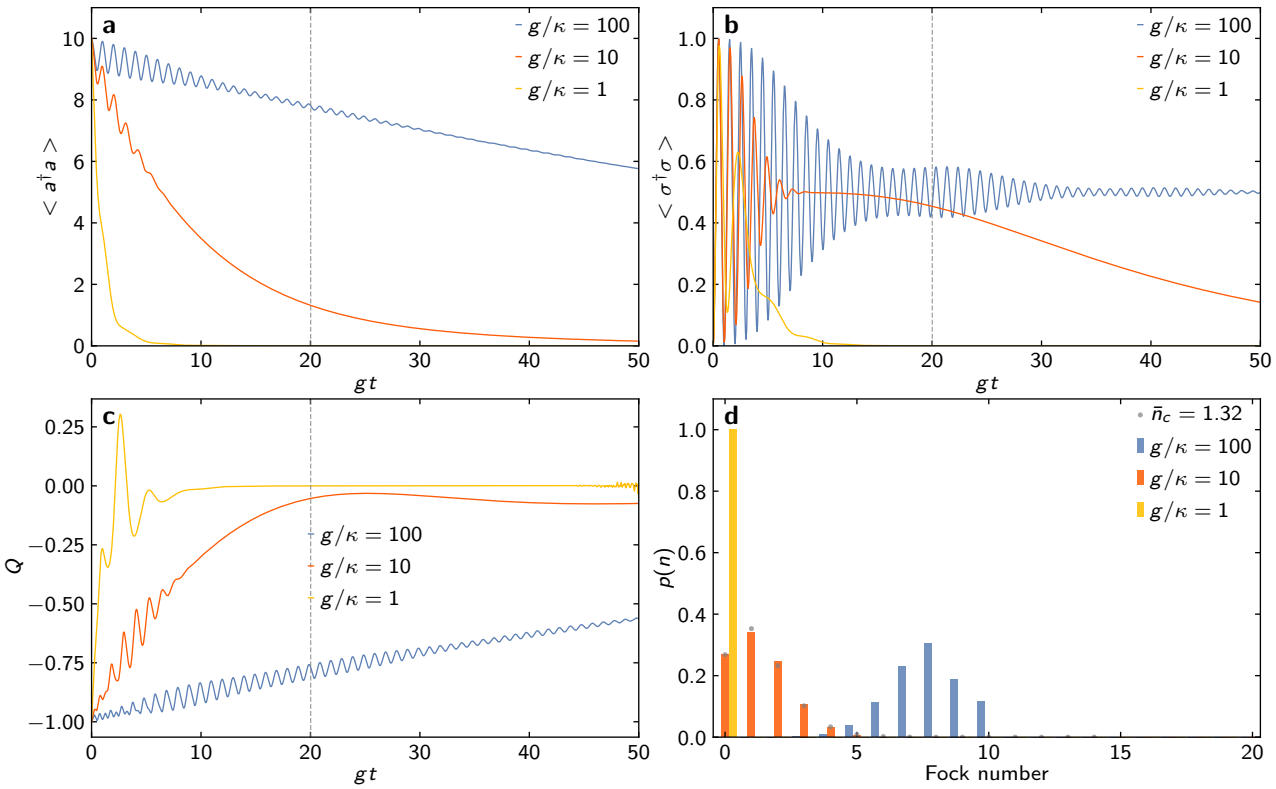

Fig. 9: Leaking cavity initially prepared in a $\bar{n} = 10$ coherent state and an atom in its ground state without driving field. **a** Expectation value of the photon number for different cavity damping rates. The atom modifies the cavity field such that it initially drives the system between the adjacent state $\bar{n} = 9$, by simultaneously absorbing and stimulated emitting a photon of the cavity field. This happens while all oscillations of different n are not fully interfering. **b** Probability of finding the atom in its excited state. Depending on the damping of the cavity field the atomic oscillation shows revivals. **c** Mandel Q parameter of the cavity field. The cavity field initially in a coherent state shows a periodic modulation form sub- to super-Possoinian statistics, as the photon is absorbed and re-emitted **d** Number state distribution of the cavity field. The gray dashed line in **a**,**b**,**c** indicates the position at which the distribution is depicted. The gray points correspond to a coherent state with mean photon number $\bar{n} = 1.32$, the mean photon number of $g/\kappa = 20$ at $gt = 20$.

measure.

The expectation values for an operator B in an ensemble described by a density matrix $\rho(t)$, is given by

$$< B(t) > = \mathrm{Tr}[\rho(t)B]. \tag{76}$$

If one is only interested in one subsystem the other subsystem can be traced out, e.g. $\rho_C(t) = \mathrm{Tr}_A[\rho(t)]$ and conversely $\rho_A(t) = \mathrm{Tr}_C[\rho(t)]$. Tr_A and Tr_C denote the partial trace over the atomic part respective cavity part of the total density matrix. The expectation value of the operators C being an operator acting only on the cavity and A, an atom operator are determined by the evolution of the individual subsystem are then also determined by the subsystems density matrix,

$$< C(t) > = \mathrm{Tr}_C[\rho_C(t)C] \qquad < A(t) > = \mathrm{Tr}_A[\rho_A(t)A]. \tag{77}$$

A system without losses can simply be described with the Schrödinger equation and does not show the full capability of this approach. By including a driving term, in principle the system would need

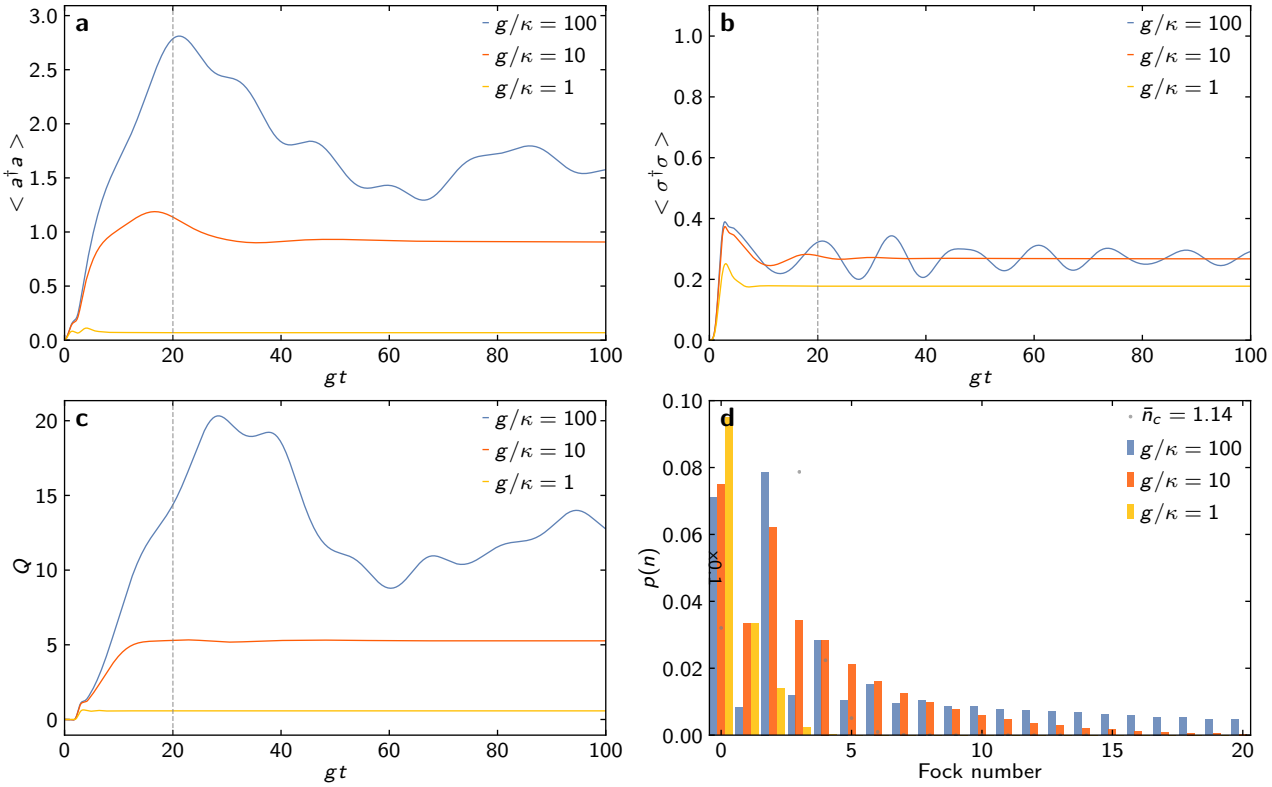

Fig. 10: Driven atom-cavity system initially in its ground state for a driving strength of $g/\eta = 2.5$. **a** Expectation value of the photon number in the cavity mode. The driving field is instantaneously switched on at $t_0 = 0$, after which the photon number quickly rises and depending on the strength of the damping quickly settles towards its steady state value, or undergoes multiple oscillations. **b** The initial built up of the cavity field results in an initial excitation probability of the atom above the steady state value. For $g/\kappa = 100$ the steady state is not reached with in the depicted range. **c** The Mandel Q parameter $Q \geq 0$, indicating a super-Possoinian photon distribution. **d** Photon distribution of the cavity field after $gt = 20$ indicated by the gray dashed line in **a-c**. All three scenarios show a significantly broadened photon distribution. For $g/\kappa = 10$ the mean photon number of $< a^\dagger a >= 1.14$ is depicted alongside a coherent distribution with the same mean photon number to illustrate the significant deviation. The $n = 0$ contribution is scaled by a factor of 0.1.

to be expanded, to also describe the evolution of the driving field. If one is only interested in the system that the field is driving, the part of the density matrix describing the driving field can be simply traced out and only the evolution of the system needs to be calculated.

The dynamics for a $n = 10$ photon Fock state in a decaying cavity are depicted in Fig. 8.

The dynamics of a coherent state in the cavity are depicted in Fig. 9. Essentially the dynamics of the coherent and number state case show similarities, such as the revival for small enough damping, but also a significant difference, where the initial collapse occurs on a much faster time scale, cf. Fig. 9.

In the next approach to the atom cavity system a driving field will be introduced, which only the cavity field is coupling to, while the interaction of the driving field with the atom will be neglected. The Hamiltonian is now made up of the Jaynes-Cummings Hamiltonian and an additional driving

field coupling to the cavity operators

$$H_{sys} = H_{JC} + \hbar \left(\Omega^\dagger(t) a(t) + a^\dagger(t) \Omega(t) \right). \tag{78}$$

The atom and cavity are initially both prepared in their respective ground state, while coherent, resonant laser light is incident on the cavity. This means, that the detuning between the driving field at angular frequency ω_L and the atom $\Delta_L = \omega_L - \omega_0$, as well as the cavity field $\Delta_C = \omega_L - \omega_0$ shall vanish, $\Delta_A = \Delta_C = 0$. The effects resulting from the interaction with the atom-cavity system on the driving field will not be considered, since the majority of photons in an experiment will be reflected from the cavity and only a small fraction of photons actually enters the cavity. Additionally the $\sqrt{n}$ scaling renders the excited states off resonant. Thus the modifications resulting from photons entering and leaving the cavity will be negligibly small. The driving field is assumed to be instantaneously turned on at $t = 0$, thus its envelope is given by $\Omega(t) = \Theta(t)\eta$, where $\Theta(t)$ is the unit step function with $\Theta(t \geq) = 1$ and zero for $t < 0$. In case of weak damping the system redistributes the photons to a state of super Possoinian variance, whereas the strongly damped systems assimilate to a distribution peaked at $n = 0$ similar to a thermal state.

Since the description so far relied on a *good* cavity, meaning that there always was only a single mode present, with varying leakage out of the cavity which hosted a perfect atom, which did not decay or decohere to any other channel. The atom will be treated in a more realistic fashion in the following.

3.3 2+1 level system interacting with a driven cavity

In the previous chapter the interaction of the cavity field with a bosonic environment, or more concrete the electromagnetic modes of free space, was included in the description of the Jaynes-Cummings model. Now the model will be further refined by including also the interaction of the two-level system inside the cavity with a bosonic bath. This interaction arises due to the fact that a cavity larger than the fundamental wavelength of the system still allows for spontaneous emission into other modes. Or to give a more intuitive picture, into the transverse direction of the non closed cavity. Thus it is possible to, in principle, drive either the cavity or the atom with an external field. With slight modifications to the Hamiltonian, which will not be performed here, it is possible to transform the solution of either system to the respective other [70]. In the following the driving field will only couple to the cavity field.

The system under consideration here will now first be described by a two-plus-one level system, where two levels are resonantly coupled by a cavity field and a third level is a dark state decoupled from the cavity field. The dynamics of the dark state $|D\rangle$ is described by a spontaneous dephasing from the excited state $|W\rangle$ with rate γ and subsequent spontaneous emission with rate Γ back to the ground state $|G\rangle$. The excited state $|W\rangle$ will also decay spontaneously with rate Γ back to the ground state. The aforementioned spontaneous processes are again described by Lindblad super-operators. The driving field is a coherent field resonant to the cavity and atom. The full master equation then reads

$$\begin{aligned} \partial_t \rho(t) =& \frac{1}{i\hbar} [\hbar g (a^\dagger \sigma_{GW} + a \sigma_{GW}^\dagger) + \hbar \Omega(t)(a^\dagger + a), \rho(t)] \\ &+ \gamma \mathcal{L}(\sigma_{DW}) \rho(t) \\ &+ \Gamma \left(\mathcal{L}(\sigma_{GW}) \rho(t) + \mathcal{L}(\sigma_{GD}) \rho(t) \right), \end{aligned} \tag{79}$$

with the transition matrices $\sigma_{ij} = |i\rangle\langle j|$. The decoupling of the atom, after being dephased into the decoupled dark state, results in a driven cavity system, in which the number of photons in the cavity grows fast compared to a coupled system. This underlines the photon blockade effect due to the $\sqrt{(n)}$ scaling of the energy separation between the individual dressed levels. If the atom is decoupled, the system is resonant for any photon number which thus increases to relatively high numbers, which is hard to calculate numerically.

In this context it is also interesting to consider the interaction strength relative to the decoherence and decay rates. The system without the dephasing to the uncoupled dark state can be roughly categorized into four regimes [71], the weak coupling regime $g \ll \Gamma, \kappa$, where the modified mode structure in the cavity enhances spontaneous emission known as the Purcell effect [18, 72]. If the coupling strength exceeds all decay rates and the rotating wave approximation still holds $\Gamma, \kappa \ll g \ll \min\{\omega, \omega_0\}$, the system enters the strong coupling regime, where the description by the Jaynes-Cummings model is valid [47, 54, 58]. Further increasing the coupling strength to $g \lesssim \omega_0$ puts the system in the ultra-strong coupling regime, where the rotating wave approximation breaks down which is accessible in state of the art experiments [73, 74]. Further increasing the coupling strength to $g \gtrsim \omega_0$ puts the system in the deep ultra-strong coupling regime which is close to being fully accessible [74], where the physics again change such that counter intuitive effects occur, e.g. the Purcell effect breaks down again [75–77].

Since the latter mentioned regimes are very hard to access or not yet fully accessible, and since the previous discussion was also following the regime, where the rotating wave approximation was valid, the further discussion will assume a system, with appropriate level structure such that the rotating wave approximation remains valid. The dynamics for a system with additional decay of the excited state but without dephasing and decoupling is not significantly different compared to the results depicted in Fig. 8 and Fig. 9. For reference in Fig. 11 the dynamics of a $\bar{n} = 10$ photon coherent and $n = 10$ Fock state are depicted for various decay rates of the excited state, while the cavity is not driven. For low damping rates the system still resides in the strong coupling regime. With increasing decay rate it transits to the weak coupling regime, where a cavity initially prepared in a coherent

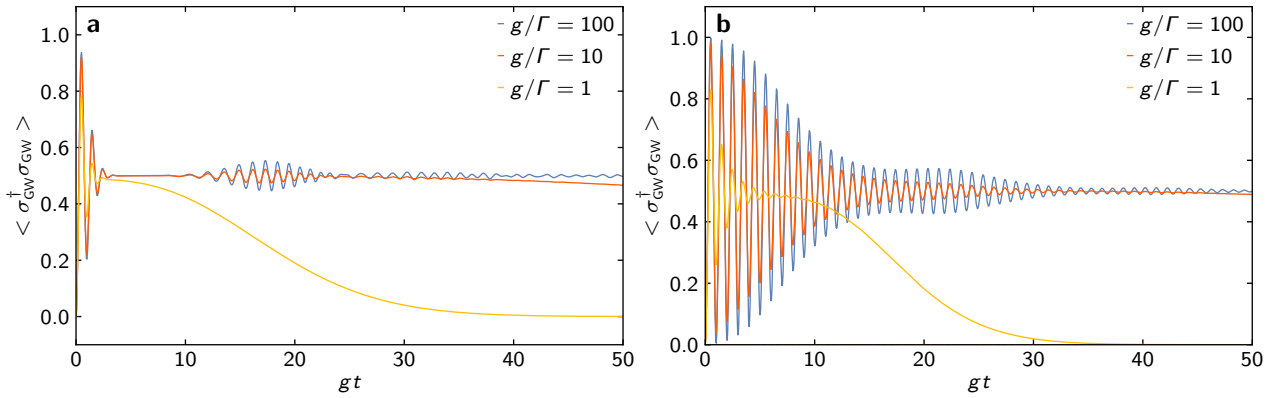

Fig. 11: Spontaneously emitting atom in a weakly damped cavity ($g/\kappa = 100$. **a** The cavity is initially in a $\bar{n} = 10$ photon coherent state, resulting in a fast collapse of the initial oscillation amplitude between the ground $|G\rangle$ and excited state $|W\rangle$ without dephasing to a dark state. **b** $n = 10$ photon Fock state leading to a decaying amplitude exhibiting some revivals for small dampings. The decay of the excited state amplitude in the case of strong damping is faster for a Fock compared to a coherent state, since the coherent state exhibits contributions from $n > 10$.

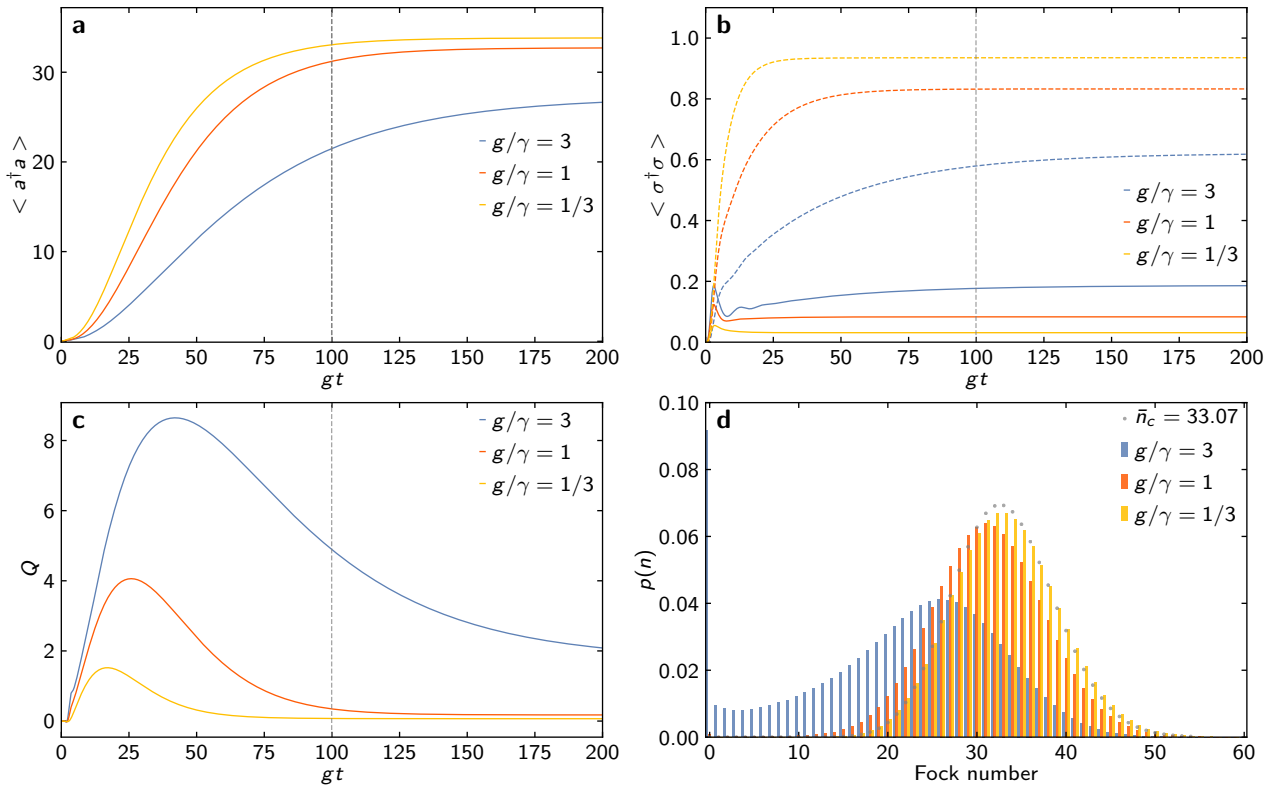

Fig. 12: Driven 2+1 level atom in a cavity for various dephasing rates into the dark state with $g/\kappa = 10$, $g/\Gamma = 10$ $g/\eta = 3$. **a** Expectation value of the photon number inside the cavity. With increasing dephasing rate the system decouples faster thus reaching an equilibrium between cavity pumping and decay on a faster time scale. **b** Expectation value of the $|W\rangle$ interacting bright state (solid line) and the decoupled dark state $|D\rangle$ (dashed line). For low enough dephasing the cavity and the atom initially show damped oscillations, which eventually are damped out due to decoupling, when a significant fraction populates the dark state. **c** Mandel-Q parameter of the cavity field. The initial vacuum state equilibrates to a coherent state, if the atom prevents the $\sqrt{n}$ scaling fast enough. The remaining excited state probability for the lowest dephasing still exhibits super Possoinian statistics. **d** Photon distribution after $gt = 100$ indicated by the gray dashed line in **a**-**c**. The decoupled system shows no significant deviation from a coherent state for $\kappa/\gamma = 1/3$.

stated shows no revivals of the oscillation amplitude in the excited state. The time scale of the decay compared to Fig. 8 and Fig. 9 are shorter, since Γ is a decay term additionally to $g = 100\kappa$.

In contrast to the aforementioned scenarios, where the system interacting with the cavity cannot decouple from the cavity field, the additional dark state provides a transition from the dressed states of the strongly interacting system to a driven cavity hosting an excited atom without any interactions with the cavity. This removes the $\sqrt{n}$ level spacing thus rendering all levels of the cavity resonant to the driving field and results in a coherent state of the cavity in steady state since the input field obeys the Possoinian statistics of a coherent driving field.

In the absence of dephasing and spontaneous emission, the time averaged value of finding the atom in the light-coupled excited state $< \sigma^\dagger_{GW} \sigma_{GW} >= 0.5$ on resonance for a sufficiently driven cavity. From this steady state strong dephasing accompanied with slow decay results in a close to unity occupation of the dark state depleting the probability in $|G\rangle$ and $|W\rangle$, cf. Fig. 12. For an initially

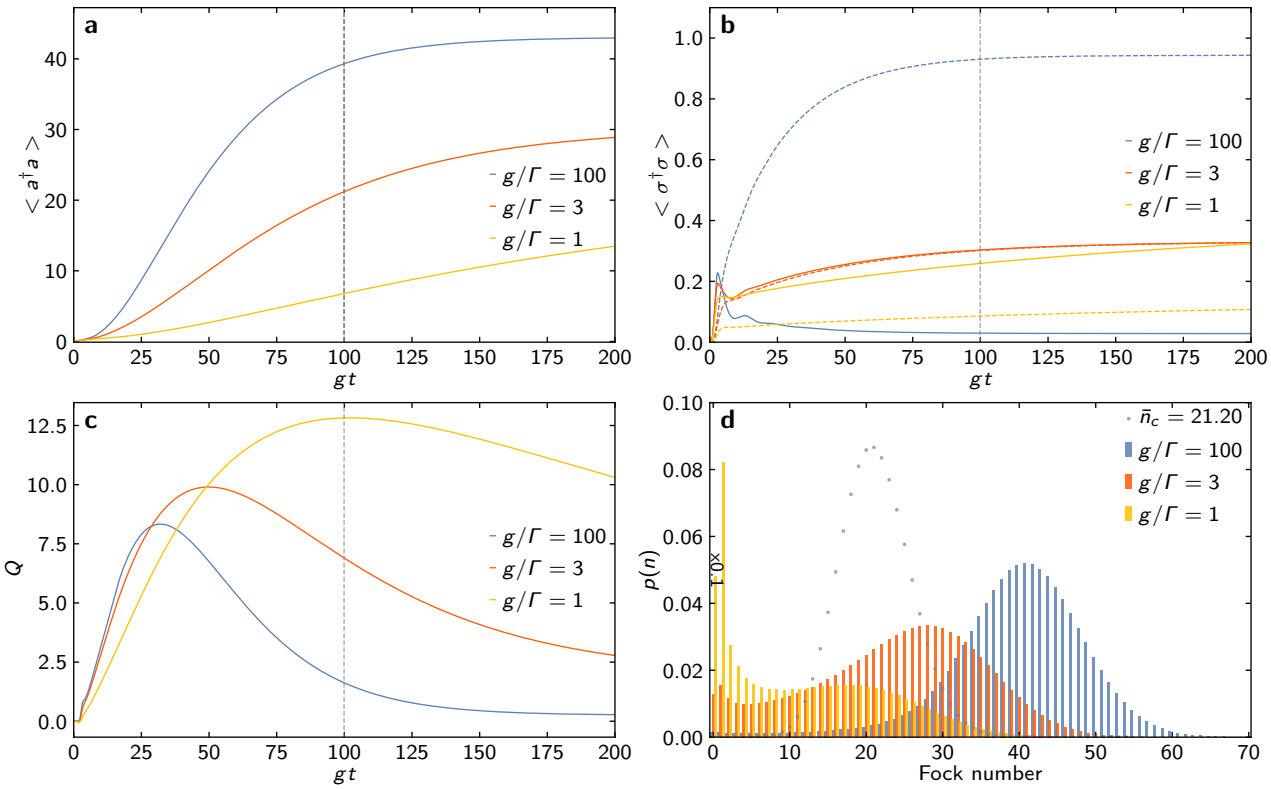

Fig. 13: Driven 2+1 level atom in a cavity for various spontaneous emission rates of the excited and dark state with $g/\kappa = 10$, $g/\gamma = 3$ $g/\eta = 3$. **a** Expectation value of the cavity photon number. **b** Expectation value of the $|W\rangle$ interacting bright state (solid line) and the decoupled dark state $|D\rangle$ (dashed line). The fast decay of the excited states $|W\rangle$ and $|D\rangle$ results in a lower occupation probability of the dark state compared to the slower decay terms. **c** Mandel-Q parameter of the cavity field. The cavity field is not entirely decoupled from the atom for higher decay rates, since the dark state decays back to the ground state relatively fast. **d** Photon distribution after $gt = 100$, indicated by the gray dashed line in **a-c**. The decay back to the ground state prevents an equilibration to a coherent state, since the atom does not mostly decouple for a fast decaying excited state. The $n = 0$ component has been rescaled by a factor of 0.1.

empty cavity the picture changes, since the excited state is almost directly decoupling from the cavity, as visible from the initial steep slope of the dephasing into the dark state, cf Fig. 12. The driven cavity then acts as a coherently driven harmonic oscillator, which settles to a coherent state. The opposite case, fast spontaneous decay while having a moderate dephasing, prevents complete decoupling thus, the entire system is still interacting. The super-Possoinian photon distribution as visible in Fig. 13 can be seen as a hallmark of the remaining interaction. Rabi oscillations are in any scenario only visible initially, on the one hand due to the Poisson statistics of the driving field and the resulting interference of the different oscillation amplitudes of the various Fock components, on the other hand due to the relaxation processes, randomly resetting the medium to its ground state, or in the case of dephasing preventing any further interaction while occupying $|D\rangle$.

The 2+1 level atom interacting with a single mode cavity field for now seems to be a relatively artificial case, since the selection of an atom exhibiting a decay channel to a uncoupled level is particularly impractical if one is interested in long coherence times. The modification of the mode structure will also suppress spontaneous decay to an entirely decoupled state. The discussed scenario

will be related to the system discussed in the following, where exactly this dynamic is inevitable, a random decoupling from the driving field. The scenario considered there will be a propagating photon field, which - in contrast to the cavity case - can facilitate a modification of the driving field *on the fly*, i.e. while propagating through the system. This is in strict contrast to the previously discussed systems, since an increase in coupling strength at fixed mode volume requires better mirrors, which in turn makes it hard to transmit an photon in or out of the cavity. In order to overcome this difficulty multiple approaches are intensely studied, where light propagates while strongly interacting with a two level system.

4 A Rydberg superatom

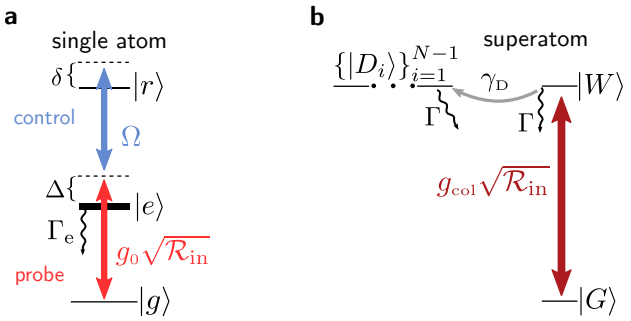

Fig. 14: Level scheme for a single atom and a Rydberg superatom. **a** Level scheme of a single three level atom in ladder configuration. The ground $|g\rangle$ and intermediate state $|e\rangle$ are coupled by a weak probe field with detuning Δ and Rabi frequency $g_0\sqrt{\mathcal{R}_{in}}$, while the intermediate state is coupled to the excited state $|r\rangle$ by a strong control field with Rabi frequency Ω. δ indicates the energy difference due to the dressing by the control field. **b** Level structure of a collective excitation within one blockade radius. The collective ground state $|G\rangle$ is coupled to the collective excited state $|W\rangle$, which can by internal dynamics among the atoms that share the same excitation dephase to a state decoupled from the driving field$|D\rangle$. As the atoms collectively couple to the driving field their interaction is greatly enhanced.

In general everything can, by sufficient preparation be a two-level system. The previously discussed interaction of a system and a resonant cavity was mostly realized in systems that are in general non perfect two-level systems. The experiments conducted by Brune, Raimond and Haroche rely on the interaction of a highly excited atom in a circular state - a Rydberg atom, with in principle infinite other states [18, 19, 22, 47]. However by exciting the atom to a circular state the dipole transitions the atom can undergo are only very limited, and thus by interacting with a cavity close to resonance the dynamics are restricted to only two levels of the atom. Further examples include superconducting LC-circuits, defects in different crystal structures, quantum dots or molecules, in any case the system can be considered to be a two-level system if the interaction with adjacent levels is negligible.

In order to justify the restriction to two-levels in a system made up of $\approx 10^4$ atoms where each individual atom provides a wealth of levels, the interaction of the atoms among each other and the interaction of each atom with light will be investigated in order to justify this strict simplification to the level scheme presented in Fig. 14.

4.1 Three levels turned into two - Adiabatic Elimination

The physics presented in the following essentially take place in three levels of the ^{87}Rb atom, the ground state $|5S^{1/2}, F = 2, m_F = 2\rangle$, the intermediate state $|5P^{3/2}, F = 3, m_F = 3\rangle$ and unless otherwise stated the $|111S^{1/2}, m_J = 1/2\rangle$ Rydberg state. For convenience they will be abbreviated by $|g\rangle$, $|e\rangle$ and $|r\rangle$. The Rabi frequencies will for now be considered to be constant and labeled $\Omega_P = g_0\sqrt{R_{in}}$ and Ω_C for the transitions $|g\rangle \leftrightarrow |e\rangle$ and $|e\rangle \leftrightarrow |r\rangle$ respectively. The Rabi frequency on the lower

transition is determined by a coupling constant g_0, given by the spatial geometry of the probe field and the incoming photon flux $\mathcal{R}_{\rangle\backslash}$; the upper transition can be considered to be classical. There is no cavity or waveguide structure modifying the mode structure of the electromagnetic field, thus all fields correspond to modes in free space. The coherent evolution of the three levels in the rotating frame can then be described by the Hamiltonian

$$H_{3L} = \hbar \begin{pmatrix} 0 & \Omega_p/2 & 0 \\ \Omega_p^*/2 & \Delta & \Omega_C/2 \\ 0 & \Omega_C^*/2 & \Delta - \delta \end{pmatrix}. \tag{80}$$

Plugging this Hamiltonian into a Schrödinger equation for the three states, with state

$$\Psi(t) = c_g(t)\,|g\rangle + c_e(t)\,|e\rangle + c_r(t)\,|r\rangle \tag{81}$$

where $|i\rangle$ is a time independent state vector, the time evolution results in three coupled differential equations for the coefficients

$$i\partial_t c_g(t) = \frac{\Omega_p}{2} c_e(t) \tag{82}$$

$$i\partial_t c_e(t) = \Delta c_e(t) + \frac{1}{2}\left(\Omega_c c_r(t) + \Omega_p^* c_g(t)\right) \tag{83}$$

$$i\partial_t c_r(t) = (\Delta - \delta) c_r(t) + \frac{\Omega_c^*}{2} c_e(t). \tag{84}$$

If the laser-field is sufficiently far detuned, from the intermediate state, i.e. $\Delta \gg \Omega_p, \Omega_c$, but the two photon detuning $\Delta - \delta$ is small, the intermediate state immediately follows the dynamics, such that it always equilibrates compared to the timescale of the other dynamics. The two resulting timescales allow for the separation of the dynamics, which is commonly referred to as *adiabatic elimination*. In the aforementioned limit of large detuning the dynamics of the intermediate state correspond to high frequency oscillations with small amplitude, compared to the dynamics occurring for $|g\rangle$ and $|r\rangle$. For sufficiently large detuning the dynamics of the intermediate state can thus be eliminated. This can be easily seen by considering the dynamics of two subspaces, with projectors P and Q, of the Hamiltonian H. The eigenvalues of QHQ are widely separated from those of PHP, and the coupling between the two subspaces is small compared to the eigenvalues of QHQ. The dynamics of interest, occurring on a slow timescale compared to the fast dynamics of H shall be accounted for in subspace P. The sum of the subspaces describes the entire system, thus $Q + P = 1$ [78]. Starting from the Schrödinger equation one finds

$$i\hbar\partial_t(P+Q)\Psi(t) = (P+Q)H(P+Q)\Psi(t) \tag{85}$$

$$i\hbar\partial_t(P\Psi(t)) = PHP(P\Psi(t)) + PHQ(Q\Psi(t)) \tag{86}$$

$$i\hbar\partial_t(Q\Psi(t)) = QHP(P\Psi(t)) + QHQ(Q\Psi(t)), \tag{87}$$

where the last two equations are obtained by multiplying with P and Q respectively and using $P^2 = P$ and $Q^2 = Q$. If the system now starts from $P\Psi(t)$, since the interaction between the subspaces is weak, the wave function of $Q\Psi(t)$ will not change significantly. Therefore setting $\partial_t Q\Psi(t) = 0$, which results in

$$i\partial_t(P\Psi(t)) = PHP(P\Psi(t)) - PHQ(QHQ)^{-1}QHP(p\Psi(t)). \tag{88}$$

Applying this to H_{3L} means setting $\partial_t c_e(t) = 0$, resolving the equations one obtains

$$i\partial_t c_g(t) = \frac{|\Omega_p|^2}{\Delta} c_g + \frac{\Omega_p^*\Omega_c^*}{\Delta} c_r(t) \tag{89}$$

$$i\partial_t c_r(t) = \frac{\Omega_p\Omega_c}{4\Delta} c_g(t) + \frac{|\Omega_c|^2}{4\Delta} c_r(t) + \delta c_r(t). \tag{90}$$

The dynamics of this system correspond to an effective two-level system where the levels are coupled by a driving field with Rabi frequency $\Omega_{eff} = \Omega_p\Omega_c/(4\Delta)$. The intermediate state's population is negligible and thus does not contribute to the dynamics. In the experimental scenario, where $|r\rangle$ is a long-lived Rydberg state and the intermediate $|e\rangle$ is the $|5P^{3/2}\rangle$ state in ^{87}Rb which exhibits a non-negligible decay rate, the contribution of $|e\rangle$ to $|r\rangle$ due to the large Rabi frequency of the coupling field between $|e\rangle$ and $|r\rangle$, leads to a decay channel for the Rydberg state. The admixture can be calculated by either diagonalizing the Hamiltonian of the two coupled levels and approximating the eigenstates for $\Omega/\Delta \ll 1$, or calculated within first order perturbation theory, which gives

$$|r'\rangle \approx |r\rangle + \frac{\Omega_c}{2\Delta}|e\rangle\,. \tag{91}$$

This results in a decay rate of the population in $|r\rangle$ due to the admixture of $|e\rangle$, which is decaying with rate Γ,

$$\Gamma_{eff} = \frac{\Omega_c^2}{(2\Delta)^2}. \tag{92}$$

The linewidth of the system can in principle be as narrow as the linewidth of the uppermost excited state, which in this specific case can be neglected, since the decay via the intermediate state is the dominant term.

By detuning the lasers that address the transitions between multiple intermediate states from the respective transition the dynamics of an in principle n-level system can be tuned to n-photon resonance, resulting in an effective two-level system. Here the dynamics of a three-level system is reduced to two levels, by detuning from the intermediate state.

4.2 The lonely interacting Rydberg Atom

Considering Rydberg atoms, highly excited states of a single atom, one of their most interesting properties is their strong interaction, which results in a vast number of phenomena. The interaction strength among cold Rydberg atoms well exceeds the time scale needed for excitation and the time scale related to motion in the trapping potential, thus positioning them as an ideal candidate for fast quantum gates [40, 79]. First implementations have been experimentally demonstrated: two atoms have been entangled by applying quantum phase gates and a $CNOT$-gate was realized [80, 81]. Furthermore the interaction enables the preparation of atomic Fock states [82] as well as the direct observation of the interaction potential among two Rydberg atoms [83–85]. The mesoscopic extent also allows for the well controllable implementation of spin Hamiltonians, resulting in multiple phenomena such as structured patterns or crystallization [86–91]. Mapping the strong interaction onto single photons enables effective interactions among photons at the level of individual quanta, which allows e.g. for the realization of single photon switches and transistors, the subtraction of a single photon from a light pulse and the observation of bound states of photons [38, 92–107]. However not only multiple Rydberg atoms interact with each other, the interaction of a Rydberg atom and one or several atoms in the ground state, can create weakly bound states of giant Rydberg molecules [108–111].

If the atomic medium is tailored such that it is small compared to the Rabi frequency of the exciting laser-field, the medium can only host a single excitation, which collectively interacts with light [38, 112–114]. The comparison of a Rabi frequency with the extent of a atomic medium at first

glance seems counter intuitive, but can be put into context by considering the potential of two Rydberg atoms as a function of distance.

Since Rydberg atoms are highly excited states, the wave function describing the highly excited, weakly bound, electron is massively boosted in size. Due the mesoscopic extent of the electronic wave function it is extremely susceptible to external electric fields admixing different orbitals to the initial wave function and thereby shifting it's energy. Considering a gedankenexperiment where one is able to excites two distant S-state, ergo isotropic, Rydberg atoms separated far enough so they cannot interact. Then taking the two Rydberg atoms closer to one another, at some point they will start to interact. Naively speaking the two charge distributions start to be influenced by one another. The charge distribution of each atom exhibits fluctuations which lead to a non-zero dipole moment for short times, which in turn induces a dipole-moment in the other atom, resembling a van der Waals interaction

$$V_{vdW}(r) = \frac{C_6}{r^6}, \tag{93}$$

where r is the inter-particle distance and C_6 the coefficient characterizing the interaction strength. The description remains valid, as long as the interaction of the atoms is relatively weak, since the picture mentioned above is only true, as long as the interaction can be treated as perturbation to the original state. This is also reflected in the shape of the r^{-6} potential, which originates from the fact that the initial state does not have a permanent dipole moment, therefore the first order correction $\propto r^{-3}$ vanishes and the lowest non-vanishing term is of second-order $\propto r^{-}6$, which can be measured in experiment [83].

Yet the pertubative description fails for interactions at shorter distances, where higher order terms need to be considered. At distances greater than the Le Roy radius, which can be roughly considered as an estimator, at which distance the wave functions of the individual Rydberg atoms start to overlap, the interaction can be considered as the interaction of the charge distributions of the four distinguishable particles, the ionic cores of the Rydberg atom and their respective electrons [115]. Depending on the state combination of the initial state the interaction can be either repulsive or attractive. For sufficiently close distances the entire interaction Hamiltonian has to be diagonalized in order to get accurate results, which may significantly deviate from a van der Waals type interaction. In Fig. 15 the interaction potential of state $|111S^{1/2}, m_J = 1/2\rangle$ with neighboring Rydberg states was calculated utilizing the *pairinteraction* software, which is presented in [115]. The behavior in the large distance limit can be approximated by a van der Waals type interaction yielding $C_6 = h\,1.488 \times 10^5\,\mathrm{GHz}\,\mu\mathrm{m}^6$.

The interaction eventually manifests itself in an energy difference between having two Rydberg atoms separated by a large distance and having two Rydberg atoms close by, as depicted in Fig. 15. The distance, where the energetic shift due to the interaction among the Rydberg atoms equals the shift of approximately one excitation bandwidth, determines an effective interaction length called *blockade radius* r_B [40, 112].

$$r_B = \left(\frac{\hbar\Omega}{C_6}\right)^{1/6}, \tag{94}$$

with Ω the excitation bandwidth, and C_6 the coefficient of the interaction. Note that the final blockade radius may be smaller, if the atom is subject to decay or decoherence mechanisms that broaden the line further than Ω. The blockade radius determines a volume within which only a single excitation can be hosted, since the excitation of an additional Rydberg atom is off resonant.

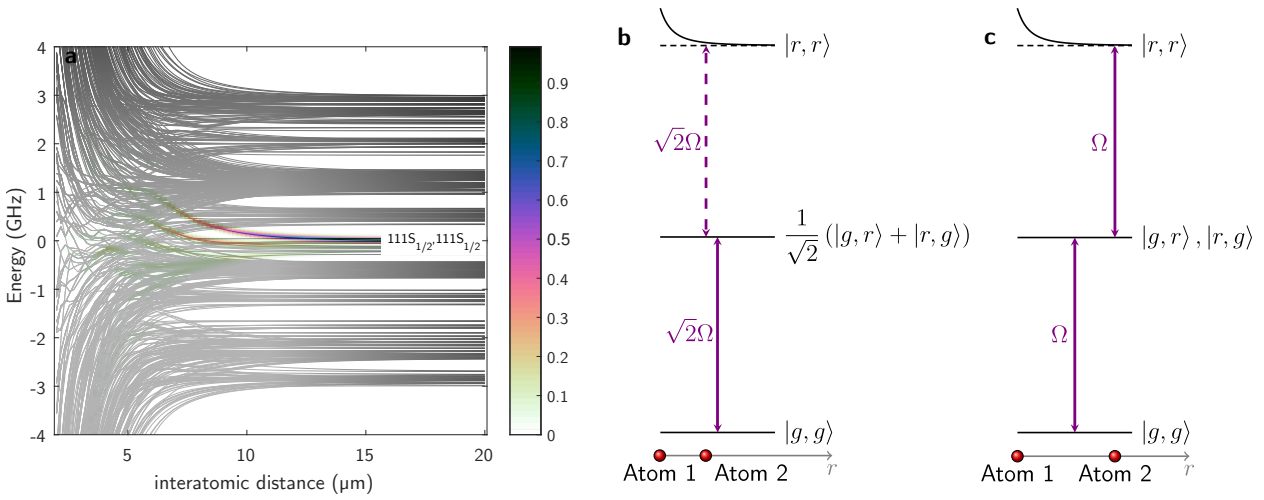

Fig. 15: Pair interaction potential of two Rydberg atoms. **a** Pair potential for Rydberg atoms in $|111S^{1/2}\rangle\,|111S^{1/2}\rangle$, and the admixture of neighboring levels, as indicated by the color code on top of the individual potential line. For clarity only $|111S^{1/2}\rangle\,|111S^{1/2}\rangle$ is labeled. With increasing interaction strength the initial pair states are significantly mixed. For interatomic distances smaller than 5 μm the result is rather an approximation, since the criterion to treat the two atoms as separate charge distributions is violated and exchange interactions need to be taken into account. **b** Atoms closer than the blockade radius exhibit a significant level shift, preventing the simultaneous excitation of two Rydberg atoms. The indistinguishability of the two particles residing within one blockade radius, results in the coupling to pair states rather than individual atoms. **c** Atoms separated further than the blockade radius, in principle probe the pair potential but are not sufficiently perturbed, thus both atoms can be excited.

The pair state is shifted out off resonance within the blockade radius. By creating an atomic medium smaller than the blockade radius, one can prepare an highly entangled atomic Fock state, in which the excitation is shared among all constituents. This will be discussed in the following.

4.3 The lonely Rydberg Atom with a twist - The Collective character of a Rydberg Superatom

As already Aristotle realized,

> "The whole is greater than the sum of its parts."

This is as well true in the case of an cold atomic cloud, being excited to a Rydberg state to form a superatom. A superatom is understood to be any cluster or arrangement of atoms exhibiting the properties of elemental atoms, such as a discrete level structure, and the possibility to only scatter a single photon at a time. In the context discussed before the superatom would be made up of all atoms residing within one blockade radius, which are coupling collectively to an incoming light field. The entire medium only allows a single excitation, thus it scatters only one photon at a time.

To emphasize the nature of this collective state of matter, the transition from the single atom to the collective picture, cf. Fig. 14, shall be performed in the following. The considered scenario shall be as follows, an atomic cloud containing N identical atoms in their ground state, which are located in

a volume which is smaller than the Rydberg blockade radius in each direction. The atomic medium shall be addressed with laser light. With less restrictions the interaction of N atoms being interfaced with electromagnetic radiation is also treated in [116, 117].

The operator describing the interaction of the atomic cloud with an incident plain wave electric field is given by the sum of all single atom operators [118]

$$V(t) = \sum_j \hbar g_0 \left(\sigma_j^\dagger a_{\mathbf{k_0}} \, \mathrm{e}^{i\mathbf{k_0}\cdot\mathbf{r}_j} \, \mathrm{e}^{-i(\nu_0-\omega_0)t} + \sigma_j a_{\mathbf{k_0}}^\dagger \, \mathrm{e}^{-i\mathbf{k_0}\cdot\mathbf{r}_j} \, \mathrm{e}^{i(\nu-\omega_0)t} \right) + \frac{1}{2} \sum_{j\neq i} V_{i,j} \sigma_j^\dagger \sigma_j \sigma_i^\dagger \sigma_i \tag{95}$$

where $\sigma_j = |g\rangle \langle r|$ is again the single atom operator relaxing an atom from the excited to the ground state and $a_{\mathbf{k_0}}$ the annihilation operator of a photon in mode k_0 with frequency $\nu_0 = c|\mathbf{k_0}|$. The atomic energy difference between ground and Rydberg state is $\hbar\omega_0$ and g_0 describes the atom-field coupling strength. The potential $V_{i,j}$ accounts for the Rydberg Rydberg interaction preventing the simultaneous excitation of two atoms. The actual shape of the potential shall not be of interest in this case, yet it justifies $\hbar g_0 \sqrt{\langle a_{\mathbf{k_0}}^\dagger a_{\mathbf{k_0}} \rangle} \ll V_{i,j}$ for any combination of i, j, essentially embodying the fact that the atomic cloud is smaller than the Rydberg blockade for any driving field of interest. Under the given assumption only singly excited states are allowed, thus any state involving two Rydberg excitations can be disregarded. Note that the transition from $|g\rangle$ to $|r\rangle$ does not necessarily need to be a direct transition from the ground to the Rydberg state, but can also be a multi-photon transition, in which case the phase relation between the fields has to be adapted.

In order to arrive at a simple expression for the excited state of the atomic cloud, which also takes into account the spatial extent of the medium, a single photon $|1_{\mathbf{k_0}}\rangle$ shall be incident on the collective ground state

$$|G\rangle = |g_1, g_2, \ldots, g_N\rangle \, . \tag{96}$$

For a single photon the interaction term can be completely neglected, and the time evolution can be evaluated assuming small interaction strengths g_0 of the single atoms. Following [118], the unitary time evolution can be approximated to give

$$U(\tau) = \mathcal{T} e^{-i/\hbar \int_{t_0}^{\tau} \mathrm{d}t' V(t')} \tag{97}$$

$$\approx 1 - i g_0 \sum_j \int_{t_0}^{\tau} \mathrm{d}t' \left(\sigma_j^\dagger a_{\mathbf{k_0}} \, \mathrm{e}^{i\mathbf{k_0}\cdot\mathbf{r}_j} \, \mathrm{e}^{-i(\nu_0-\omega_0)t'} + \sigma_j a_{\mathbf{k_0}}^\dagger \, \mathrm{e}^{-i\mathbf{k_0}\cdot\mathbf{r}_j} \, \mathrm{e}^{i(\nu-\omega_0)t'} \right) . \tag{98}$$

The initial state $|G\rangle |1_{\mathbf{k_0}}\rangle$ then evolves, assuming a resonant incident photon $\nu_0 = \omega_0$, as

$$U(\tau) |G\rangle |1_{\mathbf{k_0}}\rangle \approx |G\rangle |1_{\mathbf{k_0}}\rangle - i g_0 \tau \sum_j \mathrm{e}^{i\mathbf{k_0}\mathbf{r_j}} |g_1, g_2, \ldots, r_j, \ldots, g_N\rangle |1_{\mathbf{k_0}}\rangle \, , \tag{99}$$

which only holds for small $g_0\tau$. However one can already see that the state excited by the interaction with an incoming photon is a symmetric superposition of the individual atoms being in the excited state while all other $N-1$ atoms occupy the ground state. This state is also couple to the electromagnetic field of free space, therefore it is convenient to utilize the time evolution of the system after absorption of a photon. Its time evolution operator is given by [68, 118]

$$U_W(t) = \sum_j U_W^{(j)} = \sum_j \gamma_j^\dagger \sigma_j \tag{100}$$

$$\gamma_j^\dagger = \sum_{\mathbf{k}} \frac{g_{\mathbf{k}} \, \mathrm{e}^{-i\mathbf{k}\mathbf{r_j}}}{\nu_k - \omega_0 + \frac{i\gamma}{2}} a_{\mathbf{k}}^\dagger , \tag{101}$$

with $\gamma_j^\dagger$ describing the spontaneous emission process of a photon from atom j into mode $\mathbf{k}$, and γ is the Weisskopf-Wigner spontaneous emission rate.

Having the framework describing the excitation and relaxation of a Rydberg superatom at hand, the effects resulting from the collective excited state will be considered. The excited state of the atomic system inherits a phase relation from the electric field. A properly normalized state, the *bright* state, is

$$|W\rangle = \sum_j \mathrm{e}^{i\mathbf{k_0}\mathbf{r_j}} |r_j\rangle \,, \tag{102}$$

$|r_j\rangle$ describes the state with atom j in $|r\rangle$ and all other $N-1$ atoms in $|g\rangle$. The transition from $|G\rangle$ to $|W\rangle$ is enhanced by the number of atoms contributing to the collective dynamics, this can be easily seen by evaluating

$$\langle 0| \langle W|V(t)|G\rangle |1_{\mathbf{k_0}}\rangle = \sqrt{N} \langle 0| \langle r|V(t)|g\rangle |1_{\mathbf{k_0}}\rangle \,, \tag{103}$$

thus the transition dipole moment of the mesoscopic superatom is $\sqrt{N}$-fold enhanced compared to the single atom transition. This does not only hold for the constructed case of a single incident photon, but is also valid for a coherent field driving the superatom. However not only the excitation process is enhanced but also the relaxation process. The outgoing photon is then described by

$$\langle G| U_W |W\rangle |0\rangle = \frac{1}{\sqrt{N}} \sum_j \mathrm{e}^{i\mathbf{k_0}\mathbf{r_j}} \gamma_j^\dagger |0\rangle = \frac{\sqrt{N}}{V} \sum_{\mathbf{k}} \frac{g_{\mathbf{k}} (2\pi)^3}{\nu_k - \omega_0 + \frac{i\gamma}{2}} a^\dagger |1_{\mathbf{k}}\rangle \, \delta^{(3)}(\mathbf{k_0} - \mathbf{k}). \tag{104}$$

The atomic cloud is assumed to have a fairly high number density, such that the summation can be calculated as an integral

$$\sum_j \mathrm{e}^{i(\mathbf{k_0}-\mathbf{k})\mathbf{r_j}} \approx \frac{N}{V} \int_V \mathrm{d}^{(3)}\mathbf{r} \, \mathrm{e}^{i(\mathbf{k_0}-\mathbf{k})\mathbf{r_j}} = \frac{N(2\pi)^3}{V} \delta^{(3)}(\mathbf{k_0} - \mathbf{k}), \tag{105}$$

where V is the volume of the atomic medium. Two things shall be noted about the emission described by Eq. 104. First the direction of the spontaneously emitted photon follows the direction of the incident photon, thus rendering the system unidirectional for incoming photons, which are not scattered back, for a sufficiently smooth atomic distribution. Second the term calculated in Eq. 104 is $\propto N$, i.e. the collective decay rate, and not only the coherent interaction is collectively enhanced by the number of atoms contributing to the state [39].

The Hilbert space describing the superatom also contains $N-1$ collective dark states $\{|D_i\rangle\}_{i=1}^N$, which are orthonormal to $|W\rangle$ and $|G\rangle$ and not coupled to the light field. Considering that $|D\rangle$ and $|W\rangle$ are orthogonal,

$$0 = \sqrt{N} \langle W|D\rangle = \sum_j \sum_i \langle r_j|r_i\rangle \, \alpha_i \, \mathrm{e}^{-i\mathbf{k_0}\mathbf{r_j}} \tag{106}$$

$$= \sum_j \alpha_j \, \mathrm{e}^{-i\mathbf{k_0}\mathbf{r_j}} \,. \tag{107}$$

The interaction between state $|D\rangle$ and $|G\rangle$ is then determined by

$$\langle G|V(t)|D\rangle = \tag{108}$$

$$\sum_k \langle G| \left(\sum_j \hbar g_0 \left(\sigma_j^\dagger a_{\mathbf{k_0}} \, \mathrm{e}^{i\mathbf{k_0}\cdot\mathbf{r}_j} \, \mathrm{e}^{-i(\nu_0-\omega_0)t} + \sigma_j a_{\mathbf{k_0}}^\dagger \, \mathrm{e}^{-i\mathbf{k_0}\cdot\mathbf{r}_j} \, \mathrm{e}^{i(\nu-\omega_0)t} \right) \right. \tag{109}$$

$$\left. + \frac{1}{2} \sum_{j\neq i} V_{i,j} \sigma_j^\dagger \sigma_j \sigma_i^\dagger \sigma_i \right) |r_k\rangle \, \alpha_k$$

$$= \sum_k \sum_j \langle g| \hbar g_0 a_{\mathbf{k_0}}^\dagger \, \mathrm{e}^{-i\mathbf{k_0}\cdot\mathbf{r}_j} \, \mathrm{e}^{i(\nu-\omega_0)t} \, \delta_{j,k} |r_k\rangle \, \alpha_k \tag{110}$$

$$= \hbar g_0 a_{\mathbf{k_0}}^\dagger \, \mathrm{e}^{i(\nu-\omega_0)t} \sum_j \langle g|r_j\rangle \, \alpha_j \, \mathrm{e}^{-i\mathbf{k_0}\cdot\mathbf{r}_j} \tag{111}$$

$$= 0. \tag{112}$$

Thus, if the atoms do only interact with a single mode, as described above, the bright state $|W\rangle$ is the only state being directly addressed; all dark states cannot be directly accessed. The dark states, however are not perfectly isolated and do not decay, but they don't decay collectively enhanced but rather due to the fact that each atom can spontaneously decay and thus emit a photon with amplitude $1/N$; the dark state's spontaneous emission is not directed.

The above justification was calculated assuming a plane wave input photon field, but it can be shown, that the emission and directivity also hold for a Gaussian beam [38].

5 A two-level system strongly coupled to a waveguide

The interaction of an individual atom interacting with a single photon could be studied in the context of cavity QED, where the photon is trapped inside a resonator. The possibility to study the effects of a strongly coupled system consisting of a propagating photon field and a two-level atom coupled to it seems intriguing. Not only because it can cast light on the physics of atom-photon interaction at the quantum level for a propagating photon, but also because it enables the processing of photons, as they are transmitted through the two-level atom. Since a single atom also provides non-linear behavior depending on the input photon number, it is in principle able to mediate effective interactions among photons, which can only be studied if the light field is accessible. Since single atoms demand experimentally extremely challenging requirements in order to achieve significant coupling strength, the approach of coupling light to a collective state of matter massively simplifies the requirements, and coherent coupling on the few-photon level is achievable.

> The work presented in the following is the result of a joint effort by Asaf Paris-Mandoki, Christoph Braun, Jan Kumlin, Christoph Tresp, Ivan Mirgorodskiy, Florian Christaller, Hans Peter Büchler, Sebastian Hofferberth. [38]

5.1 Theoretical Framework

As discussed in the previous, the collective character of N two-level systems strongly interacting with an electric field, in the presence of an excitation blockade preventing more than one atom being

excited at a time, results in highly directed emission of the collective excitation. Thus an effective description considering the superatom as a single two-level system interacting with a one dimensional waveguide is well justified.

The waveguide is for simplicity assumed to to have infinite bandwidth, such that an electric field operator propagating in it can be written as

$$E(x/c,t) = \int_{-\infty}^{\infty} \frac{\mathrm{d}k}{2\pi}\, \mathrm{e}^{ickx/c}\, a_k(t), \tag{113}$$

where $a_k(t)$ annihilates a photon in mode k. Considering a two-level atom at position $x = 0$, the Hamiltonian of the resonantly coupled system in the rotating wave approximation is

$$H = \hbar \int_{-\infty}^{\infty} \frac{\mathrm{d}k}{2\pi} k\, a_k^\dagger(t) a_k(t) + \hbar\sqrt{\kappa}\left(E(0,t)\sigma^\dagger(t) + \sigma(t)E^\dagger(0,t)\right), \tag{114}$$

where the notation x/c is used in order to treat space and time equivalently. This Hamiltonian can be treated within the previously derived input-output formalism, where the wave guide represents the bath coupled to the two-level system. The bath in this case does not only provide the inevitable damping but also the driving field. In order to verify the validity of the equations, due to the broken translational symmetry of the bath Hamiltonian, which was previously not explicitly treated, the photons will now be treated as propagating waves interacting with a system. The quantity of interest is first the outgoing field for a given input field. The population inversion of the two-level system driven by a coherent field will be derived later on. The equation of motion for the field operators is again determined by the Heisenberg equation of motion, which can, as previously done, be formally integrated from $t_0 \leq t$ to its present state t

$$\partial_t a_k(t) = \frac{i}{\hbar}[H, a_k(t)] = -ick a_k(t) + -i\sqrt{\kappa}\sigma(t) \tag{115}$$

$$a_k(t) = a_k(t_0)\, \mathrm{e}^{-ick(t-t_0)} - i\sqrt{\kappa} \int_{t_0}^{t} \mathrm{d}t'\, \mathrm{e}^{-ick(t-t')}\, \sigma(t') \tag{116}$$

The solution for the time evolution of the electric field can then be found by plugging Eq. 116 into the definition of the electric field Eq. 113

$$E(x/c,t) = \int_{-\infty}^{\infty} \frac{\mathrm{d}k}{2\pi} a_k(t_0)\, \mathrm{e}^{-ick(t-t_0-x/c)} - i\sqrt{\kappa} \int_{t_0}^{t} \mathrm{d}t' \underbrace{\int_{-\infty}^{\infty} \frac{\mathrm{d}k}{2\pi}\, \mathrm{e}^{-ick(t-t'-x/c)}}_{\delta(t-x/c-t')} \sigma(t') \tag{117}$$

$$= \bar{E}(x/c, t-t_0) - i\sqrt{\kappa}\Theta(x/c)\Theta(t-x/c-t_0)\sigma(t-x/c), \tag{118}$$

recovering the result of Eq. 64 for proper x, t, t_0. Since the two-level system exhibits a fundamental nonlinearity, namely that it only interacts with a single photon at a time, the electric field can be separated into two parts. $\bar{E}$ is not interacting with the two-level system and thus just passing by, while the interacting part is described by the atomic evolution mapped back to the electric field. By only considering the evolution of the system located at $x = 0$ at times $t > t_0$, the constraints given by $\Theta(x/c)\Theta(t-x/c-t_0)$ can be resolved; assuming $\Theta(x/c=0) = 1/2$. The time evolution for any system operator $A(t)$, can equivalently be determined by calculating $\partial_t A(t) = i/\hbar[H, A(t)]$ or is determined by evaluating Eq. 60, where the input field is given by $\bar{E}$, one obtains

$$\begin{aligned} \partial_t A(t) = &- \overbrace{i\sqrt{\kappa}\left([A(t), \sigma^\dagger(t)]\bar{E}(0, t-t_o) + \bar{E}^\dagger(0, t-t0)[A(t), \sigma(t)]\right)}^{\text{coherent}} \\ &- \underbrace{\frac{1}{2}\kappa\left([A(t), \sigma^\dagger(t)]\sigma(t) - \sigma^\dagger(t)[A(t), \sigma(t)]\right)}_{\text{dissipative}}. \end{aligned} \tag{119}$$

The above expression is split into a coherent and dissipative part. It again emphasizes the effect of any coupling to a driving field - the coupling term inevitably leads to damping. This means that one cannot - no matter how strong the coupling to the waveguide κ is - enter the strong coupling regime, in which the rate related to the coherent energy exchange exceeds the rate related to the decay. In this case the decay and driving are inevitably linked.

The further analysis of this model will rely on mapping the dynamics to a density matrix, then tracing out the bath terms, i.e. the waveguide and consequently solving the equations of motion for the atomic density matrix. The solution of the atomic density matrix then gives the full information of the coupled driven system. Pictorially speaking the system is taking a single photon out of the input and later on putting it back to the output, thus the atomic evolution gives the full information in order to calculate the outgoing electric field.

The evolution of the expectation value is independent of the quantum mechanical picture, in which the solution is calculated. From Eq. 76 one can state that

$$\partial_t \langle A \rangle = \mathrm{Tr}[\partial_t A(t)\rho] = Tr[A\partial_t \rho(t)]. \tag{120}$$

Applying the unitary transformation $U = \mathrm{e}^{-i/\hbar H(t-t_0)}$ and recalling the transformation from the Schrödinger into the Heisenberg picture for the operator A and density matrix $\rho(t)$,

$$A(t) = U^\dagger A U \tag{121}$$

$$\rho(t) = U\rho U^\dagger, \tag{122}$$

Eq. 119 can be transformed to the desired picture. Using Eq. 119 after transformation to the Schrödinger picture, the cyclic property of the trace and Eq. 120, one finds after reordering the terms

$$Tr[A\partial_t\rho(t)] = Tr\left[\kappa A\left(\sigma\rho(t)\sigma^\dagger - \frac{1}{2}\left\{\sigma^\dagger\sigma, \rho(t)\right\}\right) - i\sqrt{\kappa}A\left[(\bar{E}(0,t-t_o)\sigma^\dagger + \bar{E}^\dagger(0,t-t_o)\sigma), \rho(t)\right]\right], \tag{123}$$

with the anti-commutator $A, B = AB + BA$. Assuming that the system's time dependent input field $\bar{E}(0, t-t0) = \alpha(t-t0)$ is a coherent field, the system Hamiltonian reads

$$H_0(t) = \hbar\sqrt{\kappa}(\alpha(t-t_0)\sigma^\dagger + \alpha^*(t-t_0)\sigma). \tag{124}$$

By plugging the Hamiltonian into Eq. 123, and comparing the left and right side of the equation one finds the master equation describing the system

$$\partial_t\rho(t) = -\frac{i}{\hbar}\left[H_0(t), \rho(t)\right] + \kappa\left(\sigma\rho(t)\sigma^\dagger - \frac{1}{2}\left\{\sigma^\dagger\sigma, \rho(t)\right\}\right). \tag{125}$$

After tracing out the photonic bath part, i.e. $\mathrm{Tr}_B[\rho(t)] = \rho_A(t)$, the master equation for the atomic density matrix is

$$\partial_t\rho_A(t) = -\frac{i}{\hbar}\left[H_0(t), \rho_A(t)\right] + \kappa\left(\sigma\rho_A(t)\sigma^\dagger - \frac{1}{2}\left\{\sigma^\dagger\sigma, \rho_A(t)\right\}\right). \tag{126}$$

After finding the solution to the atomic system the expectation value of the output electric field and outgoing intensity is solely determined by expectation values of the atomic operators, i.e.

$$\langle E(t-x/c)\rangle = \alpha(t-x/c) - i\sqrt{\kappa}\,\langle\sigma(t-x/c)\rangle\,\Theta(x/c) \tag{127}$$

$$\begin{aligned}\langle E^\dagger(t-x/c)E(t-x/c)\rangle =& |\alpha(t-x/c)|^2 + \kappa\,\langle\sigma^\dagger(t-x/c)\sigma(t-x/c)\rangle \\ & - i\sqrt{\kappa}\left(\alpha^*(t-x/c)\,\langle\sigma(t-x/c)\rangle - \alpha(t-x/c)\,\langle\sigma^\dagger(t-x/c)\rangle\right).\end{aligned} \tag{128}$$

Having found all equations of motion and the formal solutions for the quantities of interest, an exemplary case shall be studied in the following. A two-level system in the ground state at $t = 0$, coupled to a waveguide carrying a constant photon flux of rate r is described by the Hamiltonian and resulting equation of motion

$$H = \hbar\sqrt{\kappa r}(\sigma^\dagger + \sigma) \tag{129}$$

$$\partial_t \rho(t) = -\frac{i}{\hbar}[H, \rho(t)]. \tag{130}$$

The time dependence of the density matrix will not be explicitly stated in the following, the equations determining the solution read

$$\dot{\rho}_{11} = i\sqrt{r\kappa}(\rho_{21} - \rho_{12}) + \kappa\rho_{22} \tag{131}$$

$$\dot{\rho}_{12} = i\sqrt{r\kappa}(\rho_{11} - \rho_{22}) - \frac{\kappa}{2}\rho_{12}, \tag{132}$$

the other equations are determined by $\mathrm{Tr}[\rho] = \rho_{11} + \rho_{22}$ and $\rho_{21} = \rho_{12}^*$. By refining

$$\rho_x = \rho_{12} + \rho_{21} \tag{133}$$

$$\rho_y = \rho_{12} - \rho_{21}, \tag{134}$$

the equations reduce to

$$\dot{\rho}_x = -\kappa\rho_x \tag{135}$$

$$\dot{\rho}_y = -\frac{\kappa}{2}\rho_y - i\sqrt{r\kappa}(4\rho_{22} - 2) \tag{136}$$

$$\dot{\rho}_{22} = -i\sqrt{r\kappa}\rho_y - \kappa\rho_{22}. \tag{137}$$

The solution for ρ_x is straight forward, with $\rho_{12}(0) = 0$ it follows

$$\rho_x(t) = \rho_x(0)\,\mathrm{e}^{-\frac{\kappa}{2}t} = 0. \tag{138}$$

The remnant equations are of the form

$$\begin{pmatrix} \dot{\rho}_y \\ \dot{\rho}_{22} \end{pmatrix} = \begin{pmatrix} -\kappa/2 & -4i\sqrt{\kappa r} \\ -i\sqrt{\kappa r} & -\kappa \end{pmatrix} + \begin{pmatrix} 2i\sqrt{\kappa r} \\ 0 \end{pmatrix}. \tag{139}$$

The homogeneous system's eigenvalues read

$$\eta_\pm = -\frac{3}{4}\kappa \pm i\sqrt{4rk - \left(\frac{k}{4}\right)^2}. \tag{140}$$

With the initial conditions $\rho_{22}(0) = \rho_y(0) = 0$, i.e. the atom starts in the ground state, the solution to find the atom in the excited state is

$$\rho_{22} = \frac{4\kappa r}{\kappa^2 + 8\kappa r}\left[1 - \left(\frac{3\kappa}{4\Omega_{eff}}\sin\left(t\Omega_{eff}\right) + \cos\left(t\Omega_{eff}\right)\right)e^{-\frac{3\kappa t}{4}}\right], \tag{141}$$

with the effective Rabi frequency $\Omega_{eff} = \sqrt{4\kappa r - \left(\frac{k}{4}\right)^2}$. To emphasize the effect of the inherent coupling of driving strength and decay at a fixed photon number, a phase diagram is depicted in Fig. 16, showing the different behavior depending on coupling strength and photon rate. The dimensionless coupling constant utilized to characterize the system is

$$\lambda = \kappa\tau, \tag{142}$$

where τ is the length of the pulse that is incident on the system. The total number of photons in each individual pulse driving the system is not a fixed quantity but fluctuates about a mean value due to its coherent statistics. The mean photon number per pulse is

$$\bar{N} = \int \mathrm{d}t |\alpha(t)|^2. \tag{143}$$

The solution of the driven two level system allows for imaginary driving frequencies at $\kappa < r/64$, resulting in no oscillatory behavior, but a purely damped dynamic. A classical analog would be the overdamped case of an driven harmonic oscillator, which exponentially approaches its steady state. The energy exchange due to the driving field is still occurring, like in the classical analog, resulting in the nonzero excited state population. The above expression can be also expressed in terms of the photon number as $\lambda < \bar{N}/64$. The definition of Rabi oscillations is rather difficult, since there is no obvious indicator, however one can define a crossover at $\Omega_{eff}\tau = \pi$, which gives a critical photon number in the regime $\lambda \ll 1$

$$N_c = \frac{\pi^2}{4\lambda}. \tag{144}$$

In between these two regimes one is able to observe Rabi oscillations. The criterion is not to be confused with a perfect excitation transfer from the ground to the excited state, which is not possible within finite time, due to the damping. Yet one can achieve perfect excitation by shining in a single photon, exhibiting the waveform of a time-reversed single photon [41, 119]. The different regimes of the two-level system coupled to a waveguide can also be characterized by considering their behavior of the respective time trace of the excited state population as a function of time. The classical regime, where the system is only very weakly coupled to the driving field($\lambda \ll 1$) is recovered, in this case many photons are necessary to drive a Rabi oscillation, characterized by an overshoot of the Rydberg population. For sufficiently low photon numbers the system is not reaching its steady state within the finite width of the pulse, as visible by the continuous net absorption of photons, cf. Fig. 16 top left. For $\lambda \gg 1$ the enhanced emission results in strong damping of the system, preventing any Rabi oscillations. The driving field is strongly absorbed in the beginning, and the strong coupling leads to almost instantaneous relaxation of the system. The strong coupling also results in very fast spontaneous emission from the excited state at the end of the pulse, cf. Fig. 16 top right. In the intermediate regime, where the system is not critically damped multiple Rabi oscillations are visible even for very low photon numbers. The resulting modulation is visible in the driving field, where single photons are absorbed and either stimulated or spontaneously re-emitted into the mode. The photons interacting with the system are rearranged by the interaction with a single atom. A photon that was absorbed by the two-level atom in the ground state can subsequently stimulated by a consecutive photon to be coherently re-emitted, which leads to a higher probability of finding a photon pair. This can be considered as an effective attractive interaction between two photons mediated by a single two-level system. The opposite scenario, in which two photons simultaneously interact with the atom can be considered the opposite, since one photon is absorbed and emitted at a later instant of time, it corresponds to an effective repulsive interaction.

The region where Rabi oscillations occur is also appealing considering the effects of the outgoing wave function. The limit $\lambda \to 0$ corresponds as mentioned before to the classical limit, the interaction is so weak such that the outgoing photons are not altered, thus no correlations will arise. In the $\lambda \to \infty$ limit every incoming photon will excite the atom, but the atom will also decay on a very short time scale after the excitation. Resulting in correlations on a short time scale $\tilde{\tau}$. If the pulse is longer than this time scale, $\tau \gg \tilde{\tau}$ these correlations will not matter. In the intermediate regime the system output strongly depends on its previous history, since an photon entering the system, finding

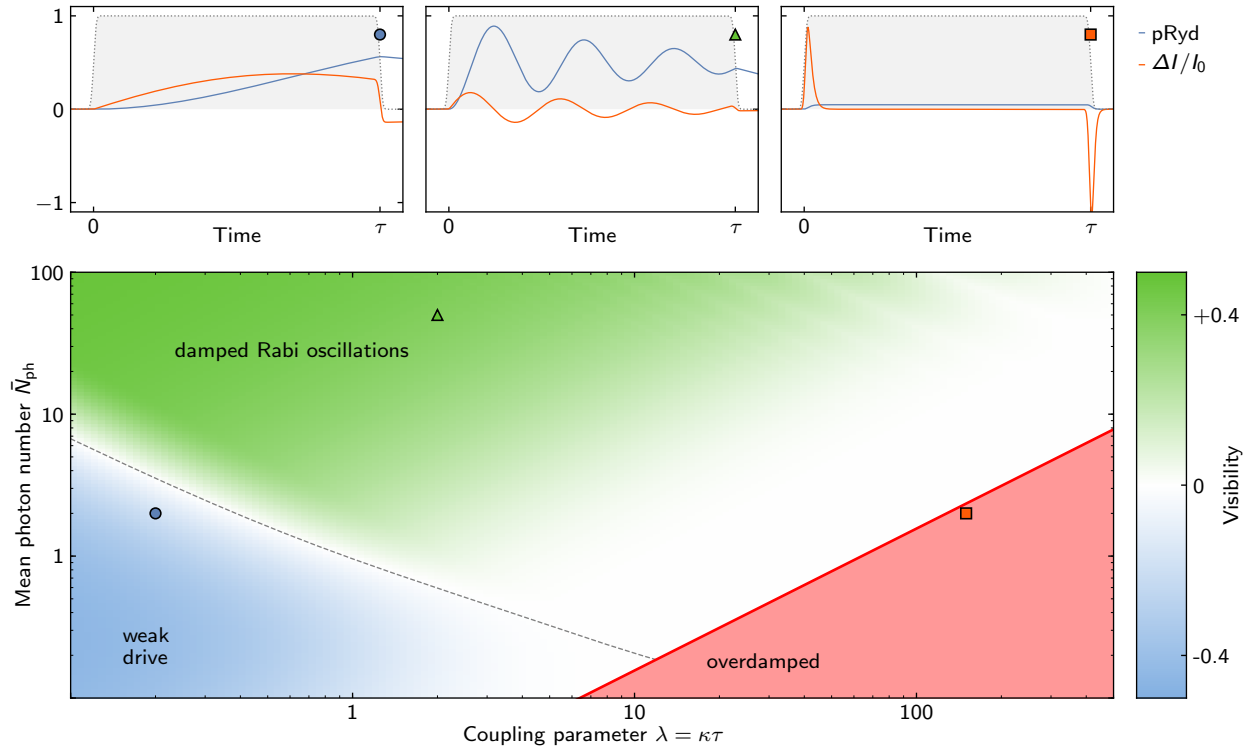

Fig. 16: Dynamical phase diagram of a driven atom in free space. (bottom) The diagram shows the visibility of Rabi oscillations, defined as $\max_{0\leq t\leq\tau}[\rho_{22}(t)] - \rho_{22}(t=\infty)$, of a two-level system driven by a propagating field. In contrast to cavity QED, the coupling and the decay of photons from the system are not independent in free-space and waveguide QED. For large coupling to the propagating mode ($\lambda = \kappa\tau \gg 1$) the enhanced emission into this mode results in an overdamped system, where the number of photons required to observe Rabi oscillations increases with coupling strength. For $\lambda \ll 1$, a large number of photons is required to drive the system with a π-pulse, defining a crossover (dashed line) between the regime of damped Rabi oscillations and the weak driving regime at lower mean photon number. The experiment, discussed in the following achieves coupling strength of $\lambda = 2.2$. (top) Exemplary solutions for the Rydberg population and relative outgoing intensity. The points indicated in the main diagram represent the coupling strength and photon number used in the respective solution. The relative modulation of the driving field I_0, $\Delta I/I_0 = (I_0 - I_{out})/I_{in}$ and is shown together with the rescaled input pulse (shaded gray).

the atom in the excited state will behave entirely different compared to a photon entering when the system is in the ground state. The resulting consequences will be studied in the following.

Note that the calculations conducted above are not specific to the initially considered setting of an atomic cloud, rather the opposite is the case. The theoretical treatment holds for any waveguide two-level system, which are being actively studied [28–32, 34–36, 120–123]. The main advantage compared to the experiments conducted in cavities comes from the fact that the output of the interaction, the driving field, is accessible after traversing the system, and not trapped inside of a resonator. The presented calculation, correct for arbitrary coupling strengths (as long as the rotating wave approximation holds), however opens up new challenges, to engineer the system such that the coupling strength can be boosted while getting control over the spontaneous emission related to it. This corresponds to a method requiring the decoupling of the coupling strength and spontaneous

decay. This can e.g. be done by simply switching on and off the coupling strength, e.g. using a two photon transition on an overall forbidden dipole transition. Another approach might rely on a waveguide exhibiting an photonic band gap that gets triggered by the presence of an atom in the excited state, thus preventing the spontaneous emission as well as the propagation of the driving field. However both approaches lack the possibility to coherently interact with multiple photons over multiple Rabi cycles.

5.2 Experimental Realization of a strongly coupled 2+1 level system in free space

Finding ways towards interacting photons is an longstanding goal[124]. If photons interact, they usually do at extremely high intensities. Finding ways to implement systems that behave differently, whether there are two photons or one photon at the input would implement a nonlinearity at the fundamental quantum level. A two-level system, both inside a cavity as well as in free space, is a nonlinear system. One manifestation is the scaling of the Rabi frequency with the square root of the photon number. Alternatively one can consider the process of absorption: after previously absorbing a photon, the consecutive photons will be transmitted, eventually leading to stimulated emission.

The limit in which individual photons result in an significant effect on the atom under consideration, other than the attenuation of a weak transmitted probe is difficult to access. It requires not only strong coupling, but also long coherence times, during which the atom remains phase coherent, allowing for continuous in phase interaction with a pulse. Even though significant progress is being made, such as an attenuation in the range of 10 % with single quantum systems such as molecules, atoms and quantum dots [29, 125, 126], the strong coupling, such that a few-photon field coherently drives the system is still outstanding.

In contrast to the aforementioned idea of coupling a *real* two-level system to a light field, we use the previously introduced collective enhancement of a Rydberg superatom [89, 112–114, 127–129].

By utilizing the implications resulting from the collective behavior, such as the highly directed emission and the increased coupling, the system under consideration is well described by the previously described theory for a coupled two-level system interacting with a 1d waveguide.

Even though the main experimental steps have already been introduced in Sec. 2, the exact preparation shall be briefly summarized [38]. To prepare the ultracold atomic ensemble that forms the single Rydberg superatom, initially ^{87}Rb atoms are captured in a magneto-optical trap (MOT) from 10^{-10} mbar rubidium background pressure in an ultra-high vacuum chamber, resulting in 5×10^6 laser-cooled atoms after 1 s of loading. After compressing the MOT by increasing the gradient of the quadrupole magnetic field, the atoms are loaded into the dipole trap formed by two crossed 1070 nm beams, intersecting under an angle of 31.4 °, and an additional elliptic dimple beam at 855 nm perpendicular to the long axis of the original trap. Subsequently, atoms are further cooled by forced evaporation for 700 ms by reducing the power of the two 1070 nm dipole trap beams. During evaporative cooling the cloud is additionally cooled during two stages of Raman Sideband Cooling. The stages are 10 ms long and occur after 89 ms and 589 ms of evaporation, eventually reaching a final cloud temperature of 6 μK. The final atomic cloud contains $\approx$ 25000 atoms in a pancake shaped harmonic trap, with a Gaussian density profile with widths $\sigma_z = 6\,\mu$m and $\sigma_r = 10\,\mu$m. The Rydberg state $|111S_{1/2}\rangle$ was chosen such that the longitudinal diameter of the cloud as well as the transverse diameter of the probe beam are significantly smaller than the minimum Rydberg blockade radius $r_b = 25.5\,\mu$m at highest photon rate $\mathcal{R}_{\text{in}} = 12.4\,\mu\text{s}^{-1}$, resulting in a fully blockaded ensemble of

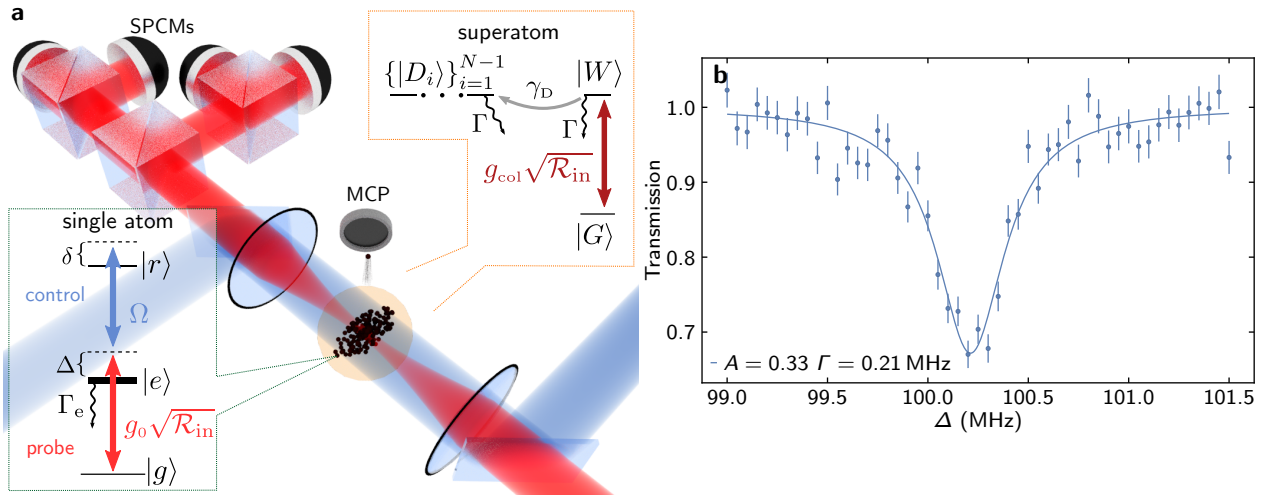

Fig. 17: Experimental Setup and absorption of the excited state on two-photon Raman resonance. **a** Experimental setup and level scheme. An ensemble of laser-cooled atoms is confined within a blockade volume using an optical dipole trap. Single-photon counting modules (SPCMs) are used to detect the light that interacts with the atoms while a multi-channel plate (MCP) detects the Rydberg atoms after ionization. A few-photon probe field (red) and a strong control field (blue) couple the single atom ground state $|g\rangle$ to a Rydberg state $|r\rangle$. Their respective Rabi frequencies are $g_0\sqrt{\mathcal{R}_{\text{in}}}$ and Ω, where g_0 is the single atom coupling constant for the probe field and $\mathcal{R}_{\text{in}}$ is the photon rate. Due to the Rydberg blockade, the whole ensemble collectively behaves like a two-level system with many-body states $|G\rangle$ and $|W\rangle$ including a loss channel to a set of collective dark states $\{|D_i\rangle\}_{i=1}^{N-1}$. **b** Absorption spectra of the $|111S_{1/2}\rangle$ Rydberg state at an intermediate state detuning of 100 MHz. Emphasizing the strong absorption of 33 % for a weak probe field of $\bar{n} = 0.94$ photons, where $\Gamma = 0.21$ MHz is the half width at half maximum.

atoms.

The restriction to a cloud smaller than the blockade radius is the essential step in achieving a strongly coupled two-level system. If the cloud size exceeds the blockade radius the position of the superatom and thus the number of atoms contributing to it varies. Each superatom, when resonantly driven, oscillates at its own Rabi frequency determined by the number of atoms that contribute to it, which will washout the contrast of the dynamics of interest. Furthermore the probability to excite more than one atom results in multiple excited states coupled due to the van der Waals interaction among the superatoms.

The single Rydberg superatom is eventually implemented by focusing a weak 780 nm probe field (beam waist $w_{\text{probe}} = 6.5\,\mu$m), together with a strong counter-propagating control field at 479 nm (beam waist $w_{\text{control}} = 14\,\mu$m) into the optically trapped atomic ensemble. The few-photon coherent probe field, with a photon rate $\mathcal{R}_{\text{in}}$, couples the ground $|g\rangle = \left|5S_{1/2}, F = 2, m_F = 2\right\rangle$ and intermediate $|e\rangle = \left|5P_{3/2}, F = 3, m_F = 3\right\rangle$ states with a Rabi frequency $g_0\sqrt{\mathcal{R}_{\text{in}}}$, where g_0 is the single-atom–single-photon coupling constant, determined by the geometry of the setup, which will be elucidated below. The control field provides coupling between $|e\rangle$ and the Rydberg state $|r\rangle = \left|111S_{1/2}, m_J = 1/2\right\rangle$ with Rabi frequency $\Omega = 2\pi \times 10$ MHz. Using a large intermediate-state detuning $\Delta = 2\pi \times 100\,\text{MHz} \gg \Gamma_e, \Omega$, the intermediate state can be adiabatically eliminated, cf Sec. 4.1. Setting the two-photon detuning δ to Raman resonance the dynamics for each atom simplify to those of a resonantly coupled two-level system between $|g\rangle$ and $|r\rangle$ with effective Rabi frequency $g_0\sqrt{\mathcal{R}_{\text{in}}}\Omega/(2\Delta)$. The decay of $|r\rangle$

is dominated by spontaneous Raman decay via the intermediate state $|e\rangle$ with rate

$$\Gamma = \Omega^2/(2\Delta)^2\Gamma_\mathrm{e}. \tag{145}$$

The experimental setup along with the relevant levels for a single and the superatom are depicted in Fig. 17. Due to the finite detuning from the intermediate state, a probe photon is transmitted through the cloud with transmission $T = 0.99$, which is for simplicity not expressed in the further description of the system, but taken into account in all evaluations.

The actual experiment starts by sending a Tukey shaped probe pulse into the atomic medium. The resulting dynamics are probed by either counting the outgoing photons on four single photon counting modules, or by applying a fast field ionization pulse at various times to probe the Rydberg population by counting the created ions on the MCP, cf. Fig. 17. The symmetric Tukey shaped pulse is described by

$$f(t, t_{rise}, t_{up}) = \begin{cases} \frac{1}{2}\left\{1 + \cos\left(\pi\left[\frac{t+t_{rise}+t_{up}/2}{t_{rise}} - 1\right]\right)\right\} & \text{if} \quad -t_{rise} - \frac{t_{up}}{2} \leq t < -\frac{t_{up}}{2} \\ 1 & \text{if} \quad -\frac{t_{up}}{2} \leq t < \frac{t_{up}}{2} \\ \frac{1}{2}\left\{1 + \cos\left(\pi\left[\frac{t+t_{up}/2}{t_{rise}}\right]\right)\right\} & \text{if} \quad \frac{t_{up}}{2} \leq t < t_{rise} + \frac{t_{up}}{2} \\ 0 & \text{otherwise,} \end{cases} \tag{146}$$

where $t_{rise} = 0.8\,\mu$s and $t_{up} = 5\,\mu$s was used in the experiments. The superatom concept introduced Sec. 4.3 needs to be refined, since in the experiment the atoms are not perfectly at rest, they dynamically dephase into the dark state subspace and consequently do not interact with the driving field. The Rabi frequency on the transition between $|G\rangle$ and $|W\rangle$ is $g_{col}\sqrt{\mathcal{R}_{in}}$ with

$$g_{col} = \sqrt{N}\frac{g_0\Omega}{2\Delta}. \tag{147}$$

The collective coupling strength g_{col} results from the collective contribution of all atoms, which boosts the single photon coupling strength by $\sqrt{N}$, as described in Sec. 4.3.

In Fig. 18**a** and **b** the resulting average photon time traces and ion signals for an input photon rate of $\mathcal{R}_\mathrm{in} = 12.4\,\mu\mathrm{s}^{-1}$ and $\mathcal{R}_\mathrm{in} = 2.6\,\mu\mathrm{s}^{-1}$ are depicted. The collectively enhanced Rabi oscillation of the Rydberg population, given by the sum of the populations in the $|W\rangle$ and the dark states $\{|D_i\rangle\}_{i=1}^{N-1}$, are observed [89, 112–114, 127–129]. Importantly, the number of Rydberg atoms throughout the whole pulse stays below one, showing that the ensemble is indeed fully blockaded and well-described as a single superatom. The coherent dynamics of the system also cause a periodic modulation of the outgoing photon rate $\mathcal{R}_\mathrm{out}$. Fig. 18**c** shows this modulation $\Delta\mathcal{R}(t) = \mathcal{R}_\mathrm{in}(t) - \mathcal{R}_\mathrm{out}(t)$ for a range of input rates, down to $\mathcal{R}_\mathrm{in} = 1.5\,\mu\mathrm{s}^{-1}$, which corresponds to a mean number of photons $\bar{N}_\mathrm{ph} = 9$ in the probe pulse. The modulation, small compared to the overall driving amplitude, results from a two-level system which can only absorb and emit a single photon. There fore the amplitude modulation cannot exceed ± 1 photon. Comparing Fig. 18**a** and **b**, the modulation for the lower input photon number is larger, yet the absolute modulation is similar.

As introduced before, a superatom consisting of N atoms provides one bright state $|W\rangle$ and $N-1$ dark states that are decoupled from the driving field. Since there is no easy procedure to measure the exact dark state, and since the dark states are not unique, the manifold of all $N-1$ dark states are considered as an additional manifold into which the excited state $|W\rangle$ can dephase, as depicted in Fig. 17. The dephasing mechanism on the one hand is due to thermal motion of the atoms during the pulse, which is assumed to be the main contribution and on the other hand due to coherent exchange interaction among the atoms within the cloud [116, 117, 120, 130–132]. In order to refine

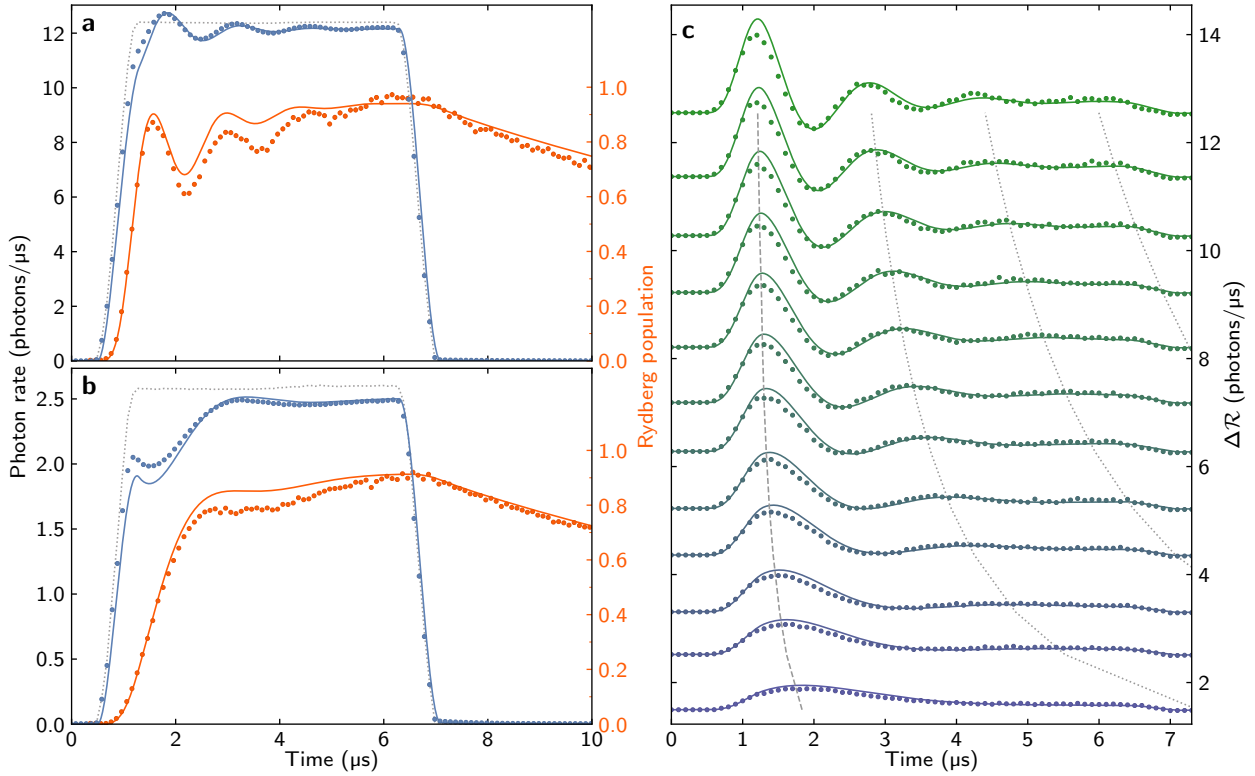

Fig. 18: Time evolution of photon signal and Rydberg population. **a** and **b** Time traces of the outgoing probe photon rate (blue points) and Rydberg population (orange points) for input pulses (dashed gray line) with peak photon rates $\mathcal{R}_{\text{in}} = 12.4\,\mu\text{s}^{-1}$ **a** and $\mathcal{R}_{\text{in}} = 2.6\,\mu\text{s}^{-1}$ **b**, corresponding to mean number $\bar{N}_{\text{ph}}$ of 71.6 and 15.1 photons in the pulse. The Rabi oscillation of the single superatom is visible both in the excited state population and in the modulation of the transmitted probe light. Solid lines are fits to the data using the theoretical model including the dark state subspace. **c** Difference signal $\Delta\mathcal{R}(t)$ between the incoming and outgoing pulses (dots) for different input photon rates $\mathcal{R}_{\text{in}}$. Each data set is vertically shifted by the corresponding $\mathcal{R}_{\text{in}}$. Solid lines are again the result of fitting the full data set with the theory model using a single set of fit parameters. Dashed lines indicate the expected positions of the Rabi oscillation peaks based on the fitted parameters, showing the scaling of the Rabi period with $1/\sqrt{\bar{N}_{\text{ph}}}$. Error bars in (a-c) are SEM and are smaller than the data points.

the previously defined description Eq. 126, two effects need to be taken into account. Firstly the superatom is made up of $\approx 10^4$ individual atoms, which decay to free space with their spontaneous decay rate Γ via the intermediate state $|e\rangle$. Secondly the dephasing of the bright state into the dark state manifold with rate γ_D. These processes are accounted for by adding two additional Lindblad terms to Eq. 126,

$$\begin{aligned}\partial_t\rho(t) = &-\frac{i}{\hbar}\left[H_0(t),\rho(t)\right] + (\kappa+\Gamma)\mathcal{L}\left[\sigma_{GW}\right]\rho(t)\\ &+\gamma_D\mathcal{L}\left[\sigma_{DW}\right]\rho(t) + \Gamma\mathcal{L}\left[\sigma_{GD}\right]\rho(t).\end{aligned} \tag{148}$$

Since the system includes now three levels the transition operators are now denoted as $\sigma_{ij} = |i\rangle\langle j|$, the Hamilton operator is identical with Eq. 124 describing the interaction between the levels $|W\rangle$ and $|G\rangle$,

$$H_0(t) = \hbar\sqrt{\kappa}(\alpha(t-t_0)\sigma^\dagger_{GW} + \alpha^*(t-t_0)\sigma_{GW}), \tag{149}$$

where the input photon rate is related to $\alpha(t) \in \mathbb{R} \forall t$ as $\mathcal{R}_{\text{in}} = |\alpha(t)|^2$. The outgoing intensity is given by evaluating Eq. 128, where similar to above the operators σ need to be replaced by σ_{GW}. The solid lines in Fig. 18**a**,**b**,**c**, are the result of fitting the above model to the respective sets of time traces. For the set in Fig. 18**a**,**b**,the obtained values read $\kappa = 0.428\,\mu\text{s}^{-1}$, $\Gamma = 0.069\,\mu\text{s}^{-1}$, and $\gamma_D = 1.397\,\mu\text{s}^{-1}$. For the set in Fig. 18**c** the parameters are found by fitting the all time traces with one set of parameters, which gives $\kappa = 0.322\,\mu\text{s}^{-1}$, $\Gamma = 0.069\,\mu\text{s}^{-1}$, and $\gamma_D = 1.326\,\mu\text{s}^{-1}$. The differences in κ and γ_D between the two data sets stem from slightly different number of atoms N in the superatom for the two experiment runs.

The experimental determination of Ω, N and Δ is straightforward, in contrast to g_0, the single-photon–single-atom coupling strength, which requires the definition of an electric field per photon. The calculation from experimental parameters will be outlined in the following. The energy of one photon $\hbar\omega_0$ is in principle infinitely transversely distributed for a Gaussian beam, in a first approximation the Gaussian beam of waist w is scaled to a box potential of width w in transverse direction, such that its integrated intensity remains constant. Now the power P of one transmitted photon corresponds to $P = \hbar\omega_0 \times \mathcal{R}$, where the photon rate $\mathcal{R}$ was used in order to arrive at a meaningful quantity, since one would otherwise rely on the definition of an arbitrary unit time. Since the final result shall be independent of the incoming photon rate the power will be rescaled by the incoming photon rate $\tilde{P} = P/\mathcal{R}$. The intensity of one photon, i.e. the energy flux per area is then given by $I = \tilde{P}/(\pi w^2)$, from which one easily finds the electric field per photon $E = \sqrt{2I/(c\epsilon 0)}$, where c is the speed of light and ϵ_0 the vacuum permittivity. The single-photon–single-atom coupling strength then results in

$$g_0 = \frac{dE}{\hbar}, \tag{150}$$

in analogy to the classical case. However the dimension of $[g_0] = 2\pi\,\text{MHz}\sqrt{\text{s}}$ is peculiar, since it depends on the mean *length* of a photon, which is inversely proportional to the rate. Thus effectively the photon is quantized within a volume given by the transverse mode and its mean length. In the presented experiment $g_0 \approx 289\,\text{Hz}\sqrt{\text{s}}$. Since the probe beam is smaller than the atomic cloud the number of atoms contributing to the superatom can be determined by measuring the resonant absorption of the probe pulse.

Following the lines of the previous findings, and the implications found for coupling to a bath in the absence of any additional decay, it follows that a single atom in free space is ultimately limited to a coupling strength equal to its spontaneous emission rate Γ. Which only holds for perfect mode-matching and is thus experimentally extremely hard to achieve [41, 119], which is further illustrated in Sec. 6. The intrinsic damping in any free space and waveguide system furthermore prevents perfect transfer of a photonic qubit to a matter qubit within a finite time [41, 119, 133, 134].

In the superatom case, the coupling $g_{col} \sim \sqrt{\kappa}$ and the decay κ into a specific mode can be boosted solely through the collective enhancement of the atom-light interaction, without any confinement of the propagating light field. As a consequence, the superatom spontaneously emits with probability $\beta = \kappa/(\kappa + \Gamma) = 0.86$ into the forward direction of the strongly coupled mode, while loss of photons due to scattering out of the propagating mode with rate Γ is minimal. The superatom thus provides the perfect test bed for quantum electrodynamics in free space.

5.3 Photon-Photon Correlations arising from the strongly coupled 2+1 level system

As previously illustrated a two-level system can mediate an effective interaction among distant photons of attractive and repulsive nature, depending on the state of the system. The effective interaction will lead to a rearrangement of the photons in the coherent pulse, which eventually results in temporal correlations of the individual photons. Having access to the full counting statistics of the outgoing

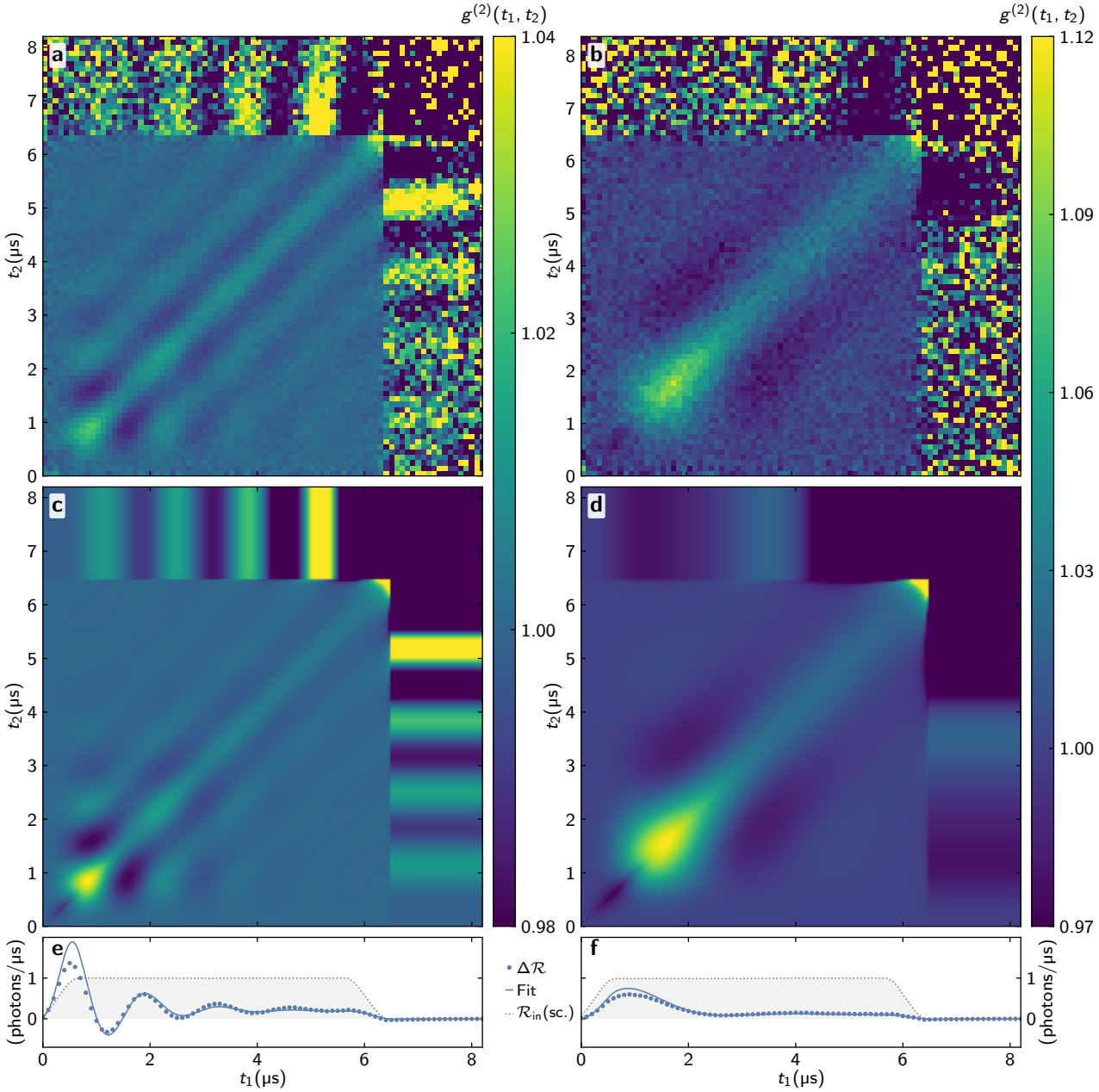

Fig. 19: Correlations of the outgoing probe field. **a** and **b** Measured two-time correlations $g^{(2)}(t_1, t_2)$ for pulses with $\mathcal{R}_{\text{in}} = 12.4\,\mu\text{s}^{-}1$ and $\mathcal{R}_{\text{in}} = 2.5\,\mu\text{s}^{-1}$ corresponding to the time traces in Fig. 18**a**,**b**. **c** and **d** Corresponding calculated correlations functions using the values of κ, Γ and γ_D obtained by fitting the time traces in Fig. 18**a**,**b**. **e** and **f** Measured (dotted) and simulated (solid) $\Delta\mathcal{R}_{\text{in}}$ together with scaled input pulses (dashed gray) for reference.

photon field, it allows to investigate how the dynamics of the coupled system result in correlations between individual outgoing probe photons. Fig. 19**a**,**b** show the measured two-time correlation functions $g^{(2)}(t_1, t_2)$ for input photon rates of $\mathcal{R}_{\text{in}} = 12.4\,\mu\text{s}^{-1}$ and $\mathcal{R}_{\text{in}} = 2.5\,\mu\text{s}^{-1}$. The superatom, while interacting with the probe pulse, periodically manipulates the light field by absorbing and stimulated emitting photons in and out of the pulse resulting in a periodic structure of bunching and antibunching features in the correlation function. The visibility of these features emphasizes the long coherence time of the superatom-photon interaction. The measurement also shows correlations beyond the probe pulse. These correlations arise due to the fact, that the system has a finite probability to be in the excited state, after the pulse has left the medium at time t_{end}, and will still emit in forward direction with rate κ. If a photon is detected at time t_i, then depending on whether the time difference $t_{end} - t_i$ to the end of the pulse is a integer multiple of the Rabi period, the spontaneously emitted photons will be bunched or antibunched. Resulting in a periodic modulation of $g^{(2)}(t_i, t_2)$ for $t_2 > t_{end}$.

The evaluation of the two-point correlation function, in contrast to the intensity expectation value, requires the determination of correlations of the operators $\sigma^{\dagger}_{GW}(t)$ at different times, i.e

$$g^{(2)}(s_1, s_2) = \frac{\langle E^{\dagger}(s_1)E^{\dagger}(s_2)E(s_2)E(s_1)\rangle}{\langle E^{\dagger}(s_1)E(s_1)\rangle\langle E^{\dagger}(s_2)E(s_2)\rangle}, \tag{151}$$

where for completeness the retarded time $s_i = t_i - x_i/c$ was used. In principle one could measure the arising correlations by only detecting photons at a fixed time t_i and moving the detectors with respect to the system, yet this is experimentally unfeasible. The correlations depicted in Fig. 19, are multi-time correlations for fixed x/c.

5.4 Quantum regression theorem

The theoretical prediction of multi-time correlations of operators in a driven dynamic system is not straight forward and requires further discussion. The time evolution of a two-time ensemble average can be calculated in a rigorous manner [67, 135], but relies on the exact history of both system and reservoir. By applying an periodic driving term to the full system, both parts, the system under consideration and the bath that it is coupled to will follow a possibly correlated periodic behavior.

The procedure outlined in [67, 135–137] and described below initially does not assume any constraints on the system under consideration, thus a modification of the bath by the system and vice versa might, dependent on the specific interaction lead to a back action of the system on the bath at a later instance of time due to their interaction.

The derivation of the master equation in Sec. 5.1, did not rely on approximation factorizing the density matrix due to the fact that the photons leaving the two-level system will not interact with the system again and thus do not result in any back action of the system on itself. This is exactly the requirement for the validity of the quantum regression theorem [138]. Thus the expectation values required to determine Eq. 151 can be determined by the quantum regression theorem without involving any additional approximations.

Starting from a full density matrix that does not need to be factorizable, the multi-time expectation value of two system operators A and B are determined by [67]

$$\langle A(t+\tau)B(t)\rangle = \text{Tr}\left[A(t+\tau)B(t)\rho(t_0)\right], \tag{152}$$

where $\tau > 0$; the entire time evolution here is determined by the time evolution of the operators A and B, Tr denotes the trace over the full density matrix $\rho(t_0)$ of system and bath. Switching to the Schrödinger picture utilizing the unitary time evolution operator $U(t, t_0)d$ for the full system, and using the cyclic property of the Tr, the expectation value reads [67, 135]

$$\begin{aligned}\langle A(t+\tau)B(t)\rangle &= \mathrm{Tr}\left[U^\dagger(t+\tau)A\underbrace{U(t+\tau,t_0)U^\dagger(t,t_0)}_{U(t+\tau,t)}BU(t,t_0)\rho(t_0)\right] \\ &= \mathrm{Tr}\left[AU(t+\tau,t)B\underbrace{U(t,t_0)\rho(t_0)U^\dagger(t,t_0)}_{\rho(t)}U^\dagger(t+\tau)\right] \end{aligned} \tag{153}$$

$$= \mathrm{Tr}_S\left[A\,\mathrm{Tr}_B\left[U(t+\tau,t)B\rho(t)U^\dagger(t+\tau)\right]\right]. \tag{154}$$

Eq. 154 then takes the form of an ensemble average of A, in a system described by the effective density matrix $B\rho(t)$ evolved in time to time $t+\tau$. Recalling Eq. 120 and using that the operator A does not act on the bath part of the density matrix the equation of motion for the effective density with respect to *tau*,

$$\chi(\tau, t) = U(t+\tau, t)B\rho(t)U^\dagger(t+\tau), \tag{155}$$

is

$$\partial_\tau \chi(\tau, t) = -\frac{i}{\hbar}[H, \chi(\tau, t)]. \tag{156}$$

Eq. 156 still relies on the dynamics of the full system including bath and system. In order to arrive at a master equation which relies solely on the dynamics of the system the bath part of the full density matrix is required to be integrated out, i.e.

$$\chi_S(\tau, t) = \mathrm{Tr}_B\left[\chi(\tau, t)\right]. \tag{157}$$

In order to express $\chi(\tau, t)$ independent of the exact dynamics of the full system, the density matrix needs to be factorizable at any time t, i.e.

$$\rho(t) = \rho_S(t) \otimes \rho_B(t), \tag{158}$$

where the indices S and B indicate the respective subsystem's density matrix, system and bath. What is neglected in the previous approximation are the possible correlations between system and bath [135], which is known as Markov approximation.

Eq. 148 can be expressed by introducing the Lindblad super-operator for the system $\tilde{\mathcal{L}}(t)$, to read

$$\partial_t \rho_S(t) = \tilde{\mathcal{L}}(t)\rho_S(t), \tag{159}$$

the formal solution to this problem can then be stated as

$$\rho_S(t) = \mathcal{T}\,\mathrm{e}^{\int_{t_0}^{t}\mathrm{d}t'\tilde{\mathcal{L}}(t')}\,\rho_S(t_0) \equiv \mathcal{V}(t, t_0)\rho_S(t_0), \tag{160}$$

given the initial density matrix $\rho_S(t_0)$. $\mathcal{T}$ denotes the time ordering operator and $\mathcal{V}(t, t_0)$ describes the time evolution operator for the density matrix from t_0 to t. The time evolution operator fulfills [67]

$$\mathcal{V}(t_0, t_0) = 1 \tag{161}$$

$$\mathcal{V}(t, t_1)\mathcal{V}(t_1, t_0) = \mathcal{V}(t, t_0). \tag{162}$$

By quenching the correlations between system and bath, i.e. applying the Markov approximation, Eq. 157 can be further simplified to give

$$\chi_S(\tau, t) = \mathcal{V}(t+\tau, t)\,\mathrm{Tr}_B\left[\chi(0,t)\right] \tag{163}$$

$$= \mathcal{V}(t+\tau, t)\{B\rho_S(t)\}. \tag{164}$$

The curly brackets denote the operator that the super-operator acts on, here $B\rho_S(t)$, since the order of operation matters for a super-operator.

Now the two-time correlation function can be calculated to be

$$\langle A(t+\tau)B(t)\rangle = \mathrm{Tr}_S\left[A\mathcal{V}(t+\tau)\{B\rho_S(t)\}\right]. \tag{165}$$

The correlation function can now be evaluated without the knowledge of the full bath dynamics, yet at the cost of assuming only short correlation times of the bath or weak interaction between bath and system for a general system. The bath and system in the case of a propagating mode coupled to a single atom do not rely on this approximation, since as stated previously, the outgoing photons do not interact with the system again and no correlations between bath and system build up [138].

Eq. 151 requires the evaluation of four operators at two different times, using the same procedure as above one finds

$$\langle A(t_0)B(t_1)C(t_1)D(t_0)\rangle = \mathrm{Tr}_S\left[BC\mathcal{V}(t_1, t_0)\{D\rho_S(t_0)A\}\right]. \tag{166}$$

Since it is not straight forward to evaluate $\mathcal{V}(t, t_0)$ for arbitrary times, it is reasonable to numerically propagate $\rho_S(t_0)$ to $\rho_S(t)$ [67],

$$\rho(t_0) = \mathcal{V}(t, t_0)\rho_S(t_0) = \mathcal{T}\,\mathrm{e}^{\int_{t_0}^{t}\mathrm{d}t'\tilde{\mathcal{L}}(t')}\,\rho_S(t_0) \tag{167}$$

$$\approx \exp\left(\sum_{n=0}^{N}\tilde{\mathcal{L}}(t_n)\Delta t\right)\rho_S(t_0) \tag{168}$$

$$= \prod_{n=0}^{N}\exp\left(\tilde{\mathcal{L}}(t_n)\Delta t\right)\rho_S(t_0). \tag{169}$$

In order to fulfill the time ordering $t_i < t_j$ for $i < j$, for simplicity the time steps are assumed to be constant, $\Delta t = t_{j+1} - t_j$ for any j. Using this procedure the correlation functions depicted in Fig. 19**c**,**d** were simulated.

The numerical results recover all features of the experimental result, including the correlations beyond the end of the pulse. The visible modulation of the correlation function for large time differences, does not only emphasize the long coherence time of the superatom, but also the possibility of entanglement between photons separated by up to $5\,\mu$s[139]. Considering two consecutive incoming photons, the first photon can either be absorbed while exciting the superatom or transmitted. The second photon then has restricted options. Depending on whether the superatom state is occupied or not, the photon can be transmitted, absorbed or lead to stimulated emission. Thus photons subsequently interacting with a single two-level system become entangled.

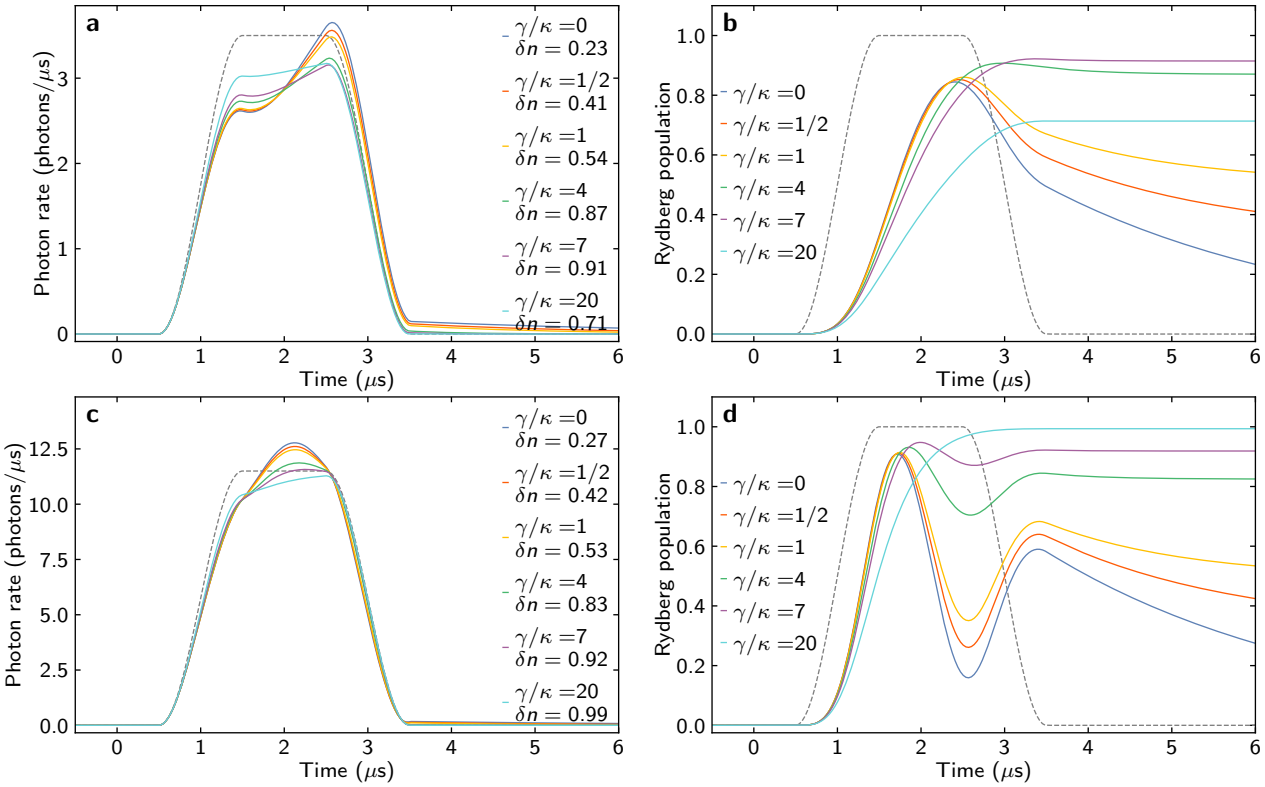

Fig. 20: Driven superatom for variable dephasing rates. **a** Output pulse for various dephasing rates γ_D and fixed coupling strength κ. The input is a coherent state $\bar{n} = 7$. δn corresponds to the number of photons absorbed from the pulse. **b** Rydberg population corresponding to **a**. For the highest dephasing rate the population only slowly accumulates in the darkstate, whereas the lower dephasing rates show that the dephasing closely follows the behavior without dephasing, thus providing efficient transfer to the dark states. **c** Identical to **a** but with input photon number $\bar{n} = 23$. The modulation of the input field varies with dephasing rate. **d** Rydberg population corresponding to **c**. Only the highest dephasing rate fully prevents any visible Rabi oscillations.

5.5 Utilizing the dephasing mechanism - a single photon absorber

The work presented in the following was a joint effort by Christoph Tresp, Christian Zimmer, Ivan Mirgorodskiy, Hannes Gorniaczyk, Asaf Paris-Mandoki, Sebastian Hofferberth [45, 98]. In this subsection the theory describing a single superatom will be used to describe the results obtained in [98].

In principle the dephasing of the collective bright state $|W\rangle$ into the dark state manifold $\{|D\rangle\}_{i=0}^{N}$ is desired to be as low as possible, since it limits the maximally achievable time the atom is actively interacting if $\gamma_D > \kappa$. If the dephasing is however properly engineered, the superatom is fully dephased within a time shorter than the input pulse, thus removing a single photon from the input pulse. This enables the collective ensemble of individual atoms to collectively absorb a single photon from arbitrary input pulse[98, 140].

The experiment is very similar to the previously described experiment described in Sec. 5.2, except for the Rydberg state $|121S_{1/2}, m_J = 1/2\rangle$ that is addressed with a Tukey pulse of $t_{rise} = 1\,\mu$s and $t_{up} = 1\,\mu$s. In order to function as a single photon absorber the system is required to deterministically

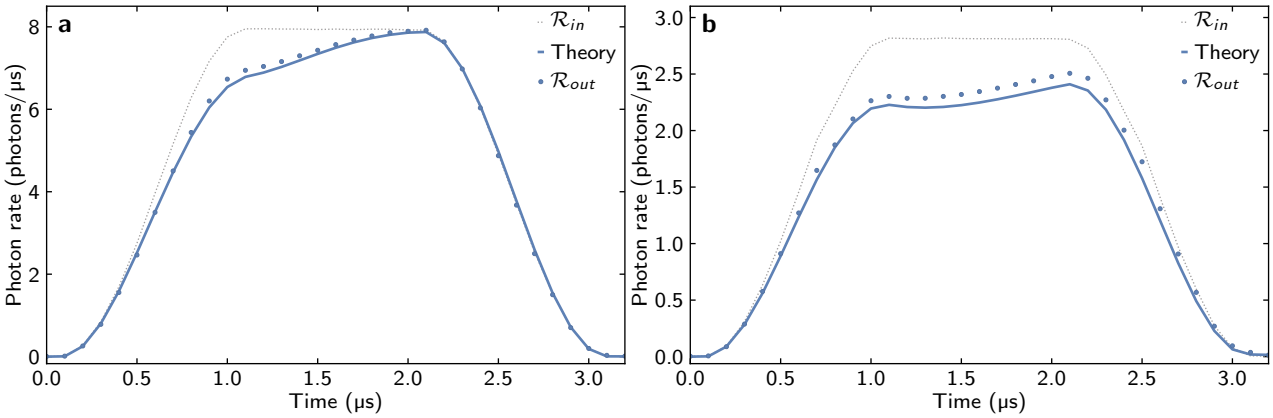

Fig. 21: Pulse distortion of the incoming pulse. **a** Output pulse shape after traversing the superatom. For input photon number of $\bar{n} = 15.76$ The pulse is mainly distorted in the first half, indicating that it absorbs a photon from the beginning of the pulse. **b** A pulse of width $\bar{n} = 5.65$ shows the same behavior the first half of the pulse exhibits a stronger deformation than the second half.

reduce the input photon number by exactly one, independent of the underlying dynamics, that occur during the pulse propagation. This requires the dephasing to be fast enough but also not to be too large, since at high dephasing rates the dynamics of the single $|W\rangle$ state are irrelevant, since the relevant timescale $\kappa \ll \gamma$, which results in an effective damping from the ground state directly into the dark state manifold. This scenario is emphasized in Fig. 20, where $\kappa = 0.3\,\mu\text{s}^{-1}$ is fixed for the Tukey pulse used in the experiment. The deterministic absorption is peaked around an optimal dephasing rate for a given driving constant κ, thus further increasing the dephasing will only allow deterministic subtraction for either sufficiently long pulses or a strong enough driving field. At some input photon rate $\mathcal{R}_{in}$, the system, as described above exhibits Rabi oscillations, which lead to a periodic modulation of the absorption probability as a function of the photon rate, since the system is then either in the ground or excited state, where an excitation resides within the cloud. The issue related to Rabi oscillations for deterministic photon subtraction results from the fact that there is a significant probability with which the superatom occupies the $|W\rangle$ state, that is then decaying in forward direction and thus emits the photon that should be absorbed. Since eventually the process always relies on the initial coherent evolution to achieve a fast excitation, the control field is turned off at the end of the pulse. This effectively freezes the excited state population and prevents decay, both collectively in forward direction and via the intermediate state.

By fitting the model presented in Sec. 5.2 to all of the data presented in [98], the coupling strength and dephasing rate can be found. The decay via the intermediate state is again given by the Rabi frequency of the control field and assumed to be mostly unaltered, i.e. $\Gamma = 0.069\,\mu\text{s}^{-1}$. The other parameters are determined to be $\kappa = 0.294\,\mu\text{s}^{-1}$ and $\gamma_D = 1.985\,\mu\text{s}^{-1}$. Two pulses containing initially $\bar{n} = 15.76$ and $\bar{n} = 5.65$ photons are depicted in Fig. 21. The deformation of the pulse ultimately results in a reduction of band width of the pulse. A photon at the front of the pulse is always exhibiting a higher probability of being absorbed, since the medium is initially in its ground state. The deformation is inevitable for a realistic system [141], however an infinitely long medium, absorbing infinitely small portions of the pulse can in principle avoid the deformation, since it couples identically to all photons in the pulse. The deformation of the pulse in the case of perfect absorption, i.e. the first photon entering the medium excites the superatom to the bright state and immediately dephases and thereby decouples from the light field, would split the pulse. The first part containing the probability amplitude of one photon will be cut off, the remaining part is unchanged. Considering

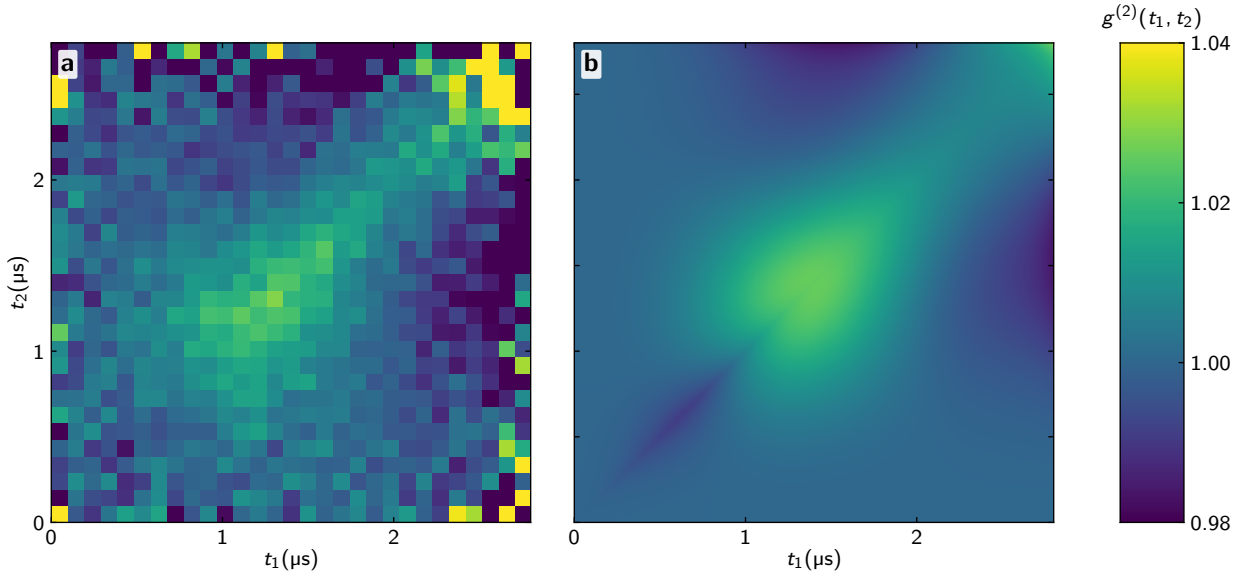

Fig. 22: Second order correlation function after photon subtraction for a coherent input pulse $\bar{n} = 15.76$. **a** Measured correlation function for the pulse in Fig. 21**a** The sub-Possoinian statistics after photon subtraction result from the immediate loss, reducing the probability of finding two photons within a time interval. After full subtraction the coherent field exhibits a photon distribution of the initial state but its actual mean value corresponds to $\bar{n} - 1$ thus leading to super-Possoinian counting statistics **b** Simulated correlation function using the model discussed before for $\kappa = 0.294\,\mu\text{s}^{-1}$, $\gamma_D = 1.985\,\mu\text{s}^{-1}$, $\Gamma = 0.069\,\mu\text{s}^{-1}$

multiple superatoms that perfectly absorb light, each absorption process will reduce the length of the pulse, thus increasing the pulse bandwidth. Having absorbed many photons, at some point the pulse bandwidth is likely to exceed the bandwidth with which a superatom can absorb a photon, thus the input wave package is in part detuned from resonance.

When considering the absorption of photons from a coherent pulse one expects the statistics of the pulse to be altered, since the width of the distribution is unchanged but one photon is missing. This leads to a super-Possonian distribution after absorbing a photon, which is visible during the time in which the pulse is distorted, cf. Fig. 22. In the intermediate vicinity of the absorption process the subtraction results in antibunching, since compared to a coherent pulse it is less likely to find a second photon in its immediate vicinity.

6 Comparing Cavity and Free Space QED

This section will attempt to outline the fundamental similarities and differences between QED in free space compared to cavity QED. The special scenario of a system decoupling from the driving field will be briefly discussed.

Note that QED, includes a wide variety of systems that are being coupled to any form of mode, the terminology atom in the following does not imply that it is a actual elementary atom. In addition the system presented in Sec. 5.1 and studied in Sec. 5.2 is very similar to a waveguide, due to the selection of one particular mode by the collective behavior of the atomic cloud. Many arguments considering the free space system therefore do also apply to a waveguide system.

The system under consideration will be a system coupling to a single photon with rate g, and a decay rate from its excited state with rate Γ.

The interaction in both systems is ultimately limited by the time that an photon can interact with the atom. In a cavity the decay of the field mode with rate κ results in an lifetime κ^{-1}; the quantization volume of the photon is given by its spatial mode inside the resonator. A photon in free space is quantized in a volume defined by its spatial extent, e.g. the area of its beam waist πw^2 and the spatial length of a pulse $c\mathcal{R}^{-1}$, where $\mathcal{R}^{-1}$ is temporal width of the pulse. In free space, or similarly in a waveguide, the electric field per photon is $\propto V^{-1/2}$ and can in principle be boosted arbitrarily by reducing the length of a pulse, yet the interaction strength cannot be boosted, as will be illustrated below. In a cavity simply reducing the volume of the mode increases the electric field per photon, while maintaining the temporal shape of the photon. Additionally increasing the finesse of the cavity, i.e. lowering κ, increases the lifetime of a photon.

The preceding discussion seems to suggest that one can in principle achieve a Rabi frequency in free space $\Omega = gE > \Gamma$, where E is the electric field of a photon and Γ the spontaneous decay rate of the atom. Simply by decreasing the pulse width further and further [119]. This result however does not take into account the spectral width of a photon, which acquires frequency components exceeding the bandwidth of the atom for pulse widths shorter than $\approx \Gamma^{-1}$. The consequences of finite bandwidth effects for an atom excited from a single photon Fock or coherent state are considered in [41, 133]. The essential result is that there is no perfect passive excitation of a matter qubit with a single photon in finite time. However an infinitely long time reversed exponential pulse, as already briefly mentioned in previous considerations, is able to perfectly excite an atom. The spontaneous emission, that the probability amplitude of being in the excited state, sends out destructively interferes with the incoming photon due to the π-phase acquired during absorption and emission and thus prevents spontaneous emission of the excited state. Once the atom's excited state population reaches unity, the atom starts to decay immediately. This process is only possible if the full solid angle is covered by the incident dipole pattern of the photon. This limitation, the immediate emission after perfect excitation, also holds for the superatom case.

To conclude this argument it has to be emphasized, that the coupling of a two-level system and a photon inside a cavity can be boosted arbitrarily, but the coupling to the full system will be drastically reduced. E.g. a photon incident on a bare, i.e. with no atom inside, high finesse cavity system, will be reflected with very high probability from the reflecting surface of the mirror, as it is the case for a photon inside the cavity.

Assuming equal mode matching to a single atom of the field inside cavity and the respective free

space field, the coupling strength of the cavity is boosted by the number of round trips a photon takes inside the cavity.

The interaction with a detuned field in free space is very similar to the detuned cavity system for an atom initially in the ground state, in both cases the states of the coupled to the dressed system approximately correspond to the bare atom states. Due to the interaction with the photon field the levels experience an additional potential. Yet the amount of photons required to observe a significant effect is different. Considering the cavity system without relaxation, such as Fig. 5**a**, where the atom is initially in the excited state. The atom in a cavity cannot decay to the ground state due to the modified mode structure in the cavity that prevents spontaneous emission. This is in strict contrast to the free space system where the mode structure is unaltered and the atom can always spontaneously decay.

Considering the effect of a cw beam interacting with a single atom, by shaping the pulse to a time reversed exponential decay, it can in principle lead to perfect extinction, by means of the mechanism described above. If the incident field is now assumed to be a multi photon field which is perfectly mode matched to the emission pattern of the atom the regime where $\Omega > \Gamma$ could be accessible. This would correspond to the strong coupling regime in cavity QED. But for a single atom a Rabi frequency exceeding the spontaneous decay rate results in saturation, i.e. power broadening of the transition, which is in turn reduces the susceptibility to an electric field [119].

One striking advantage of an atom in free space is the processing of photons on the fly. While the fundamental restriction, spontaneous emission due to coupling to a specific mode, persists. It enables the investigation of a system coupled to a continuum of modes, while specific modes strongly interact with the system. This contrasts the physics of a cavity compared to free space and to some extent also a wave guide, since a cavity always exhibits a discrete mode structure, modifying relaxation process.

A single atom strongly coupled to a cavity results in the splitting of the modes of the individual systems. Thus a photon initially resonant to the bare cavity or atom will not interact with the system due to the Rabi splitting resulting in the normal modes of the system. Thus also a cavity system can fully prevent transmission of a cw light field [59, 63]. Both systems, a single atom in free space and a single atom in a cavity can completely prevent transmission of a cw light field, based on entirely different principles. In the free space scenario interference, in the cavity case due to the photon blockade or in other words the nonlinear Rabi frequency scaling.

If the main resource of decoherence is now not due to the fact that the coupling of the system cannot be further enhanced but rather relies on the properties of the atom than the system properties, the dynamics of a cavity and free space system exhibit very similar behavior. The systems studied in Sec. 5.2 and Sec. 3.3 both exhibit an excited state that does not interact with the driving field. The dynamics of a system exhibiting a dark state displays similar behavior in free space and in a cavity. The dephasing term is independent of the underlying coupling strength. In both scenarios it enables the subtraction of a single photon. Effectively the system is decoupled from the light and subsequently transparent, manifested by the coherent state of the driven cavity Fig. 12, and the unaltered intensity of the of the outgoing pulse after photon subtraction Fig. 21.

In conclusion the interaction of a photon and an atom depends on two essential values, first the electric field within the bandwidth of the atom and second the mode structure of the environment, which remains unaltered for the free space system. Eventually any system that is not perfectly isolated, will, as long as it can be described by the derived input output relations, decay fast if it is

efficiently coupled to in- and output channels. Maybe by considering a non-Markovian system the spontaneous emission can be altered by the correlations emerging between system and bath, with e.g. an multi-pass arrangement of the pulse propagating through the system.

7 Summary

In the course of this thesis a two level system strongly coupled to a single propagating mode was investigated. The interaction mediated by the two-level system results in a periodic modulation of the outgoing photon field, as well as correlations among individual photons separated by up to 5 μs.

The crucial steps required to prepare a single Rydberg superatom were briefly summarized to give an overview of the experimental setup. The preparation of a cold atomic cloud relies on the mechanical effects of photons interacting with atoms, where the momentum of a photon results in a change of the motional state of an atom. In the further discussion the internal degrees of freedom affected by atom-photon interactions were investigated.

The first system under consideration was an atom strongly coupled to a single mode cavity. The concepts and some phenomena of cavity QED, where photons are trapped within a high finesse cavity, were investigated. Allowing for a small imperfection of the cavity, the input output formalism in the Markov approximation was derived and exemplary applied to a single excitation leaking from a cavity. Furthermore the interaction of the atom with the environment and also the possible decoupling from the cavity field was discussed.

Next the effects that come about when dealing with a dilute gas of interacting Rydberg atoms were introduced. If the atomic cloud is smaller than the characteristic length scale of the interaction, the blockade radius, the entire cloud behaves as a single superatom. The effective two-plus-one level system interacts collectively with a single propagating mode, resulting in directed emission of the photons scattered by the superatom and enhanced interaction with the photon field.

In the final part, which constitutes the main results of this work, a superatom strongly interacting with a propagating few-photon single mode light field, was investigated. The collective character enables a strong enhancement of the interaction with individual photons, thus enabling the observation of few-photon Rabi oscillations in free space. The full system including the propagating photons can be solved for a coherent input field by solely solving the density matrix of the atomic subsystem. The measurements demonstrate strong light-matter coupling in free-space. By tuning the dephasing into the darkstates the system exhibits functionality beyond the two-level system and can be utilized to absorb a single photon from an arbitrary input pulse over a wide range of photon numbers.

7.1 Outlook

The unidirectional interaction of the superatom with an incoming photon pulse enables the realization of a cascaded quantum system. The coherent interaction and state manipulation of a first system is transferred to a subsequent system, without any back action. This system will be realized by creating two individual superatoms well separated by multiple blockade radii that are both interfaced by a single mode light field. The scalability of this approach in principle allows for the realization of a cascaded quantum network paving the way towards highly correlated states of light and matter.

8 References

[1] T. Young, "The Bakerian Lecture: On the Theory of Light and Colours," Philos. Trans. R. Soc. London **92**, 12 (1802).

[2] H. Hertz, "Ueber sehr schnelle electrische Schwingungen," Ann. der Phys. und Chemie **267**, 421 (1887).

[3] H. Hertz, "Ueber einen Einfluss des ultravioletten Lichtes auf die electrische Entladung," Ann. der Phys. und Chemie **267**, 983 (1887).

[4] W. Wien, "Ueber die Energievertheilung im Emissionsspectrum eines schwarzen Körpers," Ann. der Phys. und Chemie **294**, 662 (1896).

[5] M. Planck, "Ueber irreversible Strahlungsvorgänge," Ann. Phys. **306**, 69 (1900).

[6] M. Planck, "Entropie und Temperatur strahlender Wärme," Ann. Phys. **306**, 719 (1900).

[7] O. Lummer and E. Pringsheim, "Über die Strahlung des schwarzen Körpers für lange Wellen," Verh. Dt. Phys. Ges. **2**, 163 (1900).

[8] M. Planck, "Ueber das Gesetz der Energieverteilung im Normalspectrum," Ann. Phys. **309**, 553 (1901).

[9] J. C. Maxwell, "A Dynamical Theory of the Electromagnetic Field," Philos. Trans. R. Soc. London **155**, 459 (1865).

[10] A. Einstein, "Über einen die Erzeugung und Verwandlung des Lichtes betreffenden heuristischen Gesichtspunkt," Ann. Phys. **322**, 132 (1905).

[11] L. de Broglie, *Untersuchungen zur Quantentheorie* (Akad. Verl.-Ges., Leipzig, 1927) p. 88 S.

[12] H. Sievers, "Louis de Broglie und die Quantenmechanik," (1998), arXiv:9807012 [physics] .

[13] E. Schrödinger, "Quantisierung als Eigenwertproblem," Ann. Phys. **386**, 109 (1926).

[14] E. Schrödinger, "Quantisierung als Eigenwertproblem," Ann. Phys. **385**, 437 (1926).

[15] E. Schrödinger, "Quantisierung als Eigenwertproblem," Ann. Phys. **384**, 361 (1926), arXiv:1. Konstante, D. & Rtets, V. D. M. N(g, %) =. 361–376 .

[16] E. Schrödinger, "Quantisierung als Eigenwertproblem," Ann. Phys. **384**, 489 (1926).

[17] E. Schrödinger, "ARE THERE QUANTUM JUMPS ?" Br. J. Philos. Sci. **III**, 233 (1952).

[18] P. Goy, J. M. Raimond, M. Gross, and S. Haroche, "Observation of Cavity-Enhanced Single-Atom Spontaneous Emission," Phys. Rev. Lett. **50**, 1903 (1983).

[19] F. Bernardot, P. Nussenzveig, M. Brune, J. M. Raimond, and S. Haroche, "Vacuum Rabi Splitting Observed on a Microscopic Atomic Sample in a Microwave Cavity," Europhys. Lett. **17**, 33 (1992).

[20] E. Jaynes and F. Cummings, "Comparison of quantum and semiclassical radiation theories with application to the beam maser," Proc. IEEE **51**, 89 (1963).

[21] B. W. Shore and P. L. Knight, "The Jaynes-Cummings Model," J. Mod. Opt. **40**, 1195 (1993).

[22] M. Brune, F. Schmidt-Kaler, A. Maali, J. Dreyer, E. Hagley, J. M. Raimond, and S. Haroche, "Quantum Rabi Oscillation: A Direct Test of Field Quantization in a Cavity," Phys. Rev. Lett. **76**, 1800 (1996).

[23] M. H. Anderson, J. R. Ensher, M. R. Matthews, C. E. Wieman, and E. A. Cornell, "Observation of Bose-Einstein Condensation in a Dilute Atomic Vapor," Science (80-.). **269**, 198 (1995).

[24] C. C. Bradley, C. A. Sackett, J. J. Tollett, and R. G. Hulet, "Evidence of Bose-Einstein Condensation in an Atomic Gas with Attractive Interactions," Phys. Rev. Lett. **75**, 1687 (1995).

[25] K. B. Davis, M. O. Mewes, M. R. Andrews, N. J. van Druten, D. S. Durfee, D. M. Kurn, and W. Ketterle, "Bose-Einstein Condensation in a Gas of Sodium Atoms," Phys. Rev. Lett. **75**, 3969 (1995).

[26] S. Kuhr, S. Gleyzes, C. Guerlin, J. Bernu, U. B. Hoff, S. Deléglise, S. Osnaghi, M. Brune, J.-M. Raimond, S. Haroche, E. Jacques, P. Bosland, and B. Visentin, "Ultrahigh finesse Fabry-Pérot superconducting resonator," Appl. Phys. Lett. **90**, 164101 (2007).

[27] Y.-S. Chin, M. Steiner, and C. Kurtsiefer, "Nonlinear photon-atom coupling with 4Pi microscopy," (2017), arXiv:1705.10173 .

[28] A. Maser, B. Gmeiner, T. Utikal, S. Götzinger, and V. Sandoghdar, "Few-photon coherent nonlinear optics with a single molecule," Nat. Photonics **10**, 450 (2016), arXiv:1509.05216 .

[29] M. K. Tey, Z. Chen, S. A. Aljunid, B. Chng, F. Huber, G. Maslennikov, and C. Kurtsiefer, "Strong interaction between light and a single trapped atom without the need for a cavity," Nat. Phys. **4**, 924 (2008), arXiv:0802.3005 .

[30] M. K. Bhaskar, D. D. Sukachev, A. Sipahigil, R. E. Evans, M. J. Burek, C. T. Nguyen, L. J. Rogers, P. Siyushev, M. H. Metsch, H. Park, F. Jelezko, M. Lončar, and M. D. Lukin, "Quantum Nonlinear Optics with a Germanium-Vacancy Color Center in a Nanoscale Diamond Waveguide," Phys. Rev. Lett. **118**, 223603 (2017).

[31] A. Sipahigil, R. E. Evans, D. D. Sukachev, M. J. Burek, J. Borregaard, M. K. Bhaskar, C. T. Nguyen, J. L. Pacheco, H. A. Atikian, C. Meuwly, R. M. Camacho, F. Jelezko, E. Bielejec, H. Park, M. Lončar, and M. D. Lukin, "An integrated diamond nanophotonics platform for quantum-optical networks," Science (80-.). **354**, 847 (2016).

[32] A. Goban, C.-L. Hung, J. D. Hood, S.-P. Yu, J. A. Muniz, O. Painter, and H. J. Kimble, "Superradiance for Atoms Trapped along a Photonic Crystal Waveguide," Phys. Rev. Lett. **115**, 063601 (2015).

[33] S. Rosenblum, O. Bechler, I. Shomroni, Y. Lovsky, G. Guendelman, and B. Dayan, "Extraction of a single photon from an optical pulse," Nat. Photonics **10**, 19 (2015), arXiv:1510.04042 .

[34] I. Shomroni, S. Rosenblum, Y. Lovsky, O. Bechler, G. Guendelman, and B. Dayan, "All-optical routing of single photons by a one-atom switch controlled by a single photon," Science (80-.). **345**, 903 (2014), arXiv:1512.05740 .

[35] J. Petersen, J. Volz, and A. Rauschenbeutel, "Chiral nanophotonic waveguide interface based on spin-orbit interaction of light," Science (80-.). **346**, 67 (2014).

[36] P. Lodahl, S. Mahmoodian, S. Stobbe, A. Rauschenbeutel, P. Schneeweiss, J. Volz, H. Pichler, and P. Zoller, "Chiral quantum optics," Nature **541**, 473 (2017).

[37] H. J. Kimble, "The quantum internet," Nature **453**, 1023 (2008), arXiv:0806.4195 .

[38] A. Paris-Mandoki, C. Braun, J. Kumlin, C. Tresp, I. Mirgorodskiy, F. Christaller, H. P. Büchler, and S. Hofferberth, "Free-Space Quantum Electrodynamics with a Single Rydberg Superatom," Phys. Rev. X **7**, 041010 (2017).

[39] R. H. Dicke, "Coherence in Spontaneous Radiation Processes," Phys. Rev. **93**, 99 (1954), arXiv:1407.7336 .

[40] M. D. Lukin, M. Fleischhauer, R. Cote, L. M. Duan, D. Jaksch, J. I. Cirac, and P. Zoller, "Dipole Blockade and Quantum Information Processing in Mesoscopic Atomic Ensembles," Phys. Rev. Lett. **87**, 037901 (2001).

[41] M. Stobińska, G. Alber, and G. Leuchs, "Perfect excitation of a matter qubit by a single photon in free space," EPL (Europhysics Lett. **86**, 14007 (2009).

[42] S. Chu, L. Hollberg, J. E. Bjorkholm, A. Cable, and A. Ashkin, "Three-dimensional viscous confinement and cooling of atoms by resonance radiation pressure," Phys. Rev. Lett. **55**, 48 (1985).

[43] R. Grimm, M. Weidemüller, and Y. B. Ovchinnikov, "Optical Dipole Traps for Neutral Atoms," in *Adv. At. Mol. Opt. Phys.*, Vol. 42 (2000) pp. 95–170, arXiv:9902072 [physics] .

[44] C. Braun, *Implementation of a Raman Sideband Cooling for 87Rubidium*, Bachelor thesis, Universität Stuttgart (2015).

[45] C. Tresp, *Rydberg polaritons and Rydberg superatoms - novel tools for quantum nonlinear optics*, Ph.D. thesis, Universität Stuttgart (2017).

[46] D. Wineland, C. Monroe, W. Itano, D. Leibfried, B. King, and D. Meekhof, "Experimental issues in coherent quantum-state manipulation of trapped atomic ions," J. Res. Natl. Inst. Stand. Technol. **103**, 259 (1998), arXiv:9710025 [quant-ph] .

[47] J. M. Raimond, M. Brune, and S. Haroche, "Manipulating quantum entanglement with atoms and photons in a cavity," Rev. Mod. Phys. **73**, 565 (2001).

[48] J. M. Fink, M. Göppl, M. Baur, R. Bianchetti, P. J. Leek, A. Blais, and A. Wallraff, "Climbing the Jaynes–Cummings ladder and observing its nonlinearity in a cavity QED system," Nature **454**, 315 (2008).

[49] D. I. Schuster, A. A. Houck, J. A. Schreier, A. Wallraff, J. M. Gambetta, A. Blais, L. Frunzio, J. Majer, B. Johnson, M. H. Devoret, S. M. Girvin, and R. J. Schoelkopf, "Resolving photon number states in a superconducting circuit," Nature **445**, 515 (2007), arXiv:0608693 [cond-mat] .

[50] R. J. Schoelkopf and S. M. Girvin, "Wiring up quantum systems," Nature **451**, 664 (2008).

[51] H. Walther, B. T. H. Varcoe, B.-G. Englert, and T. Becker, "Cavity quantum electrodynamics," Reports Prog. Phys. **69**, 1325 (2006).

[52] D. M. Meekhof, C. Monroe, B. E. King, W. M. Itano, and D. J. Wineland, "Generation of Nonclassical Motional States of a Trapped Atom," Phys. Rev. Lett. **76**, 1796 (1996).

[53] H. Walther, B. T. H. Varcoe, S. Brattke, and M. Weidinger, "Preparing pure photon number states of the radiation field," Nature **403**, 743 (2000).

[54] A. Wallraff, D. I. Schuster, A. Blais, L. Frunzio, R.-S. Huang, J. Majer, S. Kumar, S. M. Girvin, and R. J. Schoelkopf, "Strong coupling of a single photon to a superconducting qubit using circuit quantum electrodynamics," Nature **431**, 162 (2004).

[55] T. Werlang, A. V. Dodonov, E. I. Duzzioni, and C. J. Villas-Bôas, "Rabi model beyond the rotating-wave approximation: Generation of photons from vacuum through decoherence," Phys. Rev. A **78**, 053805 (2008).

[56] D. A. Steck, "Quantum and Atom Optics Textbook," Book , 1069 (2016).

[57] D. Braak, "Integrability of the Rabi Model," Phys. Rev. Lett. **107**, 100401 (2011), arXiv:1103.2461 .

[58] R. J. Thompson, G. Rempe, and H. J. Kimble, "Observation of normal-mode splitting for an atom in an optical cavity," Phys. Rev. Lett. **68**, 1132 (1992).

[59] A. Boca, R. Miller, K. M. Birnbaum, A. D. Boozer, J. McKeever, and H. J. Kimble, "Observation of the Vacuum Rabi Spectrum for One Trapped Atom," Phys. Rev. Lett. **93**, 233603 (2004), arXiv:0410164v1 [arXiv:quant-ph] .

[60] M. G. Raizen, R. J. Thompson, R. J. Brecha, H. J. Kimble, and H. J. Carmichael, "Normal-mode splitting and linewidth averaging for two-state atoms in an optical cavity," Phys. Rev. Lett. **63**, 240 (1989).

[61] Y. Zhu, D. J. Gauthier, S. E. Morin, Q. Wu, H. J. Carmichael, and T. W. Mossberg, "Vacuum Rabi splitting as a feature of linear-dispersion theory: Analysis and experimental observations," Phys. Rev. Lett. **64**, 2499 (1990).

[62] G. Rempe, H. Walther, and N. Klein, "Observation of quantum collapse and revival in a one-atom maser," Phys. Rev. Lett. **58**, 353 (1987).

[63] K. M. Birnbaum, A. Boca, R. Miller, A. D. Boozer, T. E. Northup, and H. J. Kimble, "Photon blockade in an optical cavity with one trapped atom," Nature **436**, 87 (2005).

[64] A. Imamoḡlu, H. Schmidt, G. Woods, and M. Deutsch, "Strongly Interacting Photons in a Nonlinear Cavity," Phys. Rev. Lett. **79**, 1467 (1997).

[65] B. R. Mollow, "Pure-state analysis of resonant light scattering: Radiative damping, saturation, and multiphoton effects," Phys. Rev. A **12**, 1919 (1975).

[66] C. W. Gardiner and M. J. Collett, "Input and output in damped quantum systems: Quantum stochastic differential equations and the master equation," Phys. Rev. A **31**, 3761 (1985).

[67] C. W. Gardiner and P. Zoller, *Quantum Noise*, 3rd ed. (Springer-Verlag, Berlin, Heidelberg, 2004) p. 450.

[68] M. O. Scully and M. S. Zubairy, *Cambridge Univ. Press* (Cambridge University Press, Cambridge, 1997) p. 630.

[69] M. Lax, "Quantum Noise. IV. Quantum Theory of Noise Sources," Phys. Rev. **145**, 110 (1966).

[70] P. Alsing and H. J. Carmichael, "Spontaneous dressed-state polarization of a coupled atom and cavity mode," Quantum Opt. J. Eur. Opt. Soc. Part B **3**, 13 (1991).

[71] Y. Wang and J. Y. Haw, "Bridging the gap between the Jaynes–Cummings and Rabi models using an intermediate rotating wave approximation," Phys. Lett. A **379**, 779 (2015).

[72] E. M. Purcell, "Spontaneous Emission Probabilities at Radio Frequencies," Phys. Rev. **69**, 681 (1946).

[73] T. Niemczyk, F. Deppe, H. Huebl, E. P. Menzel, F. Hocke, M. J. Schwarz, J. J. Garcia-Ripoll, D. Zueco, T. Hümmer, E. Solano, A. Marx, and R. Gross, "Circuit quantum electrodynamics in the ultrastrong-coupling regime," Nat. Phys. **6**, 772 (2010), arXiv:1003.2376 .

[74] F. Yoshihara, T. Fuse, S. Ashhab, K. Kakuyanagi, S. Saito, and K. Semba, "Superconducting qubit–oscillator circuit beyond the ultrastrong-coupling regime," Nat. Phys. **13**, 44 (2016), arXiv:1602.00415 .

[75] S. De Liberato, "Light-Matter Decoupling in the Deep Strong Coupling Regime: The Breakdown of the Purcell Effect," Phys. Rev. Lett. **112**, 016401 (2014), arXiv:1308.2812 .

[76] J. Casanova, G. Romero, I. Lizuain, J. J. García-Ripoll, and E. Solano, "Deep strong coupling regime of the Jaynes-Cummings model," Phys. Rev. Lett. **105**, 1 (2010), arXiv:1008.1240 .

[77] D. Ballester, G. Romero, J. J. García-Ripoll, F. Deppe, and E. Solano, "Quantum Simulation of the Ultrastrong-Coupling Dynamics in Circuit Quantum Electrodynamics," Phys. Rev. X **2**, 021007 (2012), arXiv:1107.5748 .

[78] M. Sanz, E. Solano, and Í. L. Egusquiza, "Beyond Adiabatic Elimination: Effective Hamiltonians and Singular Perturbation," (2016) pp. 127–142.

[79] D. Jaksch, J. I. Cirac, P. Zoller, S. L. Rolston, R. Côté, and M. D. Lukin, "Fast Quantum Gates for Neutral Atoms," Phys. Rev. Lett. **85**, 2208 (2000), arXiv:0004038 [quant-ph] .

[80] L. Isenhower, E. Urban, X. L. Zhang, A. T. Gill, T. Henage, T. A. Johnson, T. G. Walker, and M. Saffman, "Demonstration of a Neutral Atom Controlled-NOT Quantum Gate," Phys. Rev. Lett. **104**, 010503 (2010).

[81] T. Wilk, A. Gaëtan, C. Evellin, J. Wolters, Y. Miroshnychenko, P. Grangier, and A. Browaeys, "Entanglement of Two Individual Neutral Atoms Using Rydberg Blockade," Phys. Rev. Lett. **104**, 010502 (2010).

[82] M. Ebert, A. Gill, M. Gibbons, X. Zhang, M. Saffman, and T. G. Walker, "Atomic Fock State Preparation Using Rydberg Blockade," Phys. Rev. Lett. **112**, 043602 (2014).

[83] L. Béguin, A. Vernier, R. Chicireanu, T. Lahaye, and A. Browaeys, "Direct Measurement of the van der Waals Interaction between Two Rydberg Atoms," Phys. Rev. Lett. **110**, 263201 (2013).

[84] S. Ravets, H. Labuhn, D. Barredo, T. Lahaye, and A. Browaeys, "Measurement of the angular dependence of the dipole-dipole interaction between two individual Rydberg atoms at a Förster resonance," Phys. Rev. A **92**, 020701 (2015).

[85] D. Barredo, S. Ravets, H. Labuhn, L. Béguin, A. Vernier, F. Nogrette, T. Lahaye, and A. Browaeys, "Demonstration of a Strong Rydberg Blockade in Three-Atom Systems with Anisotropic Interactions," Phys. Rev. Lett. **112**, 183002 (2014), arXiv:1402.4077 .

[86] H. Weimer, R. Löw, T. Pfau, and H. P. Büchler, "Quantum Critical Behavior in Strongly Interacting Rydberg Gases," Phys. Rev. Lett. **101**, 250601 (2008).

[87] T. Pohl, E. Demler, and M. D. Lukin, "Dynamical Crystallization in the Dipole Blockade of Ultracold Atoms," Phys. Rev. Lett. **104**, 043002 (2010).

[88] P. Schauss, J. Zeiher, T. Fukuhara, S. Hild, M. Cheneau, T. Macri, T. Pohl, I. Bloch, and C. Gross, "Crystallization in Ising quantum magnets," Science (80-.). **347**, 1455 (2015).

[89] H. Labuhn, D. Barredo, S. Ravets, S. de Léséleuc, T. Macrì, T. Lahaye, and A. Browaeys, "Tunable two-dimensional arrays of single Rydberg atoms for realizing quantum Ising models," Nature **534**, 667 (2016).

[90] H. Bernien, S. Schwartz, A. Keesling, H. Levine, A. Omran, H. Pichler, S. Choi, A. S. Zibrov, M. Endres, M. Greiner, V. Vuletić, and M. D. Lukin, "Probing many-body dynamics on a 51-atom quantum simulator," (2017), arXiv:1707.04344 .

[91] P. Schauß, M. Cheneau, M. Endres, T. Fukuhara, S. Hild, A. Omran, T. Pohl, C. Gross, S. Kuhr, and I. Bloch, "Observation of spatially ordered structures in a two-dimensional Rydberg gas," Nature **491**, 87 (2012).

[92] C. R. Murray and T. Pohl, "Coherent photon manipulation in interacting atomic ensembles," Phys. Rev. X **7**, 66 (2017), arXiv:1702.03763 .

[93] O. Firstenberg, C. S. Adams, and S. Hofferberth, "Nonlinear quantum optics mediated by Rydberg interactions," J. Phys. B At. Mol. Opt. Phys. **49**, 152003 (2016).

[94] I. Mirgorodskiy, F. Christaller, C. Braun, A. Paris-Mandoki, C. Tresp, and S. Hofferberth, "Electromagnetically induced transparency of ultra-long-range Rydberg molecules," Phys. Rev. A **96**, 011402 (2017).

[95] H. Busche, P. Huillery, S. W. Ball, T. Ilieva, M. P. A. Jones, and C. S. Adams, "Contactless nonlinear optics mediated by long-range Rydberg interactions," Nat. Phys. **13**, 655 (2017).

[96] D. Tiarks, S. Baur, K. Schneider, S. Dürr, and G. Rempe, "Single-Photon Transistor Using a Förster Resonance," Phys. Rev. Lett. **113**, 053602 (2014), arXiv:1404.3061 .

[97] H. Gorniaczyk, C. Tresp, P. Bienias, A. Paris-Mandoki, W. Li, I. Mirgorodskiy, H. P. Büchler, I. Lesanovsky, and S. Hofferberth, "Enhancement of Rydberg-mediated single-photon nonlinearities by electrically tuned Förster resonances," Nat. Commun. **7**, 12480 (2016), arXiv:1511.09445 .

[98] C. Tresp, C. Zimmer, I. Mirgorodskiy, H. Gorniaczyk, A. Paris-Mandoki, and S. Hofferberth, "Single-Photon Absorber Based on Strongly Interacting Rydberg Atoms," Phys. Rev. Lett. **117**, 223001 (2016), arXiv:1605.04456 .

[99] T. Peyronel, O. Firstenberg, Q.-Y. Liang, S. Hofferberth, A. V. Gorshkov, T. Pohl, M. D. Lukin, and V. Vuletić, "Quantum nonlinear optics with single photons enabled by strongly interacting atoms." Nature **488**, 57 (2012).

[100] O. Firstenberg, T. Peyronel, Q.-Y. Liang, A. V. Gorshkov, M. D. Lukin, and V. Vuletić, "Attractive photons in a quantum nonlinear medium," Nature **502**, 71 (2013).

[101] J. D. Pritchard, K. J. Weatherill, and C. S. Adams, "NONLINEAR OPTICS USING COLD RYDBERG ATOMS," in *Annu. Rev. Cold Atoms Mol.*, Vol. 1 (WORLD SCIENTIFIC, 2013) pp. 301–350, arXiv:1205.4890 .

[102] H. Gorniaczyk, C. Tresp, J. Schmidt, H. Fedder, and S. Hofferberth, "Single-Photon Transistor Mediated by Interstate Rydberg Interactions," Phys. Rev. Lett. **113**, 053601 (2014).

[103] K. Jachymski, P. Bienias, and H. P. Büchler, "Three-Body Interaction of Rydberg Slow-Light Polaritons," Phys. Rev. Lett. **117**, 053601 (2016), arXiv:1604.03743 .

[104] M. F. Maghrebi, M. J. Gullans, P. Bienias, S. Choi, I. Martin, O. Firstenberg, M. D. Lukin, H. P. Büchler, and A. V. Gorshkov, "Coulomb Bound States of Strongly Interacting Photons," Phys. Rev. Lett. **115**, 123601 (2015), arXiv:1505.03859 .

[105] P. Bienias, S. Choi, O. Firstenberg, M. F. Maghrebi, M. Gullans, M. D. Lukin, A. V. Gorshkov, and H. P. Büchler, "Scattering resonances and bound states for strongly interacting Rydberg polaritons," Phys. Rev. A **90**, 053804 (2014).

[106] M. J. Gullans, J. D. Thompson, Y. Wang, Q.-Y. Liang, V. Vuletić, M. D. Lukin, and A. V. Gorshkov, "Effective Field Theory for Rydberg Polaritons," Phys. Rev. Lett. **117**, 113601 (2016).

[107] Q.-Y. Liang, A. V. Venkatramani, S. H. Cantu, T. L. Nicholson, M. J. Gullans, A. V. Gorshkov, J. D. Thompson, C. Chin, M. D. Lukin, and V. Vuletic, "Observation of three-photon bound states in a quantum nonlinear medium," (2017), arXiv:1709.01478 .

[108] V. Bendkowsky, B. Butscher, J. Nipper, J. P. Shaffer, R. Löw, and T. Pfau, "Observation of ultralong-range Rydberg molecules," Nature **458**, 1005 (2009).

[109] C. H. Greene, A. S. Dickinson, and H. R. Sadeghpour, "Creation of Polar and Nonpolar Ultra-Long-Range Rydberg Molecules," Phys. Rev. Lett. **85**, 2458 (2000).

[110] A. Gaj, A. T. Krupp, J. B. Balewski, R. Löw, S. Hofferberth, and T. Pfau, "From molecular spectra to a density shift in dense Rydberg gases," Nat. Commun. **5**, 4546 (2014), arXiv:1404.5761 .

[111] B. Butscher, J. Nipper, J. B. Balewski, L. Kukota, V. Bendkowsky, R. Löw, and T. Pfau, "Atom–molecule coherence for ultralong-range Rydberg dimers," Nat. Phys. **6**, 970 (2010).

[112] R. Heidemann, U. Raitzsch, V. Bendkowsky, B. Butscher, R. Löw, L. Santos, and T. Pfau, "Evidence for Coherent Collective Rydberg Excitation in the Strong Blockade Regime," Phys. Rev. Lett. **99**, 163601 (2007), arXiv:0701120v2 [arXiv:quant-ph] .

[113] Y. O. Dudin, L. Li, F. Bariani, and A. Kuzmich, "Observation of coherent many-body Rabi oscillations," Nat. Phys. **8**, 790 (2012), arXiv:1205.7061 .

[114] J. Zeiher, P. Schauß, S. Hild, T. Macrì, I. Bloch, and C. Gross, "Microscopic Characterization of Scalable Coherent Rydberg Superatoms," Phys. Rev. X **5**, 031015 (2015), arXiv:1503.02452 .

[115] S. Weber, C. Tresp, H. Menke, A. Urvoy, O. Firstenberg, H. P. Büchler, and S. Hofferberth, "Calculation of Rydberg interaction potentials," J. Phys. B At. Mol. Opt. Phys. **50**, 133001 (2017).

[116] R. H. Lehmberg, "Radiation from an N -Atom System. I. General Formalism," Phys. Rev. A **2**, 883 (1970).

[117] D. Porras and J. I. Cirac, "Collective generation of quantum states of light by entangled atoms," Phys. Rev. A **78**, 053816 (2008).

[118] M. O. Scully, E. S. Fry, C. H. R. Ooi, and K. Wódkiewicz, "Directed Spontaneous Emission from an Extended Ensemble of N Atoms: Timing Is Everything," Phys. Rev. Lett. **96**, 010501 (2006).

[119] G. Leuchs and M. Sondermann, "Light–matter interaction in free space," J. Mod. Opt. **60**, 36 (2013).

[120] H. Pichler, T. Ramos, A. J. Daley, and P. Zoller, "Quantum optics of chiral spin networks," Phys. Rev. A **91**, 042116 (2015).

[121] P. Lodahl, S. Mahmoodian, and S. Stobbe, "Interfacing single photons and single quantum dots with photonic nanostructures," Rev. Mod. Phys. **87**, 347 (2015).

[122] T. G. Tiecke, J. D. Thompson, N. P. de Leon, L. R. Liu, V. Vuletić, and M. D. Lukin, "Nanophotonic quantum phase switch with a single atom," Nature **508**, 241 (2014), arXiv:1404.5615 .

[123] A. F. van Loo, A. Fedorov, K. Lalumiere, B. C. Sanders, A. Blais, and A. Wallraff, "Photon-Mediated Interactions Between Distant Artificial Atoms," Science (80-.). **342**, 1494 (2013).

[124] D. E. Chang, V. Vuletić, and M. D. Lukin, "Quantum nonlinear optics — photon by photon," Nat. Photonics **8**, 685 (2014).

[125] I. Gerhardt, G. Wrigge, P. Bushev, G. Zumofen, M. Agio, R. Pfab, and V. Sandoghdar, "Strong Extinction of a Laser Beam by a Single Molecule," Phys. Rev. Lett. **98**, 033601 (2007), arXiv:0604177 [quant-ph] .

[126] A. N. Vamivakas, M. Atatüre, J. Dreiser, S. T. Yilmaz, A. Badolato, A. K. Swan, B. B. Goldberg, A. Imamoğlu, and M. S. Ünlü, "Strong Extinction of a Far-Field Laser Beam by a Single Quantum Dot," Nano Lett. **7**, 2892 (2007).

[127] E. Urban, T. A. Johnson, T. Henage, L. Isenhower, D. D. Yavuz, T. G. Walker, and M. Saffman, "Observation of Rydberg blockade between two atoms," Nat. Phys. **5**, 110 (2009).

[128] A. Gaëtan, Y. Miroshnychenko, T. Wilk, A. Chotia, M. Viteau, D. Comparat, P. Pillet, A. Browaeys, and P. Grangier, "Observation of collective excitation of two individual atoms in the Rydberg blockade regime," Nat. Phys. **5**, 115 (2009), arXiv:0810.2960 .

[129] T. M. Weber, M. Höning, T. Niederprüm, T. Manthey, O. Thomas, V. Guarrera, M. Fleischhauer, G. Barontini, and H. Ott, "Mesoscopic Rydberg-blockaded ensembles in the super-atom regime and beyond," Nat. Phys. **11**, 157 (2015).

[130] A. A. Svidzinsky, J.-T. Chang, and M. O. Scully, "Dynamical Evolution of Correlated Spontaneous Emission of a Single Photon from a Uniformly Excited Cloud of N Atoms," Phys. Rev. Lett. **100**, 160504 (2008).

[131] Y. Miroshnychenko, U. V. Poulsen, and K. Mølmer, "Directional emission of single photons from small atomic samples," Phys. Rev. A **87**, 023821 (2013).

[132] T. Caneva, M. T. Manzoni, T. Shi, J. S. Douglas, J. I. Cirac, and D. E. Chang, "Quantum dynamics of propagating photons with strong interactions: a generalized input–output formalism," New J. Phys. **17**, 113001 (2015).

[133] Y. Wang, J. Minář, L. Sheridan, and V. Scarani, "Efficient excitation of a two-level atom by a single photon in a propagating mode," Phys. Rev. A **83**, 063842 (2011).

[134] V. Leong, M. A. Seidler, M. Steiner, A. Cerè, and C. Kurtsiefer, "Time-resolved scattering of a single photon by a single atom," Nat. Commun. **7**, 13716 (2016).

[135] M. Lax, "Formal Theory of Quantum Fluctuations from a Driven State," Phys. Rev. **129**, 2342 (1963).

[136] M. Lax, "Quantum Noise. X. Density-Matrix Treatment of Field and Population-Difference Fluctuations," Phys. Rev. **157**, 213 (1967).

[137] M. Lax, "Quantum Noise. XI. Multitime Correspondence between Quantum and Classical Stochastic Processes," Phys. Rev. **172**, 350 (1968).

[138] T. Shi, D. E. Chang, and J. I. Cirac, "Multiphoton-scattering theory and generalized master equations," Phys. Rev. A **92**, 053834 (2015).

[139] E. Rephaeli and S. Fan, "Stimulated Emission from a Single Excited Atom in a Waveguide," Phys. Rev. Lett. **108**, 143602 (2012), arXiv:1204.4668 .

[140] J. Honer, R. Löw, H. Weimer, T. Pfau, and H. P. Büchler, "Artificial atoms can do more than atoms: Deterministic single photon subtraction from arbitrary light fields," Phys. Rev. Lett. **107**, 1 (2011), arXiv:1103.1319 .

[141] A. V. Gorshkov, R. Nath, and T. Pohl, "Dissipative Many-Body Quantum Optics in Rydberg Media," Phys. Rev. Lett. **110**, 153601 (2013), arXiv:1211.7060 .